Vortex Scattering in the Point Vortex Model

Karl Lydon

Aston University

Master of Science (by Research)

October, 2018

Abstract

Here we provide both a theoretical and numerical analysis of scattering in vortex collisions using the 2-D point vortex model, where both the dipole-vortex collision is considered in the three vortex case, and the dipole-dipole collision is considered in the four vortex case. We begin by presenting the basics of turbulence in classical fluids, and in quantum fluids which we then use to give an exposition of the 2-D point vortex system. The point vortex model is then given completely for the general case of N point vortices in an infinite domain. We express the system as a Hamiltonian formulation as done by Kirchhoff, with the equations of motion derived using Hamilton's canonical equations. It is then considered how to best solve the system numerically. We form a numerical simulation using the famed Dormand-Prince adaptive time step Runge-Kutta scheme, as well as an elementary controller to adjust the time-step, pseudo-code is provided to demonstrate the method. The motion of two point vortices, in both the vortex/anti-vortex and identical vortex case, is then considered both numerically and theoretically as a check of the reliability of the simulations finding precise agreement between numerical and theoretical results.

We then consider the crux of the current work, the dipole-vortex collision and the dipole-dipole collision, partly inspired by the work of Aref [H. Aref, Phys. Fluids 3 (1979), 393-400]. We solve each case numerically, with an additional theoretical treatment in the dipole-vortex case. We solve the three vortex collision for the scattering angle, minimum lengths and critical lengths. Continuing, the four vortex collision is solved for the scattering angles and the minimum lengths. We find similarities in the results of both systems, and also note an apparent mistake in Aref's work in the three vortex case, as well as noting regions of atypical vortex behavior in the four vortex case, possibly corresponding to regions of self-similar vortex collapse.

Contents

List of Figures

List of Tables

Chapter 1

Introduction

1.1 Hydrodynamic Turbulence

Problems involving the phenomenon of hydrodynamic turbulence are of critical importance to many areas and to fluid dynamics as a whole. Despite this, prediction of turbulent flows is often based on uncertainty techniques and models [2], and so instead analysis is restricted to several methods involving statistical analysis [3], non-linear dynamical system theory [4], and the central focus of this work; vortex dynamics [5, 6, 7]. Technically speaking, turbulent flow is characterized by chaotic changes in pressure and flow velocity, such behavior is composed of a complex assembly of eddy currents with no apparent regularity. This motion can be observed in any fluid where the Reynolds number, defined as the ratio between inertial forces to viscous forces, exceeds a critical value. Once the Reynolds number is greater than this critical value, viscous forces are then generally negligible and we observe the rapid velocity fluctuations already mentioned [8].

Usually we can describe fluid motion in terms of solutions of the fundamental Navier-Stokes equations. We assume that we have an incompressible Newtonian fluid of constant density ρ and constant viscosity μ, the velocity distribution of the fluid $\boldsymbol{u} \equiv \boldsymbol{u}(x, y, z, t) \in \mathbb{R}^3$ is described by the incompressible Navier-Stokes equations given here:

$$\frac{\partial \boldsymbol{u}}{\partial t} + (\boldsymbol{u} \cdot \nabla)\boldsymbol{u} = -\frac{1}{\rho}\nabla p + \frac{\mu}{\rho}\nabla^2 \boldsymbol{u} + \boldsymbol{g}, \tag{1.1}$$

$$\nabla \cdot \boldsymbol{u} = 0, \tag{1.2}$$

where (1.1) gives the Navier-Stokes momentum equations and (1.2) gives the usual incompressibility condition [9]. Note here $\boldsymbol{g} \equiv \boldsymbol{g}(x, y, z) \in \mathbb{R}^3$ represents an external field acting on the fluid (for example a gravitational field), $p \equiv p(x, y, z, t)$ is a scalar function representing pressure, and ∇ represents the differential operator common throughout vector calculus:

$$\nabla = (\frac{\partial}{\partial x}, \frac{\partial}{\partial y}, \frac{\partial}{\partial z}).$$

Similarly we define ∇^2 as the Laplacian:

$$\nabla^2 = \nabla \cdot \nabla = \frac{\partial^2}{\partial x^2} + \frac{\partial^2}{\partial y^2} + \frac{\partial^2}{\partial z^2}.$$

Solving these equations especially in the presence of turbulence is considered extremely complicated, this is due to both the non-linear $(\boldsymbol{u}\cdot\nabla)\boldsymbol{u}$ term and the complex, chaotic motion of turbulence in general. Nevertheless, turbulence has been successfully investigated using Navier-Stokes simulations in various works [10, 11, 12]. We note the $(\mu/\rho)\nabla^2\boldsymbol{u}$ term representing the

difference between velocity of a point in the fluid compared to the velocity of a small surrounding volume, hence this term corresponds to the diffusion of momentum created by the viscous forces present [9]. Hence turbulence corresponds to the limit where the nonlinear term dominates the linear terms, corresponding to highly unstable flow. If we were to ignore this term we would recover the much more simple Euler equations:

$$\begin{gathered}\frac{\partial \boldsymbol{u}}{\partial t} + (\boldsymbol{u} \cdot \nabla)\boldsymbol{u} = -\frac{1}{\rho}\nabla p + \boldsymbol{g}, \\ \nabla \cdot \boldsymbol{u} = 0.\end{gathered} \tag{1.3}$$

These equations are not as complicated as the Navier-Stokes equations, on account of lacking the diffusion term, and can easily be derived by first principles [9]. However this presents a new problem; if this term is removed then the viscous forces are no longer present, so therefore the Reynold's number as the ratio of inertial forces to viscous forces is undefined and turbulence is therefore impossible in theory under (1.3). Interestingly, it has been noted that turbulent flows can be described in the limit of vanishing viscosity as weak solutions of the Euler equations, as first suggested by Onsager [13]. We will revisit this idea later, for now we consider some other aspects of turbulence.

A major component encountered universally in turbulent flow is the presence of so-called vortices. Simply speaking, vortices can be defined as regions in the fluid around which particles outside the region rotate in circle-like orbits. These vortices are characterized by the velocity distribution of the fluid, the vorticity distribution of the fluid, and the circulation of the fluid. The vorticity in essence refers to the vector defining local rotational motion at a point in the fluid, technically calculated as the curl of velocity:

$$\boldsymbol{\omega} = \nabla \times \boldsymbol{u}, \tag{1.4}$$

where $\boldsymbol{\omega} \in \mathbb{R}^3$ represents the local vorticity at a point in the flow. Note that a fluid where $\boldsymbol{\omega} = 0$ everywhere represents what is known as irrotational fluid. We also have the circulation which is given by the line integral of the velocity field around a closed curve:

$$\kappa = \oint_C \boldsymbol{u} \cdot d\boldsymbol{s}, \tag{1.5}$$

where C is a closed curve and $d\boldsymbol{s}$ is the vector differential representing the length of a small element on the curve C. We can see how C and $\boldsymbol{\omega}$ are related by Stokes' theorem:

$$\kappa = \oint_C \boldsymbol{u} \cdot d\boldsymbol{s} = \iint_S \boldsymbol{\omega} \cdot d\boldsymbol{S}, \tag{1.6}$$

where S is a closed surface bounded by the path C. Circulation can therefore be thought of as the flux of vorticity, or vorticity can be thought of as the circulation taken using an infinitesimal curve C [14], this is shown in Fig. 1.1.

These quantities will become useful later, for now we simply note the importance of vortices to the idea of turbulent flow, and understand that they are characterized by quantities $\boldsymbol{u}, \boldsymbol{\omega}$ and κ. Certainly if one desires to model the effects of turbulent flow, then being able to accurately model the vortices formed as part of that turbulence is of prime importance. Due to the chaotic nature of turbulent flow problems involving turbulence are in general extremely complex and challenging to solve, for example, calculation of shear stresses as a result of turbulent motion proves difficult [15]. Thus it is clear that methods of approximating three dimensional turbulent systems and the vortices they contain are very attractive.

One particular method of interest here is the representation of vortices in the fluid as vortex filaments. The concept of vortex filaments is derived from the idea of vortex lines in the flow.

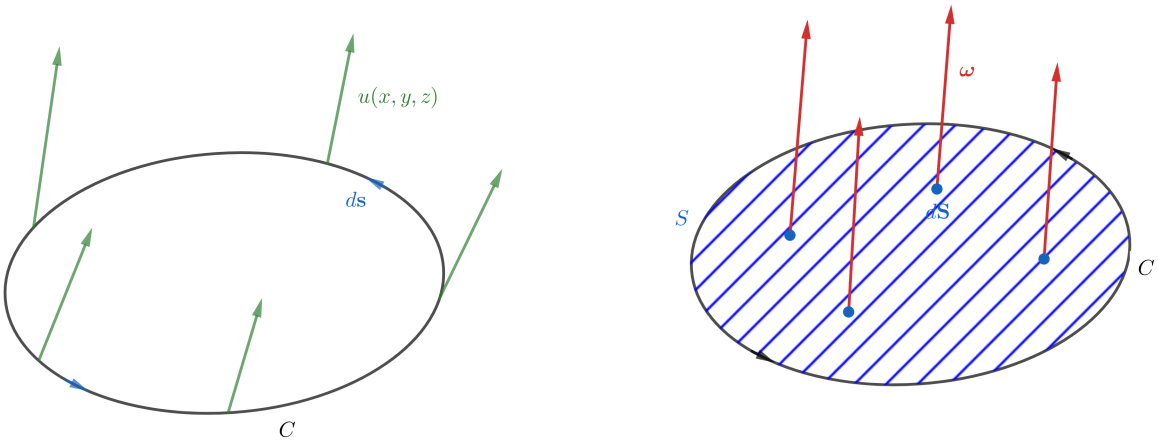

(a) κ as line integral of $\boldsymbol{u}$

(b) κ as flux of $\boldsymbol{\omega}$

Figure 1.1: Diagrams showing the geometric interpretations of κ.

We define vortex lines to be lines tangent to the local vorticity vector; by drawing vortex lines through each point of a closed curve we then have what is referred to as vortex tubes. If then we take vortex tubes to be of infinitesimal dimensions, we then have what is referred to as a vortex filament [16]. The analysis of flow using this concept was first established by Helmholtz, where he formulated several laws of vortex filament behavior now known Helmholtz's vortex theorems [17]. We reproduce the theorems here:

1. Strength of vortex filaments are constant.
2. Vortex lines move with the fluid, and must either form a closed loop, start and end at solid boundaries in the fluid, or extend to $-\infty/\infty$.
3. Fluid elements that are initially irrotational remain irrotational.

Note that it can be shown that vortex filament strength is equivalent to the circulation around it [18]. These theorems can be easily applied in modelling situations coupled with the Biot-Savart law used to describe the velocity field of the fluid imparted by the vortex filaments, a procedure common in aerodynamics. The Biot-Savart law for a vortex filament of general shape is given by the integral over all vortex lines given as:

$$\boldsymbol{u}(x, y, z) = \frac{\kappa}{4\pi} \int \frac{d\boldsymbol{\ell} \times \boldsymbol{r}}{|\boldsymbol{r}|^3}, \tag{1.7}$$

where $\boldsymbol{r} \in \mathbb{R}^3$ extends from the point of integration to the point in the fluid $P = (x, y, z)$, whereas $d\boldsymbol{\ell}$ represents the arc length element points along the filament in the direction of positive κ by right hand rule [19]. The limits of the integration will depend upon the shape of the vortex filament. We see this visualized in Fig. 1.2.

This approximation allows for a basic model of turbulent vortices where local vorticity is ignored in favor of tracking the center point of the vorticity region. Associated vortex filament methods have proved to be successful in modelling turbulence in various situations [20, 21, 22].

Another crucial approximation that can be made is to consider the turbulence in only two spatial dimensions. Analysis of turbulence in the 2-D plane is confined to a theoretical domain, as turbulent motion found in nature always manifests some degree of three dimensional phenomena. Nevertheless, the 2-D approximation to turbulence is found to accurately describe certain

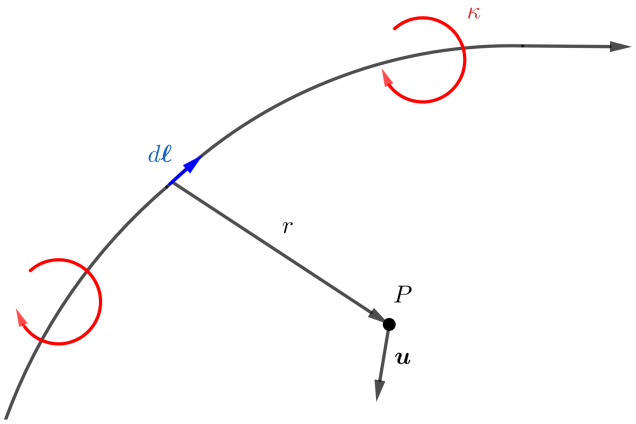

Figure 1.2: Diagram of the Biot-Savart law applied on a vortex filament.

physical systems such as oceans and atmospheres, where the ratio of lateral length to vertical length is very large [23]. The 2-D approximation also shows remarkable new phenomena that are not normally present. For example, an inverse cascade is observed [24], which in a restricted periodic domain can form a vortex condensate as analyzed in [25]. These interesting phenomena arise from the existence of new conservation laws observed in 2-D turbulence note previously present in the 3-D case, this leads to phenomena such as the condensates already mentioned and shows the 2-D turbulence being more than just a simplification of 3-D turbulence.

1.2 Turbulence in Quantum Fluids

We now move to consider possibly the most interesting aspect of turbulence, namely the concept of quantum turbulence. We can classify the turbulent flow explained in the last section into two types, classical turbulence and quantum turbulence. Whilst classical turbulence is a common occurrence that can be observed readily in nature (for example in a flowing river or stream) quantum turbulence is much rarer, only occurring in carefully designed experiment or in neutron stars. Essentially, quantum turbulence is the event of turbulent flow appearing in a superfluid i.e. a fluid with zero viscosity. Such fluids only exist at extremely low temperature very close to absolute zero [26].

The characteristic property of superfluids is the property of zero viscosity, in other words superfluids are not subject to viscous forces and so flow without a loss of energy. Normally any turbulence encountered in a classical fluid eventually decays over time as the viscous forces present causes the turbulence to decay, due to the lack of viscosity in superfluids however quantum turbulence continues indefinitely as long as the conditions for superfluidity are maintained. As the onset of turbulence is determined by the Reynold's number, which is in turn determined by the viscous forces in the fluid, under normal conditions turbulence is not possible in fluids when these viscous forces are not present as discussed previously. Nevertheless, quantum turbulence has been theorized as early as 1955 by Feynman [27], and has been observed in liquid helium [28] as a particular kind of Bose-Einstein condensate (referred to here as simply BECs). Said BECs are a peculiar phenomenon occurring as a state of matter of boson gas at extremely low temperatures and extremely low density, where once a critical temperature is reached, distinct bosons begin to occupy the lowest quantum state at the same time and so can be described by the same wave function given as the solution to the Gross-Pitaevskii equation:

$$i\hbar\frac{\partial\psi}{\partial t} = \left(-\frac{\hbar^2}{2m}\nabla_x^2 + V_{ext} + g|\psi|^2\right)\psi, \tag{1.8}$$

where ψ corresponds to the wave function in question, $\hbar$ is the reduced Planck's constant, m is the mass of the boson, V_{ext} represents an external potential, g is a measure of the atomic interactions and $|\psi|^2$ is the atomic density [29]. Note that we can express this in terms of dimensionless variables [30] i.e. if $X = x\frac{\hbar}{\sqrt{2mV_{ext}}}$, $T = \frac{tV_{ext}}{\hbar}$, and $\Psi = \sqrt{\frac{g}{V_{ext}}}$ then equation (1.8) can be expressed as:

$$i\frac{\partial \Psi}{\partial T} = (|\Psi|^2 - \nabla_X^2 - 1)\Psi. \tag{1.9}$$

This state of matter is of particular interest not only due to certain BECs exhibiting superfluidity, but also due to other interesting properties inherent to BECs; such as penetration of fine pores that would be impossible using ordinary fluids, the ability to creep upwards along walls, as well as superb heat conduction [31]. However, we must note that superfluidity does not necessarily imply the presence of a BEC, and a BEC being formed does not necessarily imply superfluidity [32].

It is clear that this exotic peculiarity is of considerable interest, as understanding of the behavior of BECs could potentially lead to a better understanding of superfluidity, and vice versa. Particularly interesting is the vortices that are formed in the event of quantum turbulence. By stirring or rotating a BEC for example one observes the formation of vortex lattices once a certain critical angular velocity is reached, as discussed these vortices will continue to rotate indefinitely. Even more peculiarly, such vortices possess quantized circulation, in other words the circulations of such vortices must be an integer multiple of the quantum value $\kappa = h/m$. Also, rotational motion is only sustained through these vortices, i.e. fluid is irrotational, $\boldsymbol{\omega} = 0$ at all points other than the vortices in question. Hence we find the Helmholtz laws of vortex motion to be satisfied in the case of quantum vortices, and as vortex widths are incredibly small (of the order of a few angstroms in ^{4}He for example [33]) we find that quantum vortices are then analogous to the vortex filaments found in the last section. Hence we can accurately describe quantum turbulence as a "tangle" of quantized identical vortex filaments, as seen in Fig. 1.3, here instead of a loose approximation vortex filaments now represent the regions of vorticity completely. This is remarkably demonstrated by Bustamante and Nazarenko [30], where it is shown that the Biot-Savart law can actually be obtained from equation (1.8), proving explicitly that vortices in quantum fluid consist of vortex filaments.

Figure 1.3: Simulation of a quantum vortex tangle, reproduced from [1].

This not only is extremely interesting but implies that modelling of quantum turbulence

is perhaps easier than modelling of the classical turbulence already discussed. This is due to vortex filaments now representing the entire physics of the situation rather than being crude approximations as is the case for classical turbulence. However, despite the obvious differences separating classical and quantum turbulence, we note that quantum fluid has in fact been expressed in terms of classical fluid equations using the Madelung transformation [34]. This essentially consists of separating the Gross-Pitaevskii into a real and imaginary part. Assume momentarily that density is not constant so now $\rho = \rho(x, y, z, t)$, now by using the Madelung transformation $\Psi = \sqrt{\rho}e^{i\phi}$ and by allowing $\boldsymbol{u}(x, y, z, t) = 2\nabla\phi(x, y, z, t)$ we obtain the equations:

$$\frac{\partial \rho}{\partial T} + \nabla \cdot (\rho \boldsymbol{u}) = 0, \tag{1.10}$$

$$\frac{\partial \boldsymbol{u}}{\partial T} + (\boldsymbol{u} \cdot \nabla)\boldsymbol{u} = -\frac{\nabla \rho^2}{\rho} + \nabla \left(2\frac{\nabla^2 \sqrt{\rho}}{\sqrt{\rho}} \right). \tag{1.11}$$

So we see that by using the Madelung transformation the Gross-Pitaevskii equation reduces to (1.10), which is the standard continuity equation found in classical fluids [9], and to (1.11), which we can see from (1.3) is identical to the Euler equation, as $\rho^2 = p$, except here we have the compressible case (in other words $\nabla \cdot \boldsymbol{u} \neq 0$). We also notice the external field $\boldsymbol{g}$ has been replaced by a "quantum pressure" term, hence we can view these as quantum compressible Euler's equations, once length scales become large enough this term becomes negligible and the original Euler's equations are reached. This result, coupled with the derivation of the Biot-Savart from (1.9) shows that quantum vortices are equivalent to vortex filaments under the given conditions, and so these vortices correspond to a discrete weak solution to the quantum Euler's equations.

One particular aspect of quantum turbulence that we have neglected to mention thus far is the possibility of freely-decaying turbulence. Despite the fact that we are investigating superfluids where vortices should remain indefinitely, it has been shown that the turbulent effects present eventually decay to form a coherent BEC via the event of vortex annihillation [35]. This interesting phenomenon is observed by Nazarenko, who found the vortices scattering momentum as sound waves before eventually colliding with other vortices leading to annihilation. Understanding of the collisions can therefore possibly lead to a better understanding of quantum turbulence and BEC formation. Hence we endeavor to investigate these collisions more closely.

1.3 Point Vortex Analogy

With this in mind, we now move to the foundation of the current work, namely the titular "point vortex" model/system. Essentially, this particular system can be considered a model of 2-D turbulent plane flow, wherein vortex tubes in the flow are made up of infinitely thin line filaments perpendicular to the plane in question. The result of this is the two dimensional vortices being represented as an assembly of discrete points. The points are then all of identical infinitesimal width and so this model serves as an ideal starting point for analyzing the collisions made by quantum vortices discussed earlier. It must be noted however that whilst point vortex widths are infinitesimal, i.e. they are indefinitely small; quantum vortices do have a finite although extremely small width. Hence the point vortex model still is only an approximation of quantum vortices.

We see that the point vortex model is in some ways a combination of the previously mentioned turbulence approximation methods. Here straight vortex filaments are "sliced" by a perpendicular plane resulting in the point vortices already described. As such it is possible

to derive some basics about point vortices using the 3-D analogue. Firstly we note that as circulation around vortex filaments is constant, it must be true that circulation around point vortices is constant. We can also derive the velocity field associated with a single vortex using (1.7) to consider a field point perpendicular to a straight line vortex filament [36], this gives the velocity field of an isolated point vortex as:

$$u_\theta = \frac{\kappa}{2\pi r}, \quad u_r = 0, \quad u_z = 0. \tag{1.12}$$

Note that here velocity is expressed is cylindrical coordinates (r, θ, z) centered about the isolated vortex, where u_r is velocity in the radial direction, u_θ represents angular velocity, and u_z represents velocity of fluid in the z direction. We note that as $u_z = 0$ motion of fluid in a plane perpendicular to a straight vortex filament is confined to the same plane. We also note the angular velocity having finite value at every point in the plane, except for the limiting case where as $r \to 0$ the angular velocity becomes a singularity. Hence a fluid particle on the 2-D follows a circular orbit about the point vortex maintaining the same separation of r. Using (1.4) and the cylindrical coordinate form for ∇ [37] we can then find the vorticity distribution as the curl of the above:

$$\boldsymbol{\omega} = \nabla \times \boldsymbol{u} = \left[\left(\frac{1}{r}\frac{\partial u_z}{\partial \theta} - \frac{\partial u_\theta}{\partial z} \right), \left(\frac{\partial u_r}{\partial z} - \frac{\partial u_z}{\partial r} \right), \frac{1}{r}\left(\frac{\partial}{\partial r}(r u_\theta) - \frac{\partial u_r}{\partial \theta} \right) \right] = (0,0,0) \quad \text{for } r \neq 0. \tag{1.13}$$

Hence fluid is irrotational as $\boldsymbol{\omega} = 0$ at all points except for where $r = 0$, which is of zero measure. These correspond to the positions of the point vortices in question, where we have a singularity in the vorticity distribution due to the singularity found in the angular velocity u_θ.

We can also form the point vortex in question in terms of a Rankine vortex. The equations of motion for a fluid in the presence of a Rankine vortex is given [9]:

$$\boldsymbol{u}_\theta = \begin{cases} \frac{\kappa r}{2\pi R^2} & \text{if } r \leq R, \\ \frac{\kappa}{2\pi r} & \text{if } r > R, \end{cases} \tag{1.14}$$

$$\boldsymbol{u}_r = \boldsymbol{u}_z = 0, \tag{1.15}$$

where here we have R representing the radius of the isolated Rankine vortex in question. We observe in Fig. 1.4 the effect of having $R \to 0$, we see the velocity of the point vortex (1.12) being recovered.

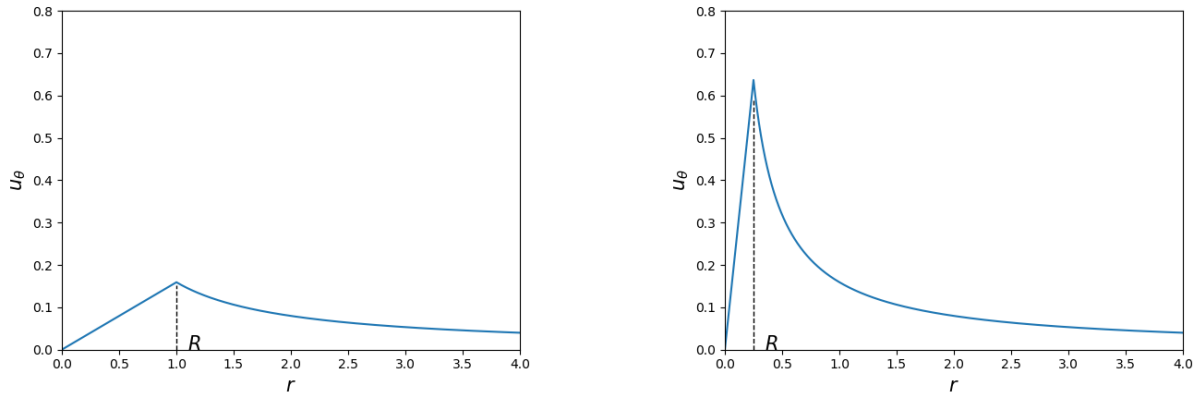

(a) R=1 (b) R=0.25

Figure 1.4: Plot of the angular velocity of fluid in the presence of a Rankine vortex with $\kappa = 1$ showing two cases of R.

We also see in Fig. 1.5 the effect on vorticity of having $R \to 0$, we observe that the vorticity approaches infinity at $R = 0$ hence the point vortex represents a singularity in the vorticity distribution.

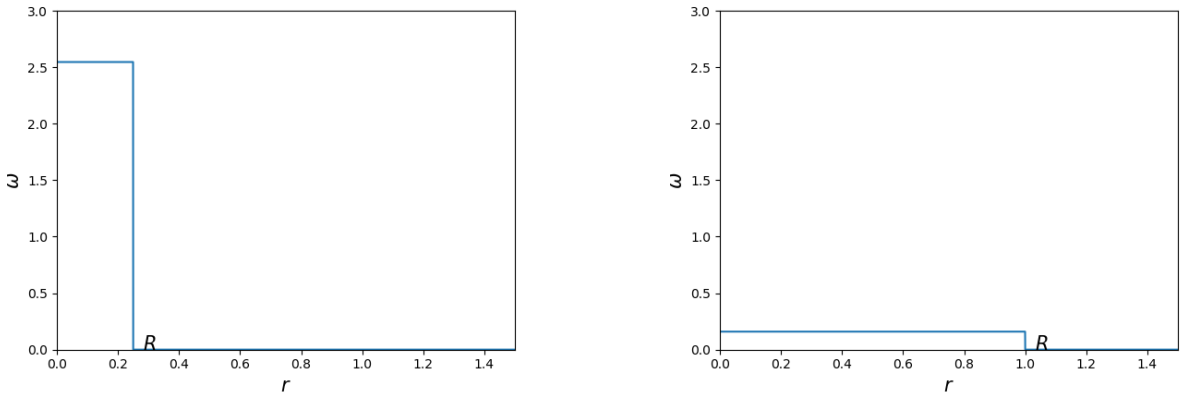

(a) R=1 (b) R=0.25

Figure 1.5: Plot of the vorticity of fluid in the presence of a Rankine vortex with $\kappa = 1$ showing two cases of R.

Therefore, by replacing a system of N ordinary vortices by N point vortices, we are essentially ignoring the structure of the underlying vorticity distribution in favor of easily approximating the regions of maximum vorticity, or in other words the vortex cores. It is therefore clear that this approximation is best used to model cases where vortex width is already extremely small, such as the case of quantum vortices, in order that point vortices remain faithful to original vortex dynamics as much as possible. We will now attempt to investigate the point vortex model more thoroughly.

Chapter 2

Point Vortex Model

2.1 Basic Theory

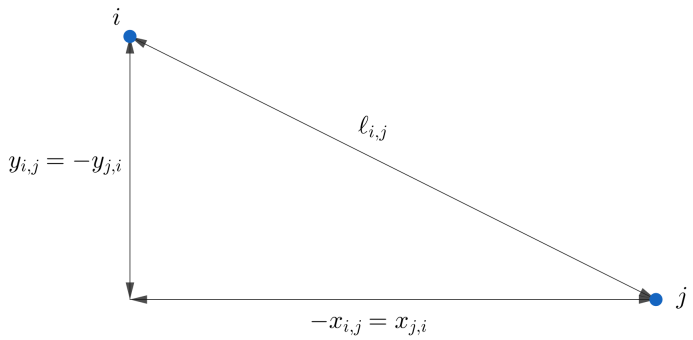

Figure 2.1: Diagram showing the fundamental vortex separations which the equations of motion are defined in terms of.

We can analyze the dynamics of the system using a Hamiltonian formulation (as done by Kirchhoff [38]). We start by expressing the equations of motion of the point vortex model. Here $\dot{x}_i$ represents the x velocity of vortex i and $\dot{y}_i$ represents the y velocity of vortex i as such:

$$\dot{x}_i = \frac{d}{dt} x_i(t),$$

where here (x_i, y_i) are the Cartesian x and y coordinates of vortex i and so on for other vortices $i = 1, 2, \ldots, N$ in the system. Note that from here we will use the shorthand $(x_i(t), y_i(t)) = (x_i, y_i)$.

$$\dot{x}_i = -\frac{1}{2\pi} \sum_j{}' \frac{\kappa_j y_{i,j}}{\ell_{i,j}^2}, \quad \dot{y}_i = \frac{1}{2\pi} \sum_j{}' \frac{\kappa_j x_{i,j}}{\ell_{i,j}^2}, \tag{2.1}$$

where here $x_{i,j} = x_i - x_j$, $y_{i,j} = y_i - y_j$, and with $\ell_{i,j}$ representing the length of the line segment spanning vortex i and vortex j, therefore:

$$\ell_{i,j}^2 = x_{i,j}^2 + y_{i,j}^2. \tag{2.2}$$

These quantities are displayed in Fig. 2.1. As according to standard Hamiltonian theory we derive the equations of motion from Hamilton's canonical equations [5]:

$$\kappa_i \dot{x}_i = \frac{\partial H}{\partial y_i}, \quad \kappa_i \dot{y}_i = -\frac{\partial H}{\partial x_i}. \tag{2.3}$$

With the Hamiltonian H given by:

$$H = -\frac{1}{4\pi} \sum_{i,j}^{N\prime} \kappa_i \kappa_j \ln(\ell_{i,j}), \tag{2.4}$$

where κ_i represents the circulation of vortex i. Note that here and throughout the remainder of this work we will use the shorthand sum notation given:

$$\sum_{\substack{j=1 \\ i \neq j}}^{N} \sum_{j=1}^{N} = \sum_{i,j}^{N\prime}.$$

It is clear that the above equations of motion are consistent with the Hamiltonian and canonical equations (note all proofs and justification from here are given in appendices, justification of above given in A.1). This then forms the point vortex system in full, so in order to solve the point vortex system we must solve the above equations of motion. It can be observed that the relative dynamics of a particular set up of vortices is the same irrespective of how they are oriented on the plane, i.e. we observe the same relative behavior regardless of translation or rotation of the system. We use Noether's theorem which states that symmetric properties of the Hamiltonian imply the existence of conserved quantities, where here we refer to Hamiltonian invariance under a transform as a symmetry. Hence according to Noether's theorem there exists three constants of motion in our system, linear momentum (in the x and y direction) and angular momentum are conserved [39]. These quantities are given as:

$$P = \sum_{i=1}^{N} \kappa_i x_i, \quad Q = \sum_{i=1}^{N} \kappa_i y_i, \quad M = \sum_{i=1}^{N} \kappa_i (x_i^2 + y_i^2). \tag{2.5}$$

We can combine these to form a conservation law that is only dependent upon the relative lengths between vortices as such:

$$R = \frac{1}{2} \sum_{i,j}^{N\prime} \kappa_i \kappa_j \ell_{i,j}^2 \equiv \left(\sum_{i=1}^{N} \kappa_i \right) M - P^2 - Q^2. \tag{2.6}$$

Note also we can define a point that is constant in the fluid, here referred to as the center of vorticity $\boldsymbol{x}_\Omega = (x_\Omega, y_\Omega)$, which can be thought of as the unique point in the flow that is the average of vortex positions weighted by the individual vortex circulations. It is easy to make analogies from this to the center of mass found in classical mechanics, as this is essentially the point vortex equivalent. We define the center of vorticity mathematically as such:

$$(x_\Omega, y_\Omega) = \frac{1}{\Omega}(P, Q). \tag{2.7}$$

where Ω is the total system circulation mathematically defined as: $\Omega = \sum_{i=1}^{N} \kappa_i$. Note that as both P, Q, and Ω are invariant with respect to time (as shown in A.2) the center of vorticity remains as a fixed point with respect to time.

Summarizing, the $N \geq 1$ point vortex dynamics is defined as a $2N$ dynamical system with four conserved quantities, the Hamiltonian and the integrals of motion above. This gives $2N-4$

degrees of freedom. Alternatively, it is possible to define the system in terms of relative motion of vortices, where we examine the vortex separations rather than absolute vortex positions. In this case the system is defined as an N dynamical system with two constants of motion, the Hamiltonian H and the combined integral of motion R. Thus such a system has $N-2$ degrees of freedom, hence whilst a system of $N=3$ vortices has one degree of freedom and so is integrable, whereas an assembly of vortices with $N>3$ generally is not [6], making the case $N=3$ of particular significance.

2.2 Numerical Code

In this section we detail the numerical methods used to solve the point vortex system. The importance of solving the system numerically is two-fold; firstly it allows us to cross examine our theoretical results to ensure reliability, second it gives a framework for solving systems comprising of more than three vortices, which is in general not possible to solve analytically as already stated. Technically, the point vortex model as described previously consists of a system of differential equations based on Hamilton's canonical equations and the conserved Hamiltonian H. This is essentially an initial value problem with the initial vortex coordinates as the initial conditions. It is then natural to assume that any standard algorithm for solving this kind of problem, such as a standard Runge-Kutta method of order 4, will suffice here. When running basic simulations on the point vortex equations using this method however we quickly find that the supposed conserved quantities actually do not remain constant with respect to time in the numerics. This is due to the phenemonon where dipole vortices being close together leads to faster dipole travel and so over a fixed time-step gives a greater error. Clearly we are in need of a more sophisticated method for solving the system.

In order to determine where the error lies we must first examine the Runge-Kutta family of algorithms in detail. To begin we briefly examine the widely known fourth order Runge-Kutta, or "RK4", method. The RK4 method and following theory is reproduced from Burden and Faires [40]. Given an ordinary differential equation and also initial value, beginning at time $t=a$ and ending at $t=b$:

$$\dot{y} = f(t,y), \quad y(a) = y_0, \quad a \leq t \leq b.$$

Note that in this case our f refers to the original equations of motion for the point vortex system, whereas the y in our case would be the original vortex positions. Here $y_i = y(t_i)$ is the unknown we wish to find. Using a step size $0 < h < 1$ such that $t_{i+1} = t_i + h$ we approximate y_{i+1} as:

$$y_{i+1} = y_i + \frac{h}{6}(k_1 + 2k_2 + 2k_3 + k_4),$$

with :

$$\begin{aligned}
k_1 &= f(t_i, y_i), \\
k_2 &= f(t_i + \frac{h}{2}, y_i + \frac{k_1}{2}), \\
k_3 &= f(t_i + \frac{h}{2}, y_i + \frac{k_2}{2}), \\
k_4 &= f(t_i + h, y_i + k_3).
\end{aligned}$$

Hence this basic Runge-Kutta method approximates y_{i+1} as the previous approximation y_i plus a weighted average of the increments k. We note the number of function calls involved in this process, i.e. the number of times it is necessary to evaluate function f at each point in time. Also, this particular Runge-Kutta method gives a local truncation error of $\mathcal{O}(h^4)$. The truncation error can be reduced by using a higher order Runge-Kutta method; however this has the effect of increasing the number of function calls required per time point whilst having little effect on conservation laws. We can also generalize the Runge-Kutta method to give order approximations. We give the arbitrary Runge-Kutta method of s stages as:

$$y_{n+1} = y_n + h \sum_{i=1}^{s} b_i k_i, \tag{2.8}$$

where

$$\begin{aligned} k_1 &= f(t_n, y_n), \\ k_2 &= f(t_n + c_2 h, y_n + h(a_{21} k_1)), \\ k_3 &= f(t_n + c_3 h, y_n + h(a_{31} k_1 + a_{32} k_2)), \\ &\vdots \\ k_s &= f(t_n + c_s h, y_n + h(a_{s1} k_1 + a_{s2} k_2 + \cdots + a_{s,s-1} k_{s-1})). \end{aligned} \tag{2.9}$$

In order to specify the particular Runge-Kutta method to be used one must provide the number of stages s, as well as the coefficients a_{ij} known as the Runge-Kutta matrix, the coefficients b_i known as the weights, and the coefficients c_i known as the nodes.

In general we note that approximations become more accurate as a higher order Runge-Kutta, and so a higher number of function calls, is used. This effect however becomes increasingly less prominent as $s > 5$, whereas the function calls continually increase resulting in a longer runtime as order increases. It is clear that in order to achieve a more accurate simulation we must either use a higher order system or reduce the step size to achieve a smaller error. However if h is reduced then we will then have an increased number of time points, in other words it will take longer to reach our endpoint $t = b$ and as such this will result in more iterations of the approximation step and so more function calls overall. Also as already discussed, by increasing the order of the system increases the amount of functions calls and so is also not an attractive option. We then need a procedure that will reduce error as much as possible such that integrals of motion are conserved, whilst at the same time not reducing the time step h, or considering Runge-Kutta methods of too high an order, unless absolutely necessary.

To solve this problem, we will introduce an adaptive time-stepping scheme. Essentially we will first execute a Runge-Kutta method of order 4 to attain a first approximation we will denote z_{i+1}, we will then apply a more accurate Runge-Kutta method of order 5 also. We will then allow this fifth order solution to be our approximation of the next time point i.e. y_{i+1}. The purpose of calculating both fourth and fifth order approximations is that it allows us to calculate an error term $|y_{i+1} - z_{i+1}|$, this represents the error of the fourth order approximation with respect to the next time point approximation y_{i+1}. Now using this error term we can adjust the step size h such that the error is below a certain threshold, such that error is kept as low as possible and that invariants are hopefully conserved. Specifically we are employing coefficients from the so called "Dormand-Prince" or "RK5(4)7M" method, introduced previously by Dormand and Prince [41]. The coefficients in this method are chosen especially to ensure highest accuracy in the fifth order approximation. Next we must decide how to adjust our time step according to

the error. We will implement the commonly used local elementary controller [42]:

$$h_{i+1} = h_i \left(\frac{\epsilon}{|y_{i+1} - z_{i+1}|} \right)^{\frac{1}{5}}, \tag{2.10}$$

where ϵ is a user defined error tolerance; the larger the value of ϵ, the larger the new step size h_{i+1} will be. We now have a complete method for solving the system of point vortices numerically, where error is as small as possible.

We give the coefficients to the Dormand-Prince method in the form of a Butcher tableau, a commonly used method for displaying the coefficients used in a Runge-Kutta family method. The Butcher tableau expresses the coefficients for a Runge-Kutta method with s stages as such:

0					
c_2	a_{21}				
c_3	a_{31}	a_{32}			
$\vdots$	$\vdots$		$\ddots$		
c_s	a_{s1}	a_{s2}	$\dots$	$a_{s,s-1}$	
	b_{11}	b_{12}	$\dots$	$b_{1,s-1}$	$b_{1,s}$
	b_{21}	b_{22}	$\dots$	$b_{2,s-1}$	$b_{2,s}$

Table 2.1: Basic Butcher tableau showing a Runge-Kutta method of arbitrary order.

With a_{ij}, b_i, c_i corresponding to the coefficients already shown in (2.8) and (2.9). We then express our Dormand-Prince method as:

0								
$\frac{1}{5}$	$\frac{1}{5}$							
$\frac{3}{10}$	$\frac{3}{40}$	$\frac{9}{40}$						
$\frac{4}{5}$	$\frac{44}{45}$	$-\frac{56}{15}$	$\frac{32}{9}$					
$\frac{8}{9}$	$\frac{19372}{6561}$	$-\frac{25360}{2187}$	$\frac{64448}{6561}$	$-\frac{212}{729}$				
1	$\frac{9017}{3168}$	$-\frac{355}{33}$	$\frac{46732}{5247}$	$\frac{49}{176}$	$-\frac{5103}{18656}$			
1	$\frac{35}{384}$	0	$\frac{500}{1113}$	$\frac{125}{192}$	$-\frac{2187}{6784}$	$\frac{11}{84}$		
	$\frac{35}{384}$	0	$\frac{500}{1113}$	$\frac{125}{192}$	$-\frac{2187}{6784}$	$\frac{11}{84}$	0	4th order
	$\frac{5179}{57600}$	0	$\frac{7571}{16695}$	$\frac{393}{640}$	$-\frac{92097}{339200}$	$\frac{187}{2100}$	$\frac{1}{40}$	5th order

Table 2.2: Butcher tableau showing the coefficients of the Dormand-Prince method.

The absolute difference between approximations give the error of the fourth order approximation as discussed previously.

To briefly summarize our numerical method, we express the coordinates of a particular vortex system in terms of the position vector $\boldsymbol{x}_i = (x_i, y_i)$. In order to solve a given system we apply the Dormand-Prince adaptive time-step method to each $\dot{x}_i$ and $\dot{y}_i$, to then approximate both x_i and y_i values at the next time point until the time end point $t = b$ is reached. Note here we use the arbitrary formulation $\dot{\boldsymbol{x}} = f(t, \boldsymbol{x})$ with $a \leq t \leq b$ and initial condition $y(t = a) = \alpha$. Coefficients are as given in the Butcher tableau in the previous section. The pseudocode for the Dormand-Prince method is given:

set a, b
set h
set h_{min}
set h_{max}
set ϵ
set vector $\boldsymbol{x}$
set vector t
$t_0 = a$
$y_0 = \alpha$
function $f(t, \boldsymbol{x})$
    return $\dot{\boldsymbol{x}}(t, \boldsymbol{x})$
end function
function CONTROLLER(i, E)
    $h = h\left(\frac{\epsilon}{E}\right)^{\frac{1}{5}}$
    if $h < h_{min}$ **then**
        $h = h_{min}$
    end if
    if $h > h_{max}$ **then**
        $h = h_{max}$
    end if

end function
function APPROXIMATE(i)
$k_1 = hf(t_i, \boldsymbol{x}_i)$
$k_2 = hf(t_i + c_2 h, \boldsymbol{x}_i + a_{21}k_1)$
$k_3 = hf(t_i + c_3 h, \boldsymbol{x}_i + a_{31}k_1 + a_{32}k_2)$
$\vdots$
$k_7 = hf(t_i + h, \boldsymbol{x}_i + a_{71}k_1 + a_{73}k_3 + a_{74}k_4 - a_{75}k_5 + a_{76}k_6)$
$RK4 = \boldsymbol{x}_i + b_{11}k_1 + b_{13}k_3 + b_{14}k_4 - b_{15}k_5 + b_{16}k_6$
$\boldsymbol{x}_{i+1} = \boldsymbol{x}_i + b_{21}k_1 + b_{23}k_3 + b_{24}k_4 - b_{25}k_5 + b_{26}k_6 + b_{27}k_7$
Controller(i, $|\boldsymbol{x}_{i+1} - RK4|$)
end function
$i = 0$
while $t_i < b$ **do**
Approximate(i)
$t_{i+1} = t_i + h$
$i = i + 1$
end while

This forms the complete numerical method we will use to solve the system.

2.3 Diagnostics: Evolution in the Two Vortex Case

Here we will consider the most basic non-trivial cases of vortex motion both theoretically and numerically in order to determine the reliability of our numerical method. We examine the case of two identical vortices in close proximity and the case of vortex and anti-vortex in close proximity.

2.3.1 Identical Vortex Evolution

First we examine the case of identical vortices in close proximity. By basic calculation we can determine velocity of each vortex in the identical vortex case. We start with two point vortices with Cartesian coordinates of vortex 1 at $(0, 0.4)$ and vortex 2 at $(0, -0.4)$ and with circulations $\kappa_1 = \kappa_2 = 1$. We calculate the velocity of each vortex by hand using (2.3) as:

$$\begin{aligned}
\dot{x}_1 &= -\frac{1}{2\pi}\frac{\kappa y_{1,2}}{\ell_{i,j}^2} = -0.19894, \\
\dot{x}_2 &= -\frac{1}{2\pi}\frac{\kappa y_{2,1}}{\ell_{1,2}^2} = 0.19894, \\
\dot{y}_1 &= \frac{1}{2\pi}\frac{\kappa x_{1,2}}{\ell_{1,2}^2} = 0, \\
\dot{y}_2 &= \frac{1}{2\pi}\frac{\kappa x_{2,1}}{\ell_{1,2}^2} = 0.
\end{aligned}$$

Each vortex in the system exerts an initial impulse upon the other giving each vortex a certain x velocity but with zero velocity in the y direction, due to starting the system with $x_1 = x_2 = 0$, however once we pass the initial time point vortex separation in the x direction $x_{ij} \neq 0$, implying each vortex will now have velocity in the y direction due to (2.3). Also it is clear from these basic calculations that $\dot{x}_1 = -\dot{x}_2$ and $\dot{y}_1 = -\dot{y}_2$ throughout the entire system. Using the length formula (2.2) we can say that:

$$
\begin{aligned}
\ell_{1,2}^2 &= (x_1 - x_2)^2 + (y_1 - y_2)^2 \\
\implies \frac{d}{dt}\ell_{1,2}^2 &= 2(x_1 - x_2)(\dot{x}_1 - \dot{x}_2) + 2(y_1 - y_2)(\dot{y}_1 - \dot{y}_2) \\
&= 2(x_1 - x_2)(-\frac{1}{2\pi}\frac{\kappa y_{1,2}}{\ell_{i,j}^2} + \frac{1}{2\pi}\frac{\kappa y_{2,1}}{\ell_{i,j}^2}) + 2(y_1 - y_2)(\frac{1}{2\pi}\frac{\kappa x_{1,2}}{\ell_{1,2}^2} - \frac{1}{2\pi}\frac{\kappa x_{2,1}}{\ell_{1,2}^2}) \\
&= \frac{\kappa}{\pi\ell_{1,2}^2}(-2x_{1,2}y_{1,2} + 2y_{1,2}x_{1,2}) = 0 \\
\implies \ell_{1,2}^2 = 0 &\implies \ell_{1,2} = 0
\end{aligned}
$$

Hence the length between vortices remain constant, noting the individual vortex velocities this implies that vortices in such a formation rotate counter-clockwise around the center of vorticity $(0, 0)$ with constant radius $\ell_{1,2} = 0.8$. We can also deduce the angular velocity of the system by first defining the polar angle and radius as:

$$
\begin{aligned}
\phi_i &= \arctan\left(\frac{y_i}{x_i}\right) \\
r_i^2 &= x_i^2 + y_i^2
\end{aligned}
$$

We see that:

$$
\begin{aligned}
\dot{\phi}_i &= \frac{\dot{y}_i x_i - \dot{x}_i y_i}{x_i^2 + y_i^2} \\
\implies \dot{\phi}_1 &= \dot{\phi}_2 = 0.12433 \\
\frac{d}{dt}r &= \frac{\dot{x}_i x_i + \dot{y}_i y_i}{r_i} \\
\implies \dot{r}_1 &= \dot{r}_2 = 0
\end{aligned}
$$

Hence we have the same angular velocity for both vortices so we can characterize the angular velocity of the entire rotation as $\dot{\phi} = 0.12433$. To check our numerical method we run a simulation with these starting coordinates and circulations and plot the results at each time point to achieve a trace of the motion (note that the light blue colors indicate vortex positions near the beginning of the simulation whilst the colour represents vortex positions towards the end).

The motion of the system in this case is shown in the Fig. 2.2:

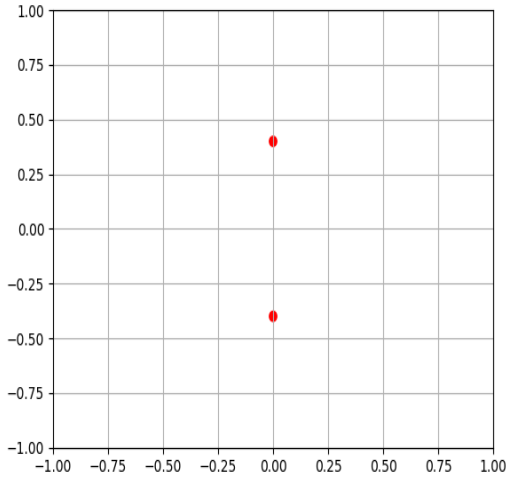

(a) Vortices at $t = 0$

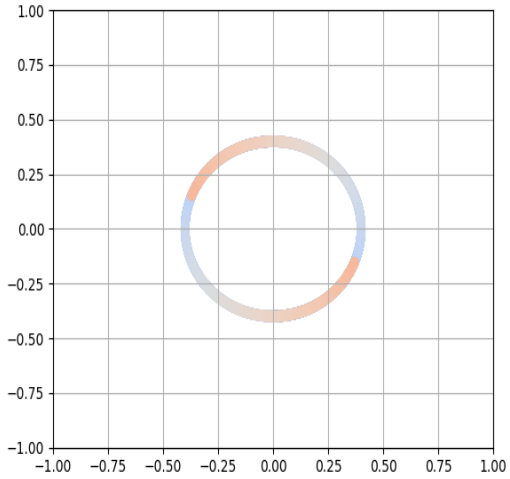

(b) Vortex motion trace

Figure 2.2: Demonstration of motion in the identical vortex case.

As we see the numerical results agree with our theoretical predictions. We also plot the velocity of our vortices as such:

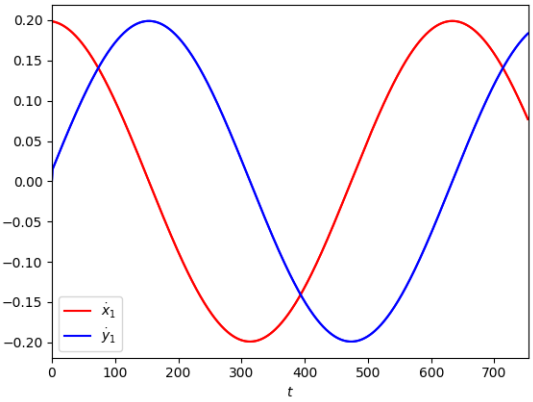

(a) Velocities of the first vortex

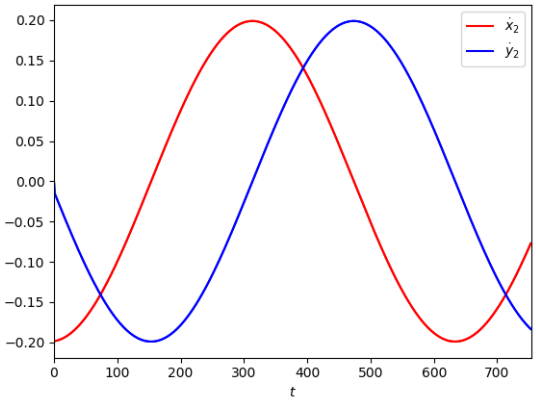

(b) Velocities of the second vortex

Figure 2.3: Velocities of each vortex in the identical vortex case.

We can also solve for the conserved quantities to make sure they agree with the numerics. We find the Hamiltonian and momentums to be:

$$
\begin{aligned}
H &= -\frac{2\ln(0.8)}{4\pi} = 0.035514 \\
P &= 0 \\
Q &= 0 \\
M &= 0.32
\end{aligned}
$$

We then solve for the conserved quantities numerically and plot:

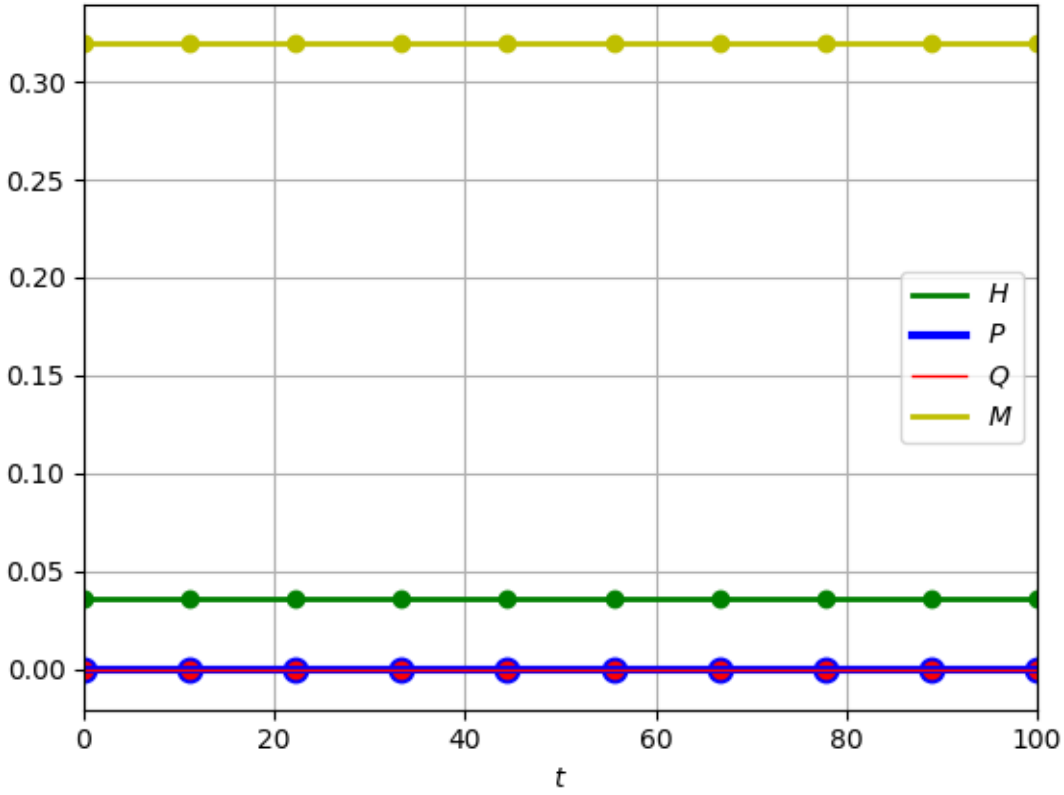

Figure 2.4: Plot of the four conserved quantities in the identical vortex case.

We represent theoretical predictions as solid lines, and the results from the numerical simulations as points. We can see in Fig. 2.4 numerically the momenta and Hamiltonian are in agreement with our theoretical predictions and are also conserved.

2.3.2 Vortex/Anti-vortex Evolution

We repeat the same process for the vortex/anti-vortex pair, this particular set up is of critical importance so from here on we will refer to this as a "dipole". Starting coordinates remain the same, but the vortex at $(0, -0.4)$ now is replaced by the anti-vortex, i.e. circulation of this vortex is $-\kappa$. We find velocities at the starting point to be:

$$\begin{aligned}\dot{x}_1 &= 0.19894\\ \dot{x}_2 &= 0.19894\\ \dot{y}_1 &= 0\\ \dot{y}_2 &= 0\end{aligned}$$

Hence we have similar results to the previous case, except here $\dot{x}_1 = \dot{x}_2$, so after the initial time point there will still be a separation of 0 in the x direction, so therefore from (2.1) there will still be no velocity in the y direction after the initial time point. We examine the length derivative as before:

$$\begin{aligned}\frac{d}{dt}\ell_{1,2}^2 &= 2(x_1 - x_2)(\dot{x}_1 - \dot{x}_2) + 2(y_1 - y_2)(\dot{y}_1 - \dot{y}_2) \\ &= \frac{x_{1,2}}{\pi\ell_{1,2}^2}(y_{1,2} - y_{1,2}) + \frac{y_{1,2}}{\pi\ell_{1,2}^2}(x_{1,2} - x_{1,2}) = 0\end{aligned}$$

So again we have a constant separation between the vortices in time. As both vortices are moving with the same x velocity, a constant separation length, and a y velocity of zero we conclude that the dipole must propagate off to infinity following a trajectory parallel to the perpendicular bisector of the vortex points. We verify this in a numerical plot as before in Fig. 2.5:

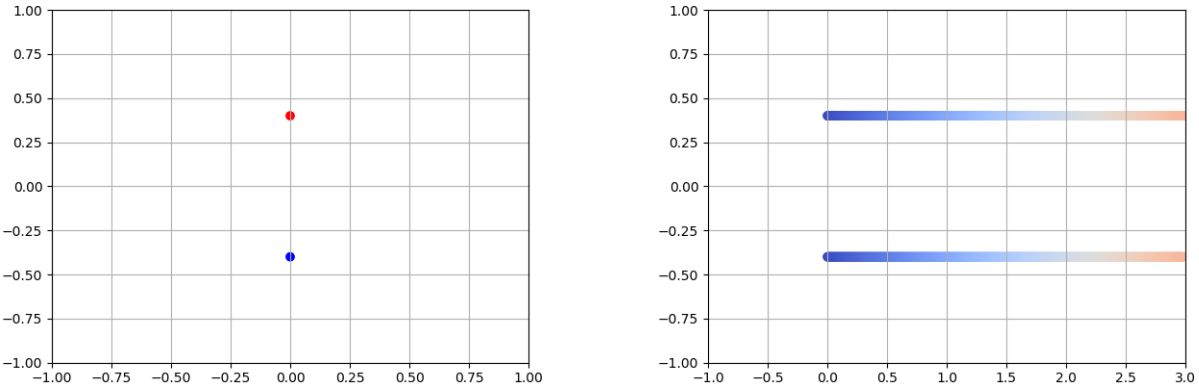

(a) Vortices $t = 0$

(b) Vortex motion trace

Figure 2.5: Demonstration of motion in the dipole case.

where here the red point represents an ordinary vortex with $\kappa = 1$ and the blue point represents the anti-vortex with $\kappa = -1$. Note that here we find the velocity is constant as predicted:

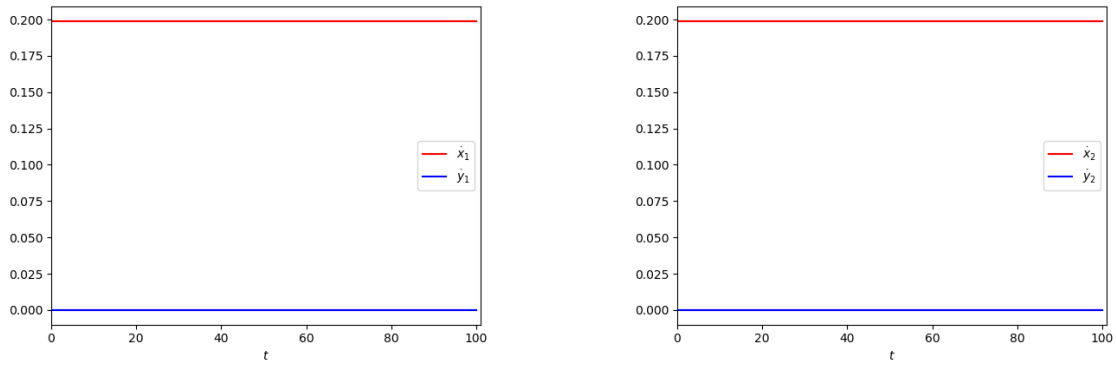

(a) Velocity of the first vortex

(b) Velocity of the second vortex

Figure 2.6: Velocities of each vortex in the dipole case.

We find conserved quantities in the dipole case to be:

$$H = \frac{2\ln(0.8)}{4\pi} = -0.035514$$
$$P = 0$$
$$Q = 0.8$$
$$M = 0$$

We again plot these quantities numerically to find:

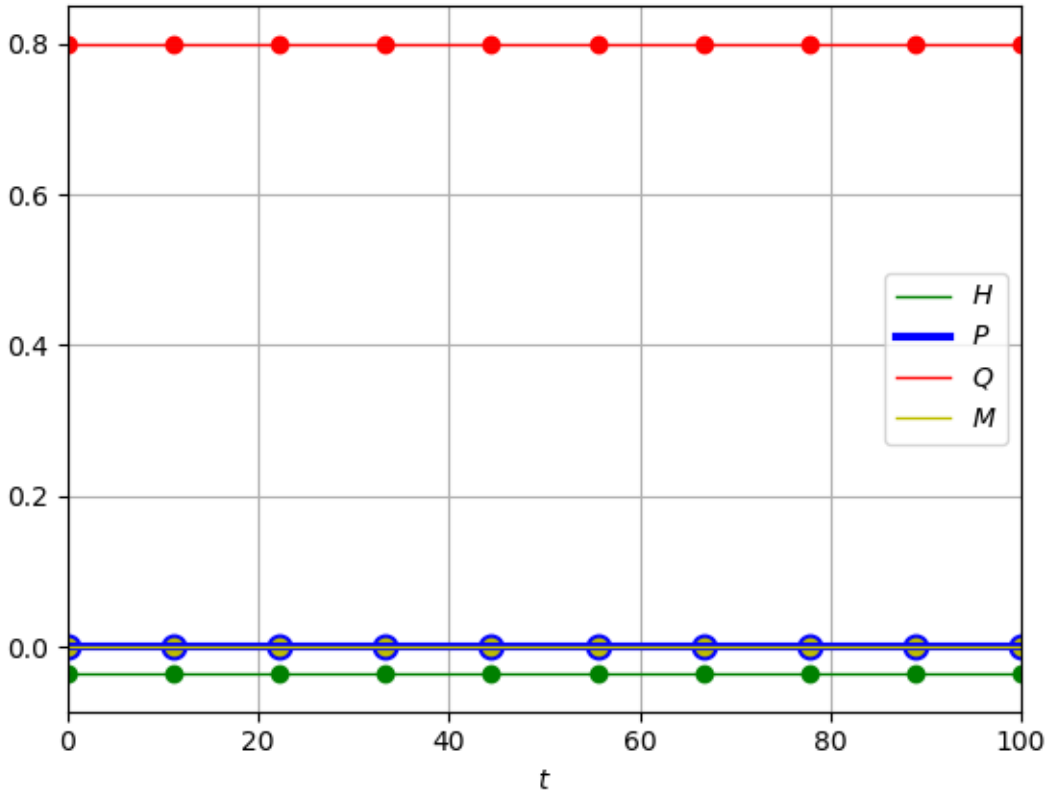

Figure 2.7: Plot of the conserved quantities with respect to time in the dipole case.

As before we see that vortex trajectories and conserved quantities of the system found numerically are in agreement with our theoretical predictions. Hence we can ensure the reliability of our numerical method, which we will now use to analyze more interesting vortex schemes.

Chapter 3

Three Vortex Scattering

3.1 Problem Statement

Here we will examine the three vortex case in detail. Specifically, we analyze the case of three vortices with circulations $\kappa_1 = \kappa_2 = 1$ and $\kappa_3 = -1$, where all vortices have equal circulation but one vortex circulation will be negative thus imparting a negative vorticity. To understand our chosen problem properly we must first refer back to the case of two vortices in close proximity. There are thus two possibilities of two vortex interaction, depending on whether we have two identical vortices, e.g. $\kappa_1 = 1$, $\kappa_2 = 1$. The other possibility is where we have a vortex and a so called "anti-vortex" in close proximity, e.g. $\kappa_1 = 1$, $\kappa_2 = -1$. The behavior of the two vortex system depends upon the velocity each vortex imparts upon the other which is a consequence of the circulation of each vortex. Hence the motion of the system is decided, in this case, on whether $\kappa_2 = 1$ or $\kappa_2 = -1$. Note that in the case where we have two identical vortices we have constant rotation about the central point, equivalent to the center of vorticity.

It is noteworthy that in the case of $\kappa_1 = 1, \kappa_2 = -1$ we have $\Omega = 0$ which implies that the center of vorticity is undefined in this case. As seen previously there is no rotation in this particular example, instead due to the vorticity each vortex imparts on the other the given dipole propagates off to infinity along the straight line trajectory perpendicular to the dipole bisector. This simple example forms the basis for the main problem which will be solved in this chapter. The natural extension for the dipole case is what will from here be referred to as the dipole-vortex collision. What this system entails is a dipole, such as the one encountered already, propagating into a collision with a stationary vortex. After collision the dipole will be deflected in some way, it is this collision and deflection which will be analyzed in this section. Such a collision is extremely interesting as in BECs it is the most basic collision which can lead to annihilation, and so understanding of these collisions may then help to better understand this phenomenon (even though no mechanism for vortex annihilation exists in the point vortex system, as this would represent two vortices occupying the same point in space, in which case the equations of motion of the system would be undefined).

This particular vortex interaction was first considered by Aref [5], from which the work in this section is partly inspired by. Here Aref considers the three vortex case in general, constructing a phase point analysis of each possible vortex set up in the three vortex case. Specifically the problem that this section addresses is contained in the appendix of Aref's work, where Aref calculates the angle of deflection (which we will refer to as the scattering angle) and also notes a region of periodic motion which is not relevant to us for reasons to be discussed later. It is interesting that basic numerics give differing results from Aref in certain regions, it will be interesting to verify and attempt to extend Aref's work.

We setup the problem as depicted in Fig. 3.1, here $L \in \mathbb{R}$ represents the x distance between the dipole and the stationary vortex, $d \in \mathbb{R}$ represents the distance between the dipole vortices,

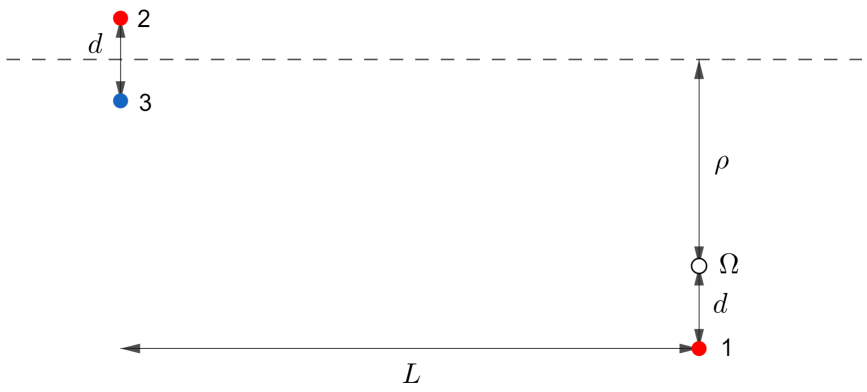

Figure 3.1: A simple diagram displaying the initial conditions of the dipole-vortex system.

and $\rho \in \mathbb{R}$ is our impact parameter, defined as the y distance between the midpoint of the dipole and the center of vorticity, here simply denoted as Ω. Note that the impact parameter has the possibility of being negative, representing the case that the midpoint of the dipole is below the center of vorticity. We also number the vortices as such.

As discussed we have that $\kappa_1 = \kappa_2 = 1$ and that $\kappa_3 = -1$. The circulation of each vortex is represented as the color of each point (red represents $\kappa = 1$, blue represents $\kappa = -1$). Here we setup the problem such that $L \gg d$ and $L \gg \rho$ at $t = 0$ to ensure the dipole has sufficient time to propagate as a dipole before being affected by the circulation of vortex 1, so a "true" collision is ensured. We then wish to analyze the different scattering regimes that occur from varying these parameters. First, we can expect that in the case where $|\rho|$ becomes very large, the dipole will barely be affected by vortex 3. Thus the dipole will 'fly-by' vortex 3 perhaps being deflected by a certain angle. We will refer to this particular regime as direct scattering. Note that as we reduce $|\rho|$ the behavior of the system changes. We note that in this case the negative vortex 1 forms a new dipole with vortex 1 and then propagates off to infinity as part of the new dipole, leaving vortex 2 behind as the stationary vortex now.

We find that indeed, the scattering we observe is dependent upon the values of ρ and d. In the region of $0 < \rho/d < 9/2$ we observe the regime of exchange scattering in this case. Whereas in the case of $\rho/d > 9/2$ or where $\rho/d < 0 \implies \rho < 0$ as expected we find the case of direct scattering. We also observe interesting behavior in the case where our combined parameter ρ/d gives the critical boundary values, i.e. $\rho/d = 0$ or $\rho/d = 9/2$. Here we find the three vortices form an equilateral triangle, with sides of fixed length, rotating about the center of vorticity $\mathbf{x}_\Omega = (0, 0)$ as a rigid-body. This rotation is analogous to the rotation of two identical vortices. In the case of two identical vortices with a distance of s between them we have rotation with angular frequency $(\kappa_1 + \kappa_2)/2\pi s^2$ where s is the distance between vortices (in our case the frequency gives $1/\pi s^2$). In the rigid-body rotation we an angular frequency of $(\kappa_1 + \kappa_2 + \kappa_3)2\pi s^2$ where here s becomes the triangle side length [5] (in our case frequency is $1/2\pi d^2$). Animations that illustrate each scattering regime can be found at [43].

3.2 Analysis

We begin analysis of the dipole-vortex collision with the critical step mentioned previously. Namely, we must be able to analyze the relative motion of the vortices, thus reducing the degrees of freedom to one when we consider the constants of motion H and R (as discussed before). It is possible to find the equations of motion for the relative lengths of the vortices

as such. Note here that as $\ell_{i,j} = \sqrt{x_{i,j}^2 + y_{i,j}^2}$ it is in fact easier to derive the length derivative by examining $\ell_{i,j}^2$ instead, due to the lack of the square root. Note here we use the same sum notation used previously, where the double prime in the summation represents a sum over k with exclusion of terms $k = i$ and $k = j$. Here $A_{i,j,k}$ is the area of the triangle spanned by vortices i, j and k. Also we define $\sigma_{i,j,k}$ with respect to said triangle such that:

$$\sigma_{i,j,k} = \begin{cases} -1 & \text{if } (i,j,k) \text{ appear clockwise,} \\ 1 & \text{if } (i,j,k) \text{ appear anti-clockwise.} \end{cases}$$

We find that the relative length derivative between vortex i and j can be expressed as:

$$\frac{d}{dt}\ell_{i,j}^2 = \frac{2}{\pi}\sum_{k}^{N}{}'' \kappa_k \sigma_{i,j,k} A_{i,j,k} \left(\frac{1}{\ell_{j,k}^2} - \frac{1}{\ell_{i,k}^2} \right), \tag{3.1}$$

where we use the sum notation:

$$\sum_{k}^{N}{}'' = \sum_{\substack{k=1 \\ k\neq i \\ k\neq j}}.$$

Hence we have the time derivative of $\ell_{i,j}^2$, detailed justification of this result can be found in A.3. It is important to realize that as:

$$\frac{d}{dt}(\ell_{i,j})^2 = 2\ell_{i,j}\frac{d}{dt}\ell_{i,j},$$

Our derivative shares the same characteristics as $\dot{\ell}_{i,j}$ as we have:

$$\frac{d}{dt}(\ell_{i,j})^2 = 0 \implies 2\ell_{i,j}\frac{d}{dt}\ell_{i,j} = 0 \implies \frac{d}{dt}\ell_{i,j} = 0 \text{ or } \ell_{i,j} = 0.$$

Hence as it is impossible for two vortices to occupy the same point, i.e. for $\ell_{i,j} = 0$, we must have that $\frac{d}{dt}(\ell_{i,j})^2 = 0 \implies \frac{d}{dt}\ell_{i,j} = 0$. Note that this equation for relative motion holds for any value of N, hence relative motion of the N vortex case is dependent upon the three vortex triangle structures such as we are studying (as each term of the sum involves a three vortex triangle), so understanding of three vortex dynamics is fundamental for understanding dynamics for systems with larger N. We write the relative motion equations for our three vortex case explicitly as:

$$\begin{aligned} \frac{d}{dt}(\ell_{1,2})^2 &= -\frac{2}{\pi}\sigma_{1,2,3}A_{1,2,3}\left(\frac{1}{\ell_{2,3}^2} - \frac{1}{\ell_{1,3}^2}\right), \\ \frac{d}{dt}(\ell_{1,3})^2 &= \frac{2}{\pi}\sigma_{1,3,2}A_{1,3,2}\left(\frac{1}{\ell_{3,2}^2} - \frac{1}{\ell_{1,2}^2}\right), \\ \frac{d}{dt}(\ell_{2,3})^2 &= \frac{2}{\pi}\sigma_{2,3,1}A_{2,3,1}\left(\frac{1}{\ell_{3,1}^2} - \frac{1}{\ell_{2,1}^2}\right). \end{aligned} \tag{3.2}$$

It is easy to see from this formulation where each length derivative gives zero, this will become useful later. For now we will note the conditions that require $\frac{d}{dt}\ell_{i,j} = 0$. It is easy to see that each $\frac{d}{dt}\ell_{i,j}$ can only equal 0 if either $A_{i,j,k} = 0$, i.e. the area of the triangle spanning

them is 0, implying that vortices are collinear. The only other possibility is if $\frac{1}{\ell_{j,k}^2} - \frac{1}{\ell_{i,k}^2} = 0 \implies \ell_{i,k} = \ell_{j,k}$, i.e. the vortices form an isosceles triangle. Therefore $\frac{d}{dt}\ell_{i,j} = 0$ if:

$$A_{i,j,k} = 0, \text{ or } \ell_{i,k} = \ell_{j,k}. \tag{3.3}$$

We know for a fact that the relative lengths are at minimum at this point simply by visualizing what each situation entails. In a regime of direct scattering for example, we picture the dipole passing the lone vortex relatively unperturbed in its path, essentially stating that the dipole will either pass vortex 1 from above or below and will continue its path whilst being deflected at some angle. It is during this passing that our dipole is either directly above or directly below the lone vortex and so all vortices are directly above each other on the same line; this collinear state gives a triangle area of 0, whereupon our dipole then propagates off to infinity. Therefore we know that this point is a minimum point. Similar logic results in the other case being classed as a minimum.

3.3 Critical Lengths

We first seek to determine the vortex separations of the system at the point in time that a critical point occurs. We will first define a point in time at which the critical interaction occurs. Then by using (3.2) and our conserved quantities we can find the lengths between vortices at this critical point, which we refer to as our "critical lengths", from here on notated as $\ell_{i,j}^*$. We will first define this critical point as the point at which our two positive vortices are closest i.e. the point at which $\ell_{1,2}$ is at minimum. To derive the critical lengths we note that by definition at this point $\ell_{1,2}$ is at minimum, now due to the conserved quantities (2.4) and (2.6) we derived, we can then solve at this point for the values $\ell_{1,3}$ and $\ell_{2,3}$. Indeed, as $\ell_{1,2}$ is at minimum at scattering then the time derivative of this quantity disappears at this point i.e.:

$$\frac{d}{dt}\ell_{1,2} = 0 \text{ at } \ell_{1,2} = \ell_{1,2}^*,$$

Therefore from (3.2) we have:

$$-\frac{2}{\pi}\sigma_{1,2,3}A\left(\frac{1}{\ell_{2,3}^2} - \frac{1}{\ell_{1,3}^2}\right) = 0. \tag{3.4}$$

This gives the following possible relations between critical lengths, note that the specific relation we obtain is dependent upon whether we have the case where $\rho/d < 0$, $0 < \rho/d < 9/2$ or $9/2 < \rho/d$:

$$\ell_{1,3}^* = \ell_{2,3}^*, \quad \ell_{1,3}^* = \ell_{1,2}^* + \ell_{2,3}^* \text{ or } \ell_{1,2}^* = \ell_{1,3}^* + \ell_{2,3}^*. \tag{3.5}$$

As already stated the first equality corresponds to the case of exchange scattering whereas the latter two correspond to direct scattering, with the particular equality chosen dependent upon whether we are in the region $\rho/d < 0$ or $\rho/d > 9/2$. Now consider the two conserved quantities below:

$$\tilde{H} \equiv e^{-2\pi H} = \frac{\ell_{1,2}}{\ell_{1,3}\ell_{2,3}}, \tag{3.6}$$

note that as this is derived from the conserved quantity (2.4) this quantity is also conserved with respect to time. Also:

$$R = \ell_{1,2}^2 - \ell_{1,3}^2 - \ell_{2,3}^2. \tag{3.7}$$

Using these integrals of motion with the constraints (3.5) we can solve for the critical lengths in each case. Note that we can express the vortex lengths $\ell_{i,j}$ in terms of the initial conditions using our parameters $\rho, d,$ and L as such:

$$\begin{aligned} \ell_{1,2} &= \sqrt{\left(\rho + \frac{3d}{2}\right)^2 + L^2}, \\ \ell_{1,3} &= \sqrt{\left(\rho + \frac{d}{2}\right)^2 + L^2}, \\ \ell_{2,3} &= d. \end{aligned} \tag{3.8}$$

So our conserved quantities can then be expressed as:

$$\tilde{H} = \frac{\sqrt{\left(\rho + \frac{3d}{2}\right)^2 + L^2}}{d\sqrt{\left(\rho + \frac{d}{2}\right)^2 + L^2}}, \tag{3.9}$$

$$R = 2\rho d + d^2. \tag{3.10}$$

3.3.1 $\ell^*_{i,j}$ in the region $0 < \frac{\rho}{d} < \frac{9}{2}$

We begin by examining the case of exchange scattering, i.e. we solve for the critical lengths in the case that $0 < \rho/d < 9/2$. This implies that $\ell^*_{1,3} = \ell^*_{2,3} = \ell^*$, as shown in Fig.3.2:

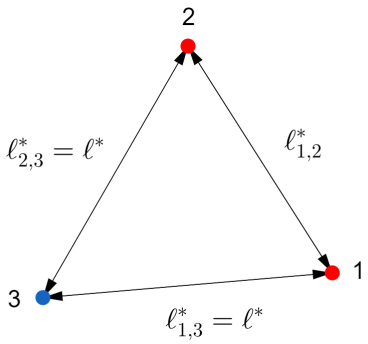

Figure 3.2: Diagram of an exchange scattering regime at the critical point, showing the relation we obtain between critical lengths.

Using the equality $\ell^*_{1,3} = \ell^*_{2,3}$ fact with (3.6) and (3.7) gives us the following system of equations:

$$\tilde{H} = \frac{\ell^*_{1,2}}{\ell^{*2}}, \tag{3.11}$$

$$R = \ell^{*2}_{1,2} - 2\ell^{*2}. \tag{3.12}$$

By solving the above system, and then expanding in terms of ρ/L and d/L using Mathematica, we have that [44]:

$$\ell^*_{1,2} = \frac{1}{\tilde{H}} + \sqrt{\frac{1}{\tilde{H}^2} + R} = d + \sqrt{2d(\rho+d)} + \mathcal{O}\left(\left(\frac{\rho}{L}\right)^2\right) + \mathcal{O}\left(\left(\frac{d}{L}\right)^2\right),$$

$$\ell^* = \sqrt{\frac{1}{\tilde{H}^2} + \frac{1}{\tilde{H}}\sqrt{\frac{1}{\tilde{H}^2} + R}} = \sqrt{d^2 + d\sqrt{2\rho d + d^2}} + \mathcal{O}\left(\left(\frac{\rho}{L}\right)^2\right) + \mathcal{O}\left(\left(\frac{d}{L}\right)^2\right).$$

3.3.2 $\ell^*_{i,j}$ in the region $\frac{\rho}{d} < 0$

Now we move to the case of direct scattering where $\rho/d < 0$. Here we note that the dipole will pass below the stationary vortex so geometrically we reason that at scattering we have the constraint $\ell^*_{1,3} = \ell^*_{1,2} + \ell^*_{2,3}$ as shown in Fig. 3.3:

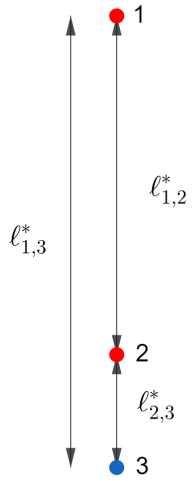

Figure 3.3: Diagram of a direct scattering regime at the critical point with the dipole passing below the stationary vortex.

Using this to solve the system of equations formed from the constraints as before we find the critical lengths in this case are:

$$\ell^*_{1,2} = -\frac{R\tilde{H}}{2} = -\frac{2\rho + d}{2} + \mathcal{O}\left(\left(\frac{\rho}{L}\right)^2\right) + \mathcal{O}\left(\left(\frac{d}{L}\right)^2\right),$$

$$\ell^*_{2,3} = \frac{R\tilde{H}}{4} + \frac{1}{2}\sqrt{R\left(\frac{R\tilde{H}^2}{4} - 2\right)} = \frac{2\rho + d}{4} + \frac{1}{4}\sqrt{4\rho^2 - 7d^2 - 12\rho d} + \mathcal{O}\left(\left(\frac{\rho}{L}\right)^2\right) + \mathcal{O}\left(\left(\frac{d}{L}\right)^2\right),$$

$$\ell^*_{1,3} = -\frac{R\tilde{H}}{4} + \frac{1}{2}\sqrt{R\left(\frac{R\tilde{H}^2}{4} - 2\right)} = -\frac{2\rho + d}{4} + \frac{1}{4}\sqrt{4\rho^2 - 7d^2 - 12\rho d} + \mathcal{O}\left(\left(\frac{\rho}{L}\right)^2\right) + \mathcal{O}\left(\left(\frac{d}{L}\right)^2\right).$$

3.3.3 $\ell^*_{i,j}$ in the region $\frac{\rho}{d} > \frac{9}{2}$

Now we are left with the case where $\rho/d > 9/2$. This again is direct scattering with $\ell^*_{1,2} = \ell^*_{1,3} + \ell^*_{2,3}$ shown in Fig. 3.4:

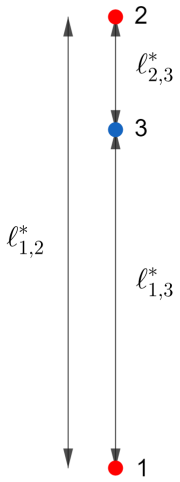

Figure 3.4: Diagram of a direct scattering regime at the critical point this time with the dipole passing above the stationary vortex.

Following the same process as in other cases we find that the critical lengths in this case are given by:

$$\ell^*_{1,2} = \frac{R\tilde{H}}{2} = \frac{2\rho+d}{2} + \mathcal{O}\left(\left(\frac{\rho}{L}\right)^2\right) + \mathcal{O}\left(\left(\frac{d}{L}\right)^2\right),$$

$$\ell^*_{1,3} = \frac{R\tilde{H} - \sqrt{R^2\tilde{H}^2 - 8R}}{4} = \frac{2\rho+d}{4} - \frac{1}{4}\sqrt{4\rho^2 - 12\rho d - 15d^2} + \mathcal{O}\left(\left(\frac{\rho}{L}\right)^2\right) + \mathcal{O}\left(\left(\frac{d}{L}\right)^2\right),$$

$$\ell^*_{2,3} = \ell^*_{1,2} - \ell^*_{1,3} = -\frac{2\rho+d}{4} + \frac{1}{4}\sqrt{4\rho^2 - 12\rho d - 15d^2} + \mathcal{O}\left(\left(\frac{\rho}{L}\right)^2\right) + \mathcal{O}\left(\left(\frac{d}{L}\right)^2\right).$$

Hence we can give the full critical lengths in Table 3.1, note that terms of order $(\rho/L)^2$ and $(d/L)^2$ are omitted.

	$\frac{\rho}{d} < \frac{9}{2}$	$0 < \frac{\rho}{d} < \frac{9}{2}$	$\frac{9}{2} < \frac{\rho}{d}$
$\ell^*_{1,2}$	$-\frac{2\rho+d}{2}$	$d + \sqrt{2d(\rho+d)}$	$\frac{2\rho+d}{2}$
$\ell^*_{1,3}$	$-\frac{2\rho+d}{4} + \frac{1}{4}\sqrt{4\rho^2 - 7d^2 - 12\rho d}$	$\sqrt{d^2 + d\sqrt{2\rho d + d^2}}$	$\frac{2\rho+d}{4} + \frac{1}{4}\sqrt{4\rho^2 - 12\rho d - 15d^2}$
$\ell^*_{2,3}$	$\frac{2\rho+d}{4} + \frac{1}{4}\sqrt{4\rho^2 - 7d^2 - 12\rho d}$	$\sqrt{d^2 + d\sqrt{2\rho d + d^2}}$	$-\frac{2\rho+d}{4} + \frac{1}{4}\sqrt{4\rho^2 - 12\rho d - 15d^2}$

Table 3.1: Complete critical lengths in each case.

3.4 Minimum Lengths

3.4.1 $\min_{\forall t\in\mathbb{R}} \ell_{i,j}$ in the region $\frac{\rho}{d} < 0$

We now turn our attention to the minimum lengths of the system. Which we will refer to here as $\min_{\forall t\in\mathbb{R}} \ell_{i,j}$. It is important to note that the minimum lengths of the system are not necessarily the same as the critical lengths of the system, rather we seek to find when each $\ell_{i,j}$ is at minimum over the entire system, although there may be some similarities. Firstly, in deriving this we note that by definition of the previous section the system critical point occurs when $\ell_{1,2}$ is at minimum, therefore the minimum length of this particular vortex separation will be the same as the critical length found in the previous section i.e. $\ell^*_{1,2} = \min_{\forall t\in\mathbb{R}} \ell_{1,2}$ so:

$$\min_{\forall t\in\mathbb{R}} \ell_{1,2} = \begin{cases} -\frac{2\rho+d}{2} + \mathcal{O}((\frac{\rho}{L})^2) + \mathcal{O}((\frac{d}{L})^2) & \text{if } \frac{\rho}{d} < 0, \\ d + \sqrt{2d(\rho+d)} + \mathcal{O}((\frac{\rho}{L})^2) + \mathcal{O}((\frac{d}{L})^2) & \text{if } 0 < \frac{\rho}{d} < \frac{9}{2}, \\ \frac{2\rho+d}{2} + \mathcal{O}((\frac{\rho}{L})^2) + \mathcal{O}((\frac{d}{L})^2) & \text{if } \frac{\rho}{d} > \frac{9}{2}. \end{cases}$$

Hence we only have to derive the minimum lengths of $\ell_{1,3}$ and $\ell_{2,3}$. First we consider the direct scattering case of $\rho/d < 0$. We note that in the case of direct scattering our dipole approaches the stationary vortex and propagates off relatively unperturbed. This implies that minimum lengths in this case occur in the critical region. For example, we reason that the minimum length of $\ell_{1,3}$ must occur at the critical point, as the dipole gets increasingly close to the stationary vortex, scatters, then propagates off to infinity. Therefore in this case the minimum length is again the same as the critical length. Mathematically $\ell^*_{1,3} = \min_{\forall t\in\mathbb{R}} \ell_{1,3}$ so we find:

$$\min_{\forall t\in\mathbb{R}} \ell_{1,3} = -\frac{2\rho+d}{4} + \frac{1}{4}\sqrt{4\rho^2 - 7d^2 - 12\rho d} + \mathcal{O}((\frac{\rho}{L})^2) + \mathcal{O}((\frac{d}{L})^2).$$

Now for the final minimum length in this case we observe an interesting phenomenon found in the critical lengths, we note that $\ell^*_{2,3} < d$, implying that the vortices become closer together than their initial separation. This implies that the effect of the stationary vortex at this point causes an "attraction" effect onto the positive vortex of our dipole, pulling the vortices together at scattering. After the scattering is complete the dipole will relax back to its original separation d. This implies that again the minimum length in this case is given by the critical length:

$$\min_{\forall t\in\mathbb{R}} \ell_{2,3} = \frac{R\tilde{H}}{4} + \frac{1}{2}\sqrt{R(\frac{R\tilde{H}^2}{4} - 2)} = \frac{2\rho+d}{4} + \frac{1}{4}\sqrt{4\rho^2 - 7d^2 - 12\rho d} + \mathcal{O}((\frac{\rho}{L})^2) + \mathcal{O}((\frac{d}{L})^2).$$

Hence all minimum lengths in the case of $\rho/d < 0$ are actually the same as the scattering lengths. We can justify the reasoning in this section by providing a trace plot of a sample vortex evolution similar to the traces produced in Chapter 2:

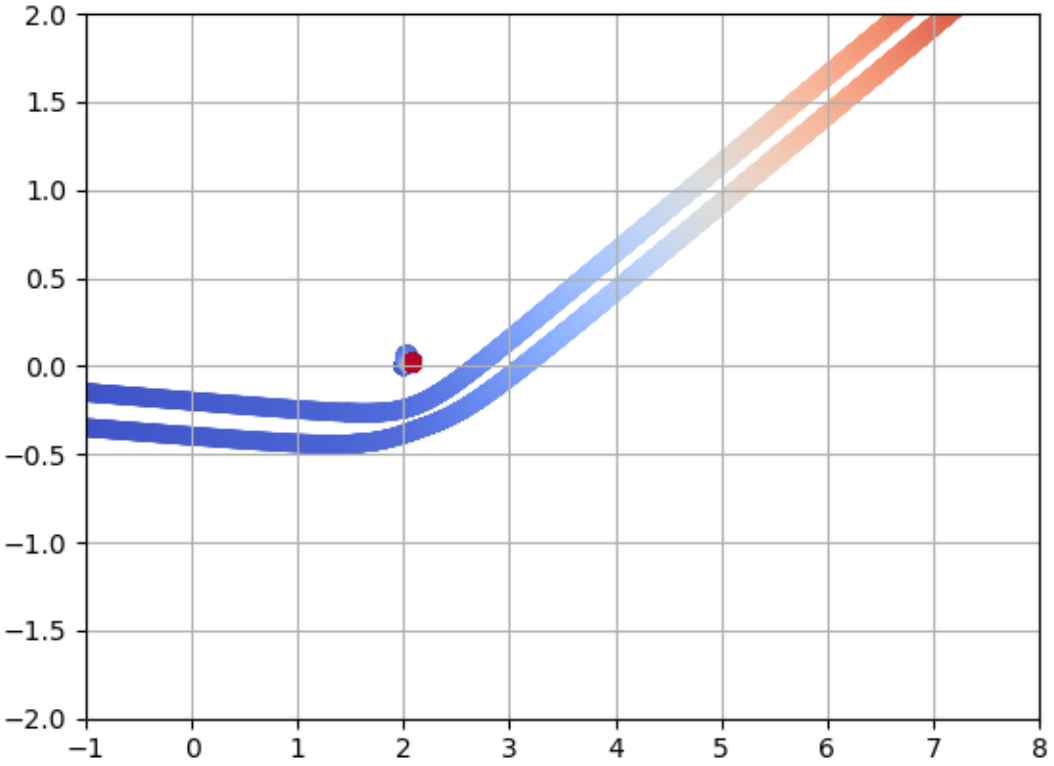

Figure 3.5: Trace of sample vortex evolution in the case of $\frac{\rho}{d} < 0$.

We see the predicted behavior, with dipole separation reaching the $\min_{\forall t \in \mathbb{R}} \ell_{2,3} < d$ value at the critical point then relaxing back to the original separation of d.

3.4.2 $\min_{\forall t \in \mathbb{R}} \ell_{i,j}$ in the region $0 < \frac{\rho}{d} < \frac{9}{2}$

Now we examine minimum lengths in the exchange scattering case. We note that the two lengths we are interested in, i.e. $\ell_{1,3}$ and $\ell_{2,3}$, form dipole separations during different phases of the scattering. First, we see that the length of $\ell_{2,3}$ must become larger after scattering takes place, as the new dipole formed by vortices 1 and 3 propagates off to infinity. This implies that the minimum length $\min_{\forall t \in \mathbb{R}} \ell_{2,3}$ must occur at or before scattering. We see that actually the critical length is larger than the starting separation d, this implies that $\ell_{2,3}$ increases up to the critical point, or in other words the minimum length of the separation $\ell_{2,3}$ must be its starting separation, so:

$$\min_{\forall t \in \mathbb{R}} \ell_{2,3} = d.$$

Now in the case of $\ell_{1,3}$, we reason that the length must become smaller as evolution of the system occurs and the new dipole propagates off. We reason therefore that the dipole will relax to the original separation d as $t \to \infty$ and so the minimum length in this case will also be d. Therefore:

$$\min_{\forall t \in \mathbb{R}} \ell_{1,3} = d.$$

We produce another vortex trace to visualize the evolution as before:

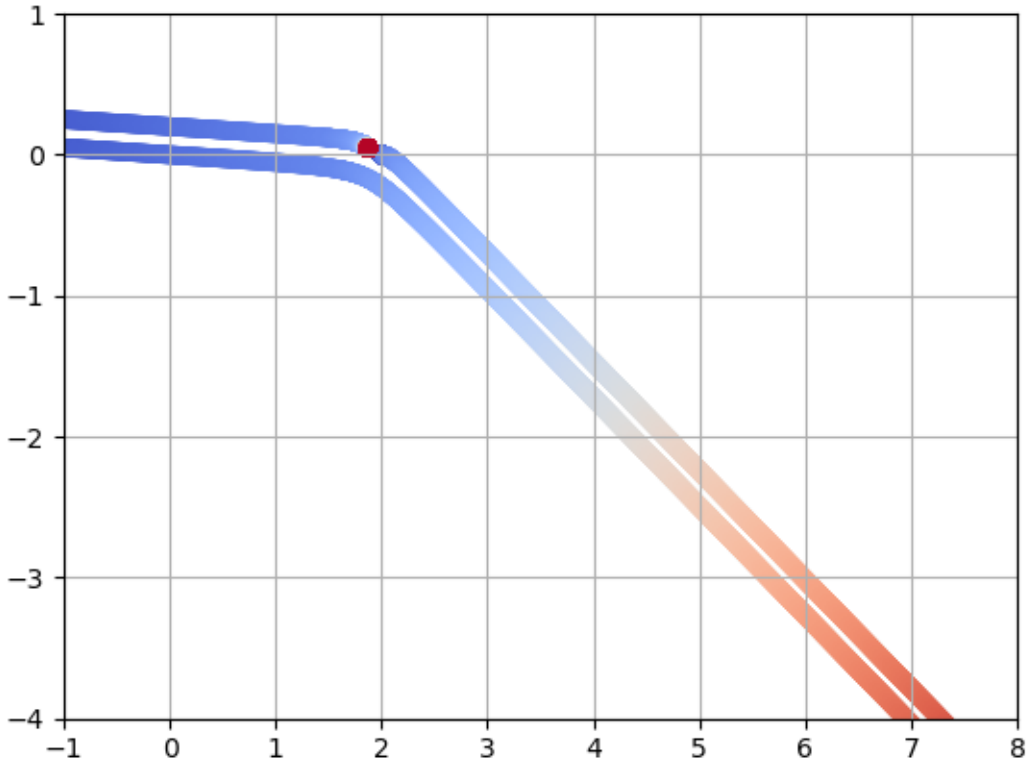

Figure 3.6: Trace of sample vortex evolution in the case of $0 < \frac{\rho}{d} < \frac{9}{2}$.

Again we see what we predicted with dipoles maintaining the same initial separation d.

3.4.3 $\min_{\forall t \in \mathbb{R}} \ell_{i,j}$ in the region $\frac{\rho}{d} > \frac{9}{2}$

We now consider the final direct scattering case. We observe that this case is slightly different from the previous direct scattering case in terms of the behavior of lengths at scattering. We observe an attraction effect similar to the first direct scattering case, except here the dipole passes above the stationary vortex. This key difference has the consequence of forcing the vortices of the dipole further away from each other at scattering, after which they will relax back to their original separation d as $t \to \infty$. This implies that the minimum length in this case will be the original separation, therefore:

$$\min_{\forall t \in \mathbb{R}} \ell_{2,3} = d.$$

Now all that is left is to derive the final minimum $\min_{\forall t \in \mathbb{R}} \ell_{1,3}$. Again we see that this length must start off relatively large, become smallest near scattering, and finally become ever larger as $t \to \infty$. Therefore we reason that again this minimum must be the same as the critical length i.e.:

$$\min_{\forall t \in \mathbb{R}} \ell_{1,3} = \frac{2\rho + d}{4} + \frac{1}{4}\sqrt{4\rho^2 - 12\rho d - 15d^2} + \mathcal{O}((\frac{\rho}{L})^2 + \mathcal{O}((\frac{d}{L})^2).$$

Now we once again form the evolution trace:

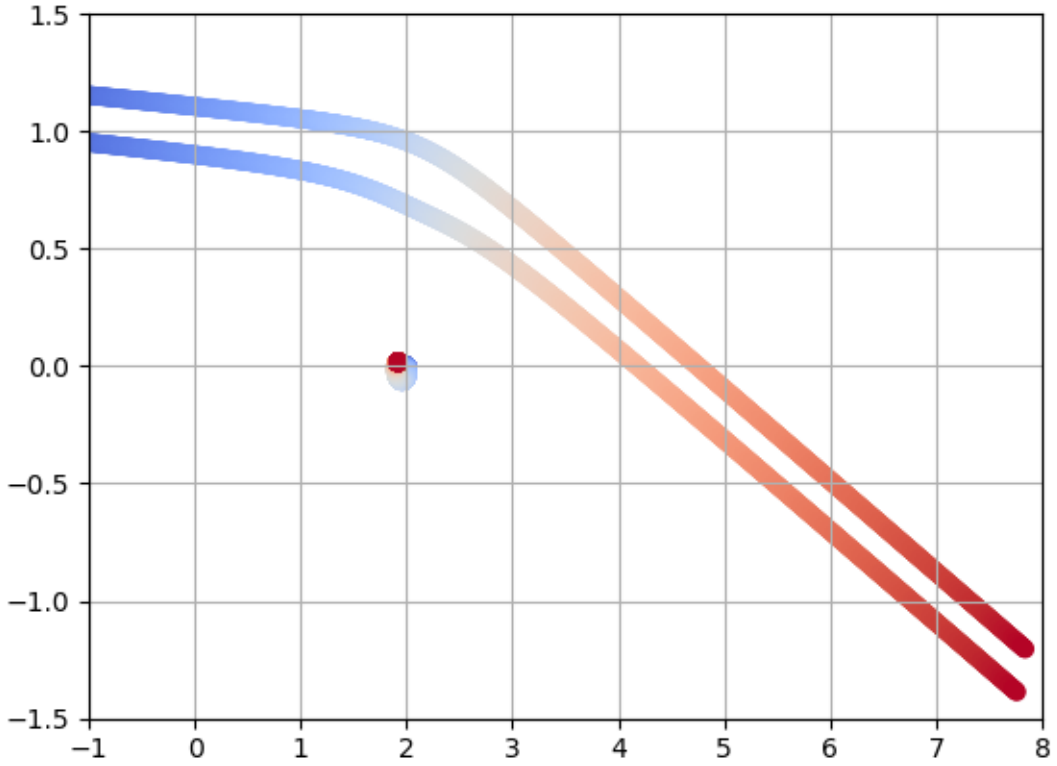

Figure 3.7: Trace of sample vortex evolution in the case of $\frac{\rho}{d} > \frac{9}{2}$.

So finally we have a complete picture of the separations possible over the entire dipole-vortex interaction, we summarize the results in the table below (note that for the sake of brevity $\mathcal{O}((\rho/L)^2)$ and $\mathcal{O}((d/L)^2)$ terms are omitted again):

	$\frac{\rho}{d} < 0$	$0 < \frac{\rho}{d} < \frac{9}{2}$	$\frac{9}{2} < \frac{\rho}{d}$
$\min_{\forall t \in \mathbb{R}} \ell_{1,2}$	$-\frac{2\rho+d}{2}$	$d + \sqrt{2d(\rho+d)}$	$\frac{2\rho+d}{2}$
$\min_{\forall t \in \mathbb{R}} \ell_{1,3}$	$-\frac{2\rho+d}{4} + \frac{1}{4}\sqrt{4\rho^2 - 7d^2 - 12\rho d}$	d	$\frac{2\rho+d}{4} + \frac{1}{4}\sqrt{4\rho^2 - 12\rho d - 15d^2}$
$\min_{\forall t \in \mathbb{R}} \ell_{2,3}$	$\frac{2\rho+d}{4} + \frac{1}{4}\sqrt{4\rho^2 - 7d^2 - 12\rho d}$	d	d

Table 3.2: Complete minimum separations in each case.

3.5 Scattering Angles

Finally we compute the angle at which the dipole is deflected with respect to the center of vorticity, referred to here as the scattering angle. We define the scattering angle as the change of polar angle of vortex 3, i.e. change of ϕ_3, in the limit of t from $-\infty$ to ∞. It is important that we define the scattering angle from the third vortex, as this vortex remains part of the dipole regardless of whether we have the case of exchange scattering or direct scattering. In

contrast vortex 2 becomes a stationary vortex in the case of exchange scattering so if we were to solve for the change in angle of this vortex we would receive a result not reflective of the "true" scattering angle of the dipole. Hence the choice of defining the scattering angle in terms of ϕ_3 is justified.

Mathematically we notate the scattering angle as $\Delta\phi$ and define this as done by Aref:

$$\Delta\phi = \lim_{t\to\infty} \phi_3 - \lim_{t\to-\infty} \phi_3 \tag{3.13}$$

To solve for this we use a strategy employed by Aref in the previously mentioned work [5], which was also used by Novikov in his work on three identical vortices [7]. We summarize our method as such; first we express our relative lengths in dimensionless form, then it is necessary to formulate an equation of motion in terms of our dimensionless variables, which we will finally use coupled with the angle derivative $\dot{\phi}_3$ to express our scattering angle $\Delta\phi$.

To begin we use our conserved quantity R to define quantity C as:

$$C = \frac{R}{N\left(\prod_{i=1}^{N} \kappa_i\right)}, \tag{3.14}$$

Thus if we apply (3.14) to our case we have that:

$$\ell_{1,2}^2 - \ell_{2,3}^2 - \ell_{1,3}^2 = -3C. \tag{3.15}$$

It is easy to see that this quantity is invariant of time using (3.2).

We then define dimensionless variables b_m (here m can refer to any of the vortex indices) as:

$$b_1 = \frac{\ell_{2,3}^2}{C}, \quad b_2 = \frac{\ell_{1,3}^2}{C}, \quad b_3 = -\frac{\ell_{1,2}^2}{C}. \tag{3.16}$$

From (3.15) we find that these variables then obey the constraint:

$$b_1 + b_2 + b_3 = 3. \tag{3.17}$$

Also, if we define a new conserved quantity θ determined by the initial conditions as:

$$\theta = |C|e^{-4\pi H}. \tag{3.18}$$

This then gives the constraint:

$$\frac{b_1 b_2}{|b_3|} = \frac{1}{\theta}. \tag{3.19}$$

Now, what we have essentially done is express the dipole-vortex collision in terms of the dimensionless relative lengths b_m, which we then found to obey the constraints (3.17) and (3.19). As discussed before this then reduces the system to one degree of freedom. We can categorize the scattering regimes in terms of the new quantities C and θ. We find that where $C > 0$ and $\theta < \frac{1}{3}$ we observe a regime of exchange scattering, whereas if instead $\theta > \frac{1}{3}$ we observe the case of direct scattering. Now in the case where $C < 0$, if $\theta < \frac{8}{3}$ we observe again the regime of exchange scattering, whereas if $\theta > \frac{8}{3}$ we observe direct scattering.

Next we seek to find the equations of motion in terms of our dimensionless quantities, of particular interest is the derivative $\dot{b}_3$. This is because of how b_3 depends upon the length $\ell_{1,2}$. We note that as vortices 1 and 2 are identical these vortices can never form a dipole, whereas other vortex pairs can either form a dipole or begin the collision process as a dipole in the case of vortices 2 and 3. This means that essentially we can encapsulate the collision using

the equation of motion of b_3. Hence we solve for the dimensionless equation of relative motion which gives:

$$\dot{b}_3 = \pm\frac{\sqrt{\theta}}{C\pi b_3}\sqrt{(|b_3| - \frac{9}{4}\theta)\left[(3-b_3)^2 - 4\frac{|b_3|}{\theta}\right]}. \tag{3.20}$$

Now we can use the above to solve for where $\frac{d}{dt}b_3 = 0$. Note that this implies $\frac{d}{dt}\ell_{1,2}^2 = 0$ so the solutions we obtain will correspond to the situations found in (3.3). Notice however that there are three values of b_3 that give the result $\dot{b}_3 = 0$, due to the quadratic term within the square root. To show this we write the cases of the above equation explicitly as:

$$\dot{b}_3 = \begin{cases} \pm\frac{\sqrt{\theta}}{C\pi b_3}\sqrt{-(b_3 + \frac{9}{4}\theta)\left[(3-b_3)^2 + 4\frac{b_3}{\theta}\right]} & \text{if } C > 0, \\ \pm\frac{\sqrt{\theta}}{C\pi b_3}\sqrt{(b_3 - \frac{9}{4}\theta)\left[(3-b_3)^2 - 4\frac{b_3}{\theta}\right]} & \text{if } C < 0. \end{cases}$$

Now in the case of $C > 0$ we obtain the roots of the above equation as:

$$b_3 = -\frac{9}{4}\theta, \quad b_3 = -\frac{1}{\theta}[1 \pm \sqrt{1-3\theta}]^2.$$

We classify these roots to refer to later as:

$$\alpha(\theta) = -\frac{9}{4}\theta, \quad \beta(\theta) = -\frac{1}{\theta}[1-\sqrt{1-3\theta}]^2, \quad \gamma(\theta) = -\frac{1}{\theta}[1+\sqrt{1-3\theta}]^2. \tag{3.21}$$

Notice also in the case that $C < 0$ we have similar results for the roots:

$$b_3 = \frac{9}{4}\theta, \quad b_3 = \frac{1}{\theta}[1 \pm \sqrt{1+3\theta}]^2,$$

which correspond to $\alpha(-\theta), \beta(-\theta), \text{and } \gamma(-\theta)$. We will refer to the roots in this case as:

$$\alpha(-\theta) = \bar{\alpha}, \quad \beta(-\theta) = \bar{\beta}, \quad \gamma(-\theta) = \bar{\gamma}. \tag{3.22}$$

Now using these roots we can express $\dot{b}_3$ as (here for shorthand we write b_3 as simply b):

$$\dot{b} = \begin{cases} \pm\frac{\sqrt{\theta}}{C\pi b}\sqrt{[\alpha-b][\beta-b][\gamma-b]} & \text{if } C > 0, \\ \pm\frac{\sqrt{\theta}}{C\pi b}\sqrt{[b-\bar{\alpha}][b-\bar{\beta}][b-\bar{\gamma}]} & \text{if } C < 0. \end{cases} \tag{3.23}$$

Therefore we can see in each case there exists three cases where $\dot{b}_3 = 0$. It can be shown that β and γ, or $\bar{\beta}$ and $\bar{\gamma}$, correspond to where $\ell_{1,3} = \ell_{2,3}$. We also have the root α, which by elimination must correspond to the collinear case found in direct scattering where either $\ell_{1,2} = \ell_{1,3} + \ell_{2,3}$ or $\ell_{2,3} = \ell_{1,2} + \ell_{1,3}$, depending upon whether we have α or $\bar{\alpha}$. Thus we can think of the root α as representing the degenerate case of the triangle inequality, in other words α is a boundary point of which b_3 cannot pass as this would imply the vortices and the lengths between them no longer form a triangle, an obvious impossibility. It is interesting that there are two roots corresponding to the case $b_1 = b_2$. This is due to the fact that there exists a region of periodic relative motion that occurs when in the initial conditions $|b_m|$ are close to being equal. As this does not correspond to our case (due to how large L is at $t = 0$, $|b_3|$ will then start very large also) we will not consider this here. This case is considered in detail in the appendix of Aref's fundamental work [5].

We now continue the derivation of the scattering angle, by expressing the system now in polar coordinates. We express the position of vortex i now as (ϕ_i, r_i) where ϕ_i is the angle

spanned from horizontal by the line segment joining vortex i to the center of vorticity and r_i is the length of this line segment. Therefore we have that:

$$\phi_i = \arctan\left(\frac{y_i}{x_i}\right), \tag{3.24}$$

$$r_i = \sqrt{y_i^2 + x_i^2}. \tag{3.25}$$

We now seek to find the equations of motion of the system, namely the equation of motion $\dot{\phi}_3$ which will allow us to calculate the scattering angle of the collision. We find that the new polar coordinates satisfy Hamilton's canonical equations as such:

$$\frac{\partial H}{\partial \phi_i} = \kappa_i r_i \dot{r}_i, \quad \frac{\partial H}{\partial r_i} = -\kappa_i r_i \dot{\phi}_i. \tag{3.26}$$

From this we can express the desired expression $\dot{\phi}_3$ in terms of the variable b_3 as:

$$\dot{\phi}_3 = \frac{\theta}{4\pi C} \frac{9 - 3b_3 + \frac{4}{\theta}|b_3|}{(6 - b_3)|b_3|}. \tag{3.27}$$

Now we define the scattering angle of vortex 3 as:

$$\Delta\phi_3 = \lim_{t\to+\infty} \phi_3 - \lim_{t\to-\infty} \phi_3 = \int_{-\infty}^{+\infty} \dot{\phi}_3 \, dt. \tag{3.28}$$

To evaluate this integral we must first examine the behavior of the variable b_3 with respect to time. We first observe the case of direct scattering. If $C > 0$ we have a negative b_3, so in the limit of $t \to -\infty$ we have that $b_3 \to -\infty$ (as $t \to -\infty \implies L \to \infty$ so $|b_3|$ becomes increasingly large). So therefore as $t \to +\infty$ then b_3 becomes less negative until it reaches the point $b_3 = \alpha$, note that during this motion $\dot{b}_3 > 0$. Note also that in the case of $C > 0$ and $\theta > 1/3$ the other roots of $\dot{b}_3$ then become complex so it is impossible for b_3 to reach these points, hence as $t \to \infty$, b_3 will reach the stationary point α after which it will rebound back to infinity $b_3 \to -\infty$. Similar motion occurs in the direct scattering case of $C < 0$, with instead as $t \to -\infty$, we have $b_3 \to +\infty$, then as $t \to +\infty$ we have $b_3 \to \bar{\alpha}$ and then $b_3 \to +\infty$. Now, in the exchange scattering case we have similar motion where either $b_3 \to \gamma \to -\infty$ or $b_3 \to \bar{\gamma} \to +\infty$ as $t \to \infty$. Using this explanation for the behavior of b_3 and (3.20) and (3.27) we can express the scattering angle integrals in each case as such:

$$\Delta\phi = \begin{cases} \frac{\sqrt{\theta}}{2} \int_{-\infty}^{\gamma} \frac{9-(3+\frac{4}{\theta})b \; db}{\sqrt{(\alpha-b)(\beta-b)(\gamma-b)}} & \text{if} \quad C > 0, \theta < \frac{1}{3}, \\ \frac{\sqrt{\theta}}{2} \int_{-\infty}^{\alpha} \frac{9-(3+\frac{4}{\theta})b \; db}{\sqrt{(\alpha-b)(\beta-b)(\gamma-b)}} & \text{if} \quad C > 0, \theta > \frac{1}{3}, \\ \frac{\sqrt{\theta}}{2} \int_{\bar{\gamma}}^{\infty} \frac{9-(3-\frac{4}{\theta})b \; db}{\sqrt{(b-\bar{\alpha})(b-\bar{\beta})(b-\bar{\gamma})}} & \text{if} \quad C < 0, \theta < \frac{8}{3}, \\ \frac{\sqrt{\theta}}{2} \int_{\bar{\alpha}}^{\infty} \frac{9-(3-\frac{4}{\theta})b \; db}{\sqrt{(b-\bar{\alpha})(b-\bar{\beta})(b-\bar{\gamma})}} & \text{if} \quad C < 0, \theta > \frac{8}{3}. \end{cases} \tag{3.29}$$

We note that in each case the integral is of a rational function of b_3 and a square root term that contains a cubic in b_3. So by definition the scattering angles are in the form of elliptic integrals, which cannot in general be expressed in terms of elementary functions [45]. However, by simple substitutions such as given by Labahn and Mutrie [46], we can reduce each of the scattering angle integrals into a combination of the so-called Legendre normal forms.

The particular normal forms which we will use here are the first complete elliptic integral $K(k)$ and the third complete elliptic integral $\Pi(n,k)$ given by:

$$K(k) = \int_0^1 \frac{d\phi}{\sqrt{1-k^2\sin^2\phi}}, \quad \Pi(n,k) = \int_0^1 \frac{d\phi}{(1+n\sin^2\phi)\sqrt{1-k^2\sin^2\phi}}, \tag{3.30}$$

where k is the elliptic eccentricity and n is a constant independent of other variable referred to as the "characteristic". Note that n and k have differing values depending upon which case of scattering occurs. Expressing the scattering angles in terms of the standardized Legendre integrals is useful for the purpose of plotting numerically which we will see later. We then express each scattering angle in the same form:

$$\Delta\phi = \sqrt{a_1}\left[a_2 K(k) + a_3 \Pi(n,k)\right], \tag{3.31}$$

where each $a_i = a_i(\theta)$ depends upon which case of scattering occurs. Combined with Table 3.3 equation (3.31) details the scattering angles in each case. Note that in the case $C > 0, \theta > 1/3$ we define the variable $A^2 = (\gamma-\alpha)(\beta-\alpha)$:

	a_1	a_2	a_3	k^2	n
$C>0, \theta<\frac{1}{3}$	$\frac{\theta}{\alpha-\gamma}$	3	$\frac{4}{\theta}$	$\frac{\alpha-\beta}{\alpha-\gamma}$	$\frac{6-\alpha}{\alpha-\gamma}$
$C>0, \theta>\frac{1}{3}$	$\frac{\theta}{A}$	$(3+\frac{4}{\theta}+\frac{9+\frac{24}{\theta}}{\alpha+A-6})$	$\frac{(\frac{A}{\alpha-6}-1)(9+\frac{24}{\theta})}{2(\alpha+A-6)}$	$\frac{A-\frac{\beta+\gamma}{2}+\alpha}{2A}$	$-\frac{(\alpha+A-6)^2}{4A(\alpha-6)}$
$C<0, \theta<\frac{8}{3}$	$\frac{\theta}{\bar{\gamma}-\bar{\beta}}$	3	$-\frac{(9-\frac{24}{\theta})(\bar{\alpha}-\bar{\gamma})}{(\bar{\alpha}-6)(6-\bar{\gamma})}$	$\frac{\bar{\alpha}-\bar{\beta}}{\bar{\gamma}-\bar{\beta}}$	$\frac{\bar{\alpha}-6}{6-\bar{\gamma}}$
$C<0, \theta>\frac{8}{3}$	$\frac{\theta}{\bar{\alpha}-\bar{\beta}}$	$\frac{3\bar{\gamma}-\frac{4}{\theta}\bar{\gamma}-9}{\bar{\gamma}-6}$	$-\frac{(9-\frac{24}{\theta})(\bar{\gamma}-\bar{\alpha})}{(\bar{\gamma}-6)(6-\bar{\alpha})}$	$\frac{\bar{\gamma}-\bar{\beta}}{\bar{\alpha}-\bar{\beta}}$	$\frac{\bar{\gamma}-6}{6-\bar{\alpha}}$

Table 3.3: Table giving the a_i coefficients and n and k parameters in each scattering case.

3.6 Numerical Results

Finally, we now solve the three vortex collision numerically using the algorithm detailed in Chapter 2. In the process of doing this we compare our results to the theoretical results already derived in previous sections. We run a series of numerical simulations, with key parameters $d = 0.2$ and $L = 10$, ensuring that the conditions $\rho/L \ll 1$ and $d/L \ll 1$ hold. We use a range of ρ values such that we have a decent range of our parameter ρ/d, we choose to run simulations within the range $-2 < \rho/d < 5.5$ for the scattering and minimum lengths, and use a range of $\rho/d \in [-4.5, 10.5]$ in the simulations for scattering angles. We also note the importance of choosing an appropriate time end-point and appropriate minimum time-step bound h_{min}. This is of particular importance as we must ensure the simulation runs long enough such that scattering can actually occur within the simulation; otherwise we will end up solving for key quantities before scattering has actually taken place, hence giving erroneous results. We begin with the critical and minimum lengths of the system.

3.6.1 Critical Lengths

The critical lengths of the system are displayed in Fig. 3.8.

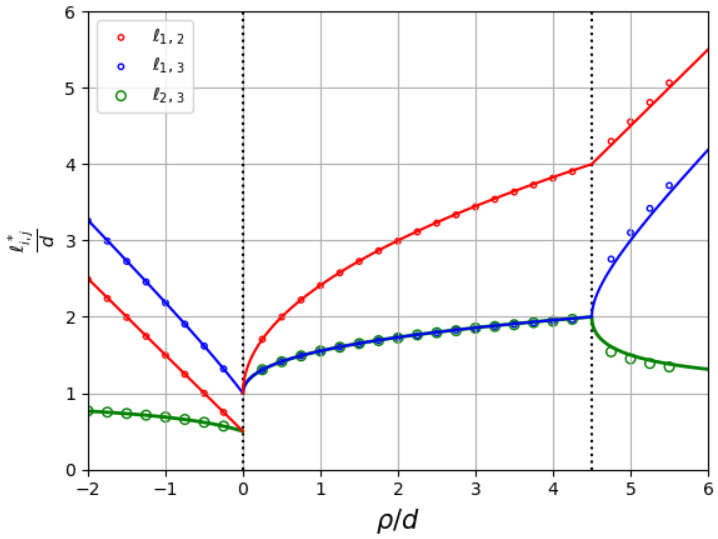

Figure 3.8: Numerical results plotted against the theoretical derivations for the critical lengths.

Here we use solid lines on the plot indicate the theoretical results for a given length, whilst the dots corresponding to the same color indicate the numerical results found for this length. Note the theoretical predictions and the numerical results agree remarkably, with only slight deviation most prominent in the case where $\rho/d > 9/2$. Note the critical lengths decrease as $\rho/d \to 0$, approaching the limiting case of $\rho/d = 0$ whereupon we numerically compute $\ell^*_{1,2} = \ell^*_{2,3} = 0.5d$, we also assume as that $\ell^*_{1,3}$ must equal $0.5d$ at this point as corollary to the fact that $\rho/d = 0$ corresponds to rigid body motion of the equilateral triangle of vortices. The same also occurs as $\rho/d \to 9/2$ where $\ell_{1,3}$ and $\ell_{2,3}$, here represented by a single line as they are equal in this case, are both seen approaching the value $2d$. We see also that past this final rigid body case as $\rho/d \to \infty$, the scattering lengths $\ell^*_{1,2}$ and $\ell^*_{1,3}$ continually increase, whilst the length $\ell^*_{2,3}$ between dipole vortices continually decreases, the same behavior is observed for where ρ/d. Intuitively this is obvious, as $|\rho| \to \infty$ the dipole passes ever more further above or below the stationary vortex, this implies that $\ell^*_{1,2}$ and $\ell^*_{1,3}$ become increasingly large as the dipole impact parameter becomes large. Also as we reason that the effect of the stationary vortex circulation becomes less apparent as $|\rho|$ becomes larger, such that the dipole separation is less and less effected by the stationary vortex. Hence as $|\rho| \to \infty$ we see that $\ell_{2,3} \to d$, i.e. the dipole is so far above or below the stationary vortex at scattering it retains its initial separation and so in this limit we have a constant $\ell_{2,3} = d$ throughout the entire evolution.

3.6.2 Minimum Lengths

We use the same procedure to plot the minimum lengths, shown in the Fig. 3.9:

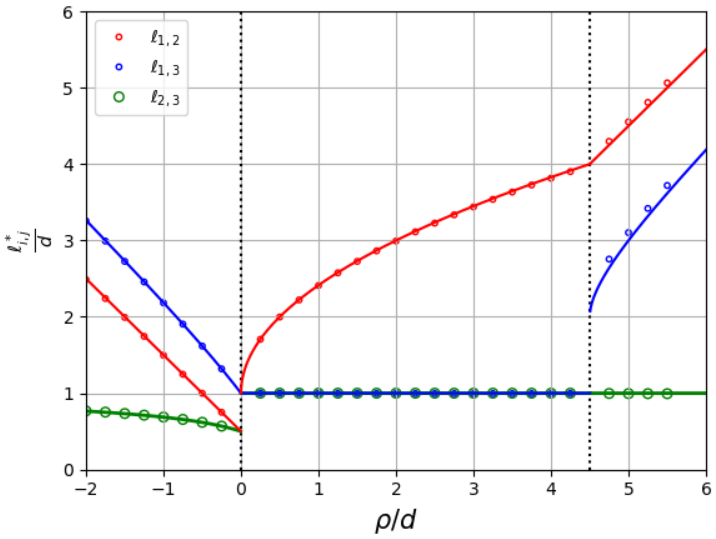

Figure 3.9: Numerical results plotted against the theoretical derivations for the minimum lengths.

Again, the theoretical and the numerical results agree completely. We observe the same behavior as predicted, the minimum lengths in the case of $\rho/d < 0$ occur at the scattering point and hence are the same as we found for the critical lengths. In the case where $0 < \rho/d < 9/2$ we again see only two lines as here $\min_{\forall t \in \mathbb{R}} \ell_{1,3} = \min_{\forall t \in \mathbb{R}} \ell_{2,3} = d$, highlighting the interesting phenomena that $\ell_{1,3} \to d$ after scattering, implying the separation of the newly formed dipole of vortex 1 and 3 after scattering relaxes to the initial length of the first dipole of vortex 2 and 3. After the second boundary $\rho/d = 9/2$ is passed, the behavior is again what we expected. Where $\min_{\forall t \in \mathbb{R}} \ell_{1,2}$ and $\min_{\forall t \in \mathbb{R}} \ell 1, 3$ become increasingly large as the dipole passes further above or below the dipole and again these lengths occur at the critical point. Now observe the behavior of $\ell_{2,3}$ in this region. Notice that whereas our other two minimums in this region have minimums that occur at scattering, the minimum $\ell_{2,3}$ does not correspond to its value at scattering. This again is in line with our predictions, as the dipole approaches the scattering point its separation actually increases, up until after scattering whereupon the dipole relaxes back to its original separation d, meaning this initial length is the minimum separation in this case.

3.6.3 Scattering Angles

Finally, we run simulations solving for the scattering angles of the system. In order to solve for the scattering angles we run simulations as before, here using the C++ standard library "atan2" function, which maps the scattering angle onto a $\Delta\theta \in [-\pi, \pi]$ domain. This however may pose a problem as the scattering angle formulae derived earlier extend past this range up to the value 2π, hence as the numerical results are the focus of this section we translate the entire theoretical results by π (note that this makes no difference to the overall results as the scattering angle is only relevant when a given point of reference is specified). We use the atan2 function to calculate the angle between dipole trajectories with respect to the center of vorticity at the start and end of the simulation, with our results shown in Fig. 3.10.

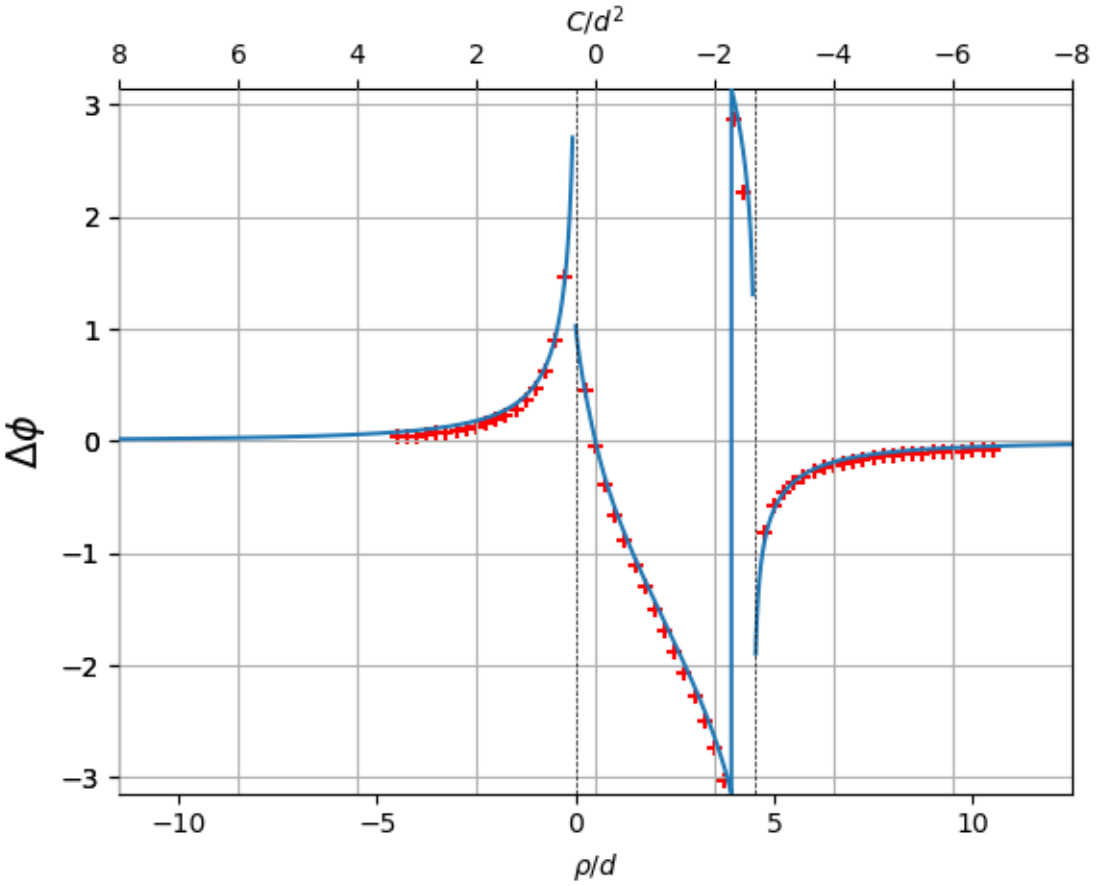

Figure 3.10: Numerical results as compared to theoretical results of the scattering angle.

Here we plot results both with respect to our original parameter ρ/d and also with respect to C/d^2, we are allowed to do this as in the limit $\rho \ll L$ and $d \ll L$ we have:

$$\theta = \frac{|C|}{d^2}.$$

Hence plotting in this way allows us to visualize the results in terms of the derived quantities C and θ. We have the following relation between the two parameters:

$$\frac{C}{d^2} = -\frac{1}{3}\left(2\frac{\rho}{d} - 1\right).$$

Note here the blue curve represents theoretical results, whilst the red crosses represent the numerical solution, we again see excellent agreement between the separate results. First we notice the behavior of the angle in the case that $|\rho| \to \infty$, we see as is to be expected that the scattering angle decreases as ρ increases in magnitude, due to the stationary vortex not affecting the dipole as much when $|\rho|$ is large, to the point that the scattering angle is zero for large enough $|\rho|$. We also see that the two rigid-body cases at $\rho/d = 0$ and $\rho/d = 9/2$ both act as asymptotes to the system, here represented as the dashed lines. This again is to be expected as in these cases the vortices perpetually rotate about the center of vorticity and so the scattering angle $\Delta\phi_3$ will in effect be infinite. It is also interesting to note both numerical and theoretical plots are of a different sign from Aref's original plot in the case where $\rho/d > 9/2$, or where $C/d^2 < -8/3$, suggesting a possible mistake in Aref's work [5]. We also notice in Table 3.3 that the exchange scattering coefficient $4/\theta$ is in our case positive whereas it is negative in Aref's case, suggesting another mistake.

Chapter 4

Four Vortex Scattering

4.1 Problem Statement

Here we consider the four vortex collision as an extension of the previously considered dipole-vortex collision, whereupon instead of a dipole colliding with a stationary vortex, the dipole instead collides with an identical dipole propagating towards the same target point. This is another basic collision that is possible in the BECs already mentioned, where instead of a dipole in the condensate meeting a stationary vortex it instead collides with another propagating dipole. This collision is then fundamental to the formation of BECs as already mentioned and so we attempt to investigate this collision also. It is also possible that a propagating dipole in the fluid may also collide with rotating identical vortices, although this collision is not investigated here.

The concept of the four vortex collision differs from the previously considered case in that as discussed the $N = 4$ vortex system is in general not integrable [6]. This means that finding analytical solutions such as found before for the three vortex case may not possible here. Interestingly however in works by Aref [47] and Eckhardt [48], it can be shown that the four vortex case can be integrated as long as the following conditions hold; first, the sum of all circulations must be zero, and also total linear momentum must be zero. Mathematically we represent these conditions as such:

$$\kappa_1 + \kappa_2 + \kappa_3 + \kappa_4 = 0, \tag{4.1}$$

$$P = Q = 0. \tag{4.2}$$

It is clear that as we have identical dipoles with identical circulations $\pm\kappa$ then condition (4.1) holds. Note that if we examine (4.2) using (2.5) however we have that:

$$\kappa_1 x_1 + \kappa_2 x_2 + \kappa_3 x_3 + \kappa_4 x_4 = 0,$$
$$\kappa_1 y_1 + \kappa_2 y_2 + \kappa_3 y_3 + \kappa_4 y_4 = 0.$$

Now if we say that $\kappa_1 = \kappa, \kappa_2 = -\kappa, \kappa_3 = \kappa, \kappa_4 = -\kappa$ we obtain the relations:

$$\frac{x_1 + x_3}{2} = \frac{x_2 + x_4}{2}, \quad \frac{y_1 + y_3}{2} = \frac{y_2 + y_4}{2},$$

therefore in order for a particular four vortex interaction in our case to be integrable it must hold that vortex pairs of equal circulation share the same midpoint.

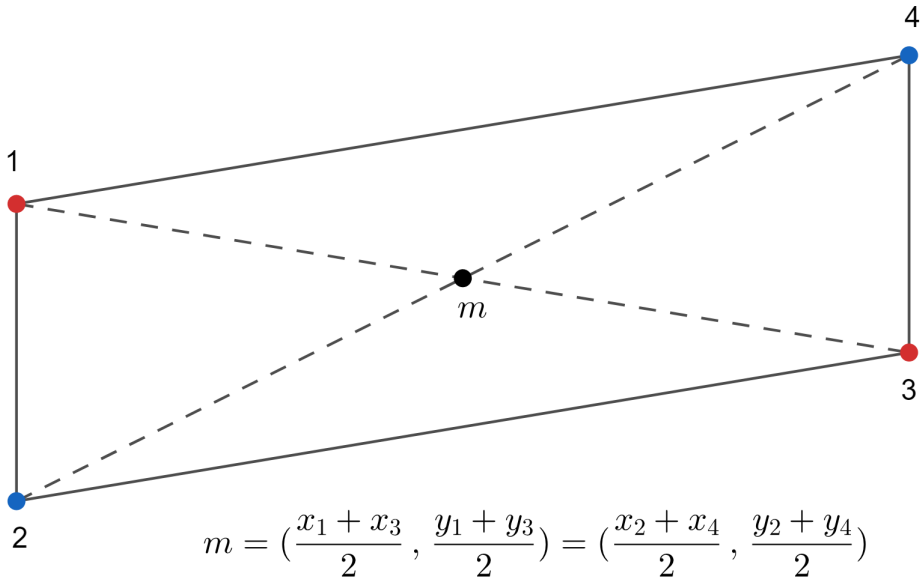

Figure 4.1: Visualization of the integrability conditions (4.1) and (4.2), showing the parellelogram spanned by the vortices.

As seen in Fig. 4.1, the conditions for integrability imply that a system of four vortices with the given circulations is integrable if the vortices span a parallelogram as shown. Unfortunately this represents a special case where vortex dipole trajectories are exactly parallel, which has a low probability of occurring in actual quantum turbulence. Due to this we plan to consider dipole-dipole collisions where trajectories are not exactly parallel to achieve a more universal appreciation of these collisions. As we are considering the dipole-dipole collision this way the parallelogram configuration seen does not hold in our case and so the problem we consider is definitively not integrable. Hence we instead restrict the analysis to a purely numerical treatment using the already established procedure used in the previous chapter. A similar set up has already been investigated by Aref [49], it is notable that Aref has also considered the cases of dipoles with slightly different circulations, whereas we consider the dipoles as completely identical. It is interesting that in the case of Aref chaotic scattering (a phenomenon they refer to as "chattering") occurs, Aref also states that this can occur in the limiting case of identical vortex pairs even though this case seems more regular. It will be interesting to investigate whether we can observe the chaotic scattering found by Aref in our numerical simulations.

We set up the problem as such; we consider a dipole with circulations $\kappa_1 = 1, \kappa_2 = -1$ propagating towards the origin O which will serve as a "target point". Note we cannot use the center of vorticity as a reference point as before as in this case $\Omega = 0$ and so the center of vorticity is undefined. We denote the initial separation from the target point as L_1, representing the distance from the midpoint of the dipole to the origin. With this in mind, we then consider another dipole, again with circulations $\kappa_3 = 1, \kappa_4 = -1$, also propagating towards the target point with L_2 denoting the distance of the midpoint of this dipole to the origin. Due to the symmetries of such a system we can combine these parameters in the form of the dimensionless parameter $L = L_2/L_1$, keeping L_1 the same whilst varying L_2. Note that in effect this is the same as changing the impact parameter in the three vortex case. We also denote ϕ as the angle between the line segments joining the dipole midpoints to the target point. We note the symmetries present in the parameters, namely the dynamics of the system where $\phi \in [0, \pi]$ is identical to when $\phi \in [\pi, 2\pi]$ and so we will only consider the case where $\phi \in [0, \pi]$. Similarly, we note the symmetry present about the impact parameter value $L = 1$, by a simply change

of label we can show the dynamics of the system where $0.5 < L < 1$ is identical to where $1 < L < 1.5$. An illustration of this system is given in Fig. 4.2.

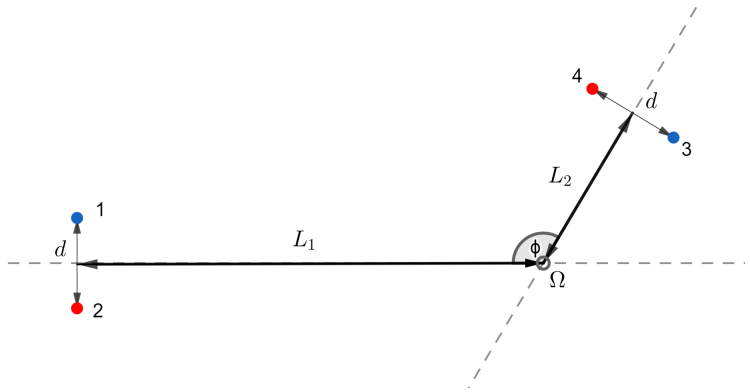

Figure 4.2: Diagram of the four vortex collision.

We will vary the values of L and ϕ in order to observe the behavior of the system and the differing cases that arise. Note that as before we must also ensure that scattering occurs, so the simulation must be run for long enough i.e. with a sufficiently large time endpoint. We also must make sure that L_1 and L_2 are sufficiently large such that dipoles are able to first propagate towards the target without initially being effected by the other dipole. We observe from basic simulations that, similar to the three-vortex case, there exists regimes of both direct and exchange scattering in the collision of two dipoles. In the case of direct scattering the particular combination of L and ϕ causes the dipoles to "miss" each other, or in other words, each dipole passes the target point without any major effects other than maybe a small deflection. This is in contrast to the case of exchange scattering, where we examine the initial dipoles being broken whilst new dipoles are formed which then propagate to infinity. Specifically in this case at scattering we see vortex 1 and vortex 2 separating as well as vortex 3 and vortex 4 separating, we then see vortex 1 and vortex 4 form a new dipole, and vortex 2 and vortex 3 form a new dipole, which then both propagate off to infinity. An example of this type of scattering occurs at the boundary $\phi = \pi$, where the new dipoles are scattered at right angles to the original dipole trajectories, note that for this particular ϕ value the system dynamics are invariant with respect to L. It is easy to see the analogy to three vortex scattering when we consider the different scattering regimes, although no form of rigid-body rotation can exist here, on account of the center of vorticity being undefined.

4.2 Results

4.2.1 Direct and Exchange Scattering Regions

We run a number of simulations for the four vortex case as described above, we allow ϕ to vary between $(0, \pi)$ whilst we allow L to vary between $[0.4375, 1]$. This ensures that the full dynamics of the system is encapsulated, with both the direct scattering and exchange scattering cases being simulated in full. Note that the behavior at $\phi = \pi$ is already established, so we do not need to include this point in the analysis. As before we solve for the scattering angle using the Dormand-Prince algorithm. We first begin by solving numerically for the regions of where direct and exchange scattering occur in this case, in order to better understand the effect our parameters have on the dynamics of the system and so we are able to put later results into context. We vary L and Φ as stated and find regions of scattering as displayed in Fig. 4.3.

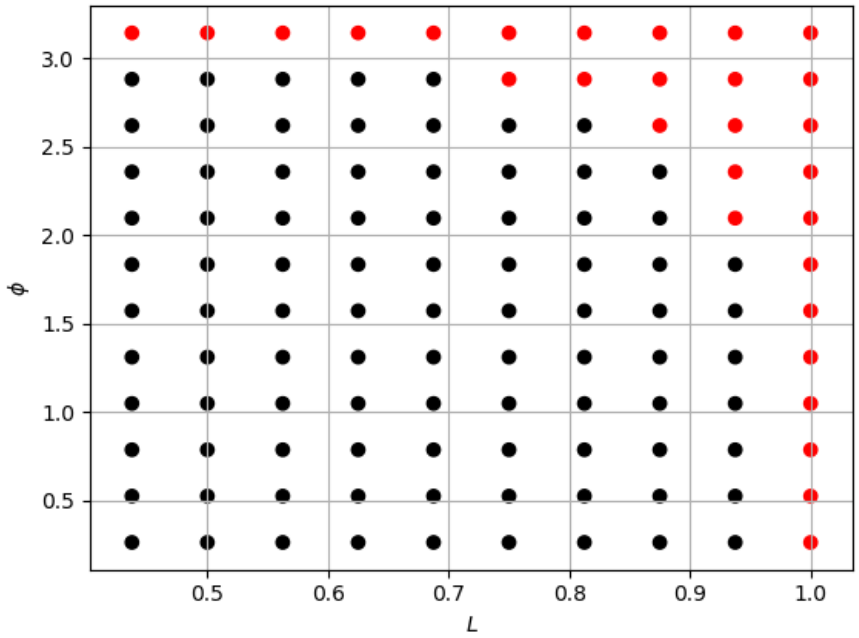

Figure 4.3: Plot displaying the regions of exchange/direct scattering.

There, red marks indicate exchange scattering and black marks indicate direct scattering. First we note the large region of direct scattering as opposed to the region of exchange scattering. We see that exchange scattering occurs more as $\phi \to \pi$, up to the limit $\phi = \pi$ where we observe exchange scattering regardless of the value of L. As discussed previously this is due to $\phi = \pi$ representing a "head on" collision, where the relative dynamics is the same regardless of the value of L. We also observe exchange scattering more as $L \to 1$, and again observing exchange scattering at the limit point $L = 1$ regardless of the value of ϕ. This is interesting, as we have here shown that there exists certain values of a given parameter L or ϕ whereupon the type of scattering we observe is not affected by the value of our other parameter. Whilst the same relative collision was observed in the case of $\phi = \pi$ for all values of L, it is noteworthy that we will observe a different collisions with different scattering dynamics with $L = 1$ as ϕ is varied.

4.2.2 Scattering Angles

As previously done in the three vortex collision we wish to investigate the angle of deflection, by varying the parameters ϕ and L as done previously we calculate the angle of deflection of vortex 1 with respect to the origin for each case of ϕ and L, and here notate the scattering angle as θ. Note that due to the results found in the previous section (i.e. the range of parameters we are considering is dominated by direct scattering) we will from here restrict the range of ϕ further, from here we will only consider ϕ in the range $[\pi/2, \pi)$. We notate this data elegantly as a heat map in Fig. 4.4:

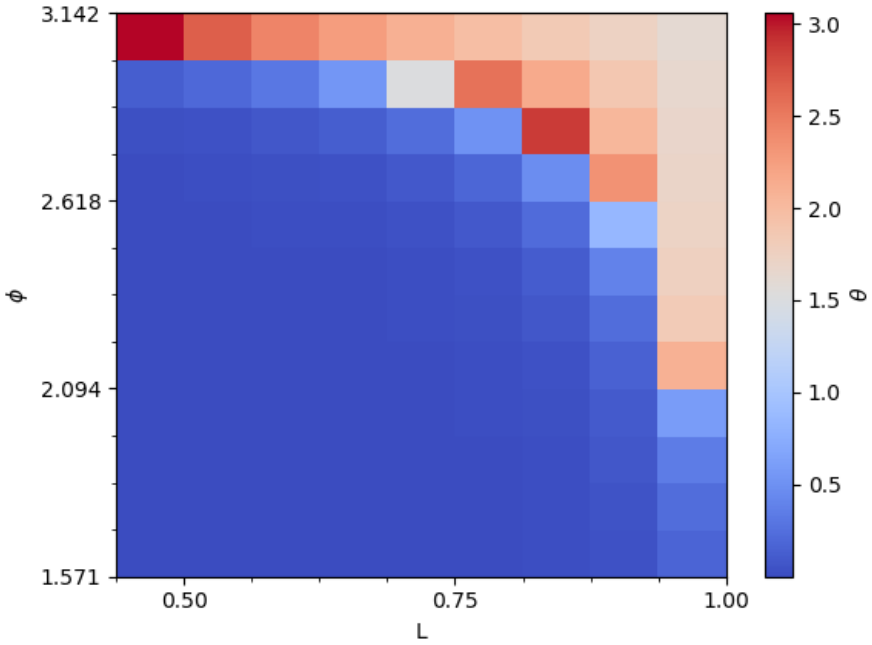

Figure 4.4: Heat map of the scattering angles in the four vortex case.

We note the large amount of space whereupon barely any scattering take place i.e. where $\theta \approx 0$. For example in the region where $L < 0.75$, we note that the dipoles pass each other with barely any effect on each other, other than when ϕ is very close to the limit case $\phi = \pi$. We see also when comparing to Fig. 4.3 that in general the deflection angle is greatest when exchange scattering occurs, compared to the direct scattering where only small deflection is observed. It is also evident that the most scattering occurs with $\phi \approx \pi$, this is to be expected as this represents where dipoles form a more head on collision and so greater scattering effects are observed as they interact. This also shows that scattering angle in the four vortex case is then more dependent upon the angle of incidence ϕ rather than the proportion of the dipole lengths L. Overall we note the scattering is much more regular than perhaps other four vortex dipole collisions where $\kappa_1 \neq \kappa_3$ and $\kappa_2 \neq \kappa_4$, indeed Aref's so-called vortex chattering cannot be observed here. With that said there seems to be large jumps in the scattering angle θ at certain points as the incidence angle ϕ increases, the most prominent occurring at $L = 0.875, \phi = 2.87979$ and $L = 0.5, \phi = 3.01069$. By examining Fig. 4.3 we see that this sudden increase in scattering angle tends to occur at the border of the direct scattering and exchange scattering regions. Indeed, there seems to be a sudden increase in scattering angle at every point on the direct/exchange boundary, after which the scattering angle θ tends to $\theta = \pi/2$ as $\phi \to \pi$. Strangely however, this sudden jump also appears on the boundary $L = 1$, which as discussed is a region of purely exchange scattering. It is as of yet unclear what vortex dynamics must occur at these boundaries of direct and exchange scattering, we found in the three-vortex case that these correspond to rigid-body rotation, but as discussed this is not possible here so the answer is not quite so simple. It is noteworthy however that in the paper by Aref analyzing three vortex motion he observes a self-similar vortex collapse, it is possible that as rigid body rotation is not possible that this collapse is maybe responsible for the behaviour observed at region boundaries.

4.2.3 Minimum Lengths

Finally we consider the minimum lengths over the entirety of each vortex evolution as done in the dipole-vortex collision. We vary the parameters L and ϕ as before and plot our results again as heatmaps in Fig. 4.5:

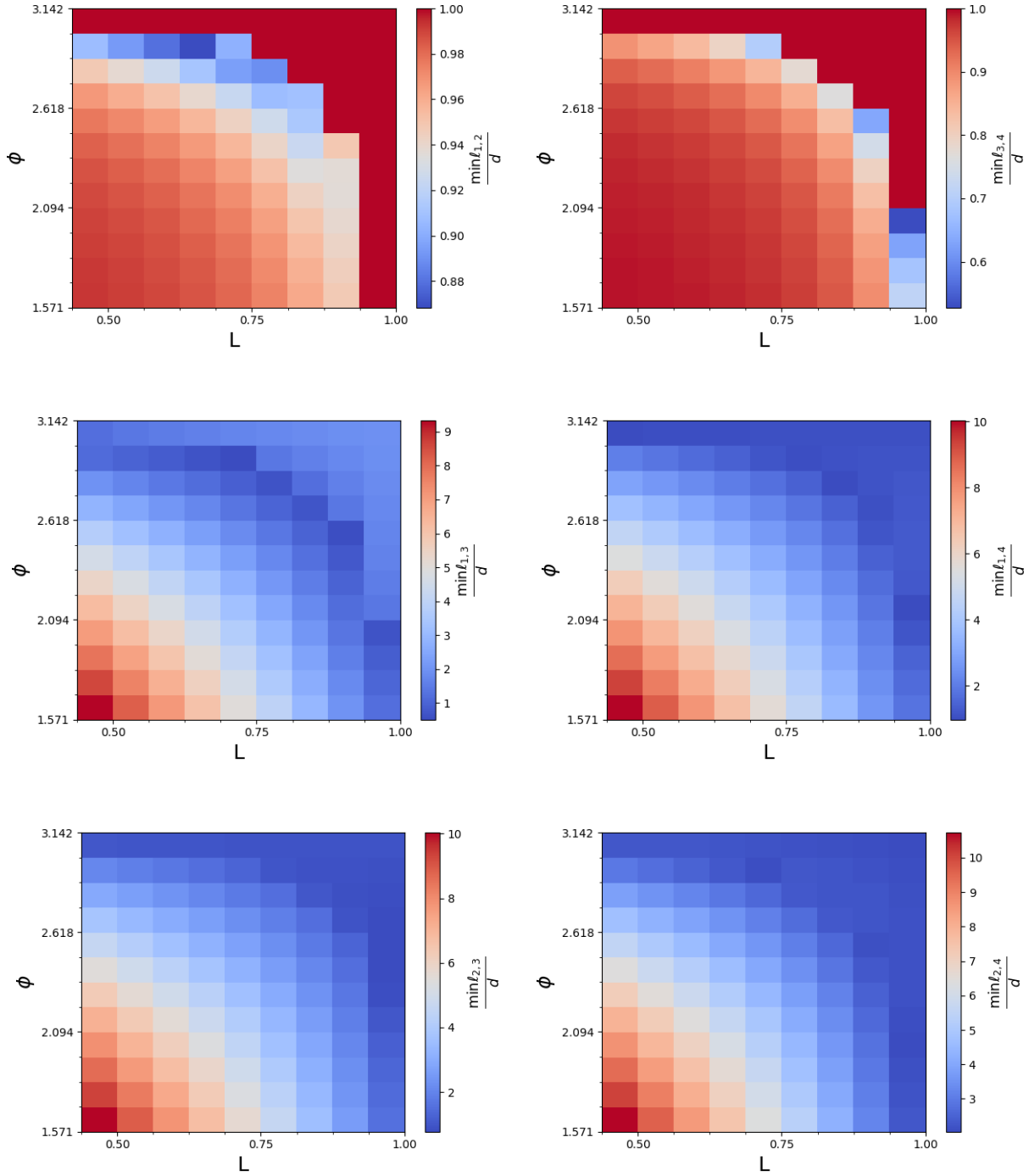

Figure 4.5: Minimum length heatmaps in the four vortex case.

Despite the four vortex collision being defined by six relative separations, we note that the minimum length plots all take very similar forms. We see that the heat maps for the minimum length of $\ell_{1,2}$ and minimum length of $\ell_{3,4}$ both illustrate roughly the same results in the respective scattering regions, as well as lengths $\ell_{1,3}, \ell_{1,4}, \ell_{2,3}$, and $\ell_{3,4}$ all displaying similar

results. Intuitively this should be obvious, as the lengths that give similar heatmaps are more or less corresponding to the same separations (e.g. $\ell_{1,2}$ and $\ell_{3,4}$ both refer to the separation of the initial dipoles). Indeed, we see that the minimum lengths for the four vortex case can be summarized in only two basic forms, the form given by the dipole separations $\ell_{1,2}$ and $\ell_{3,4}$, and the form given by separations from vortices of one dipole to vortices of the other. We also note some interesting features regarding the regions observed. Namely we see that the minimum lengths of each separation is at the absolute lowest respective value in each case at the boundary of direct scattering and exchange scattering, whereas the largest minimum separation occurs in the bottom left corner of each heatmap, this makes sense as in this region the dipoles essentially miss each other completely. Also, we note that the minimum length of every vortex separation in the exchange scattering region is $\approx d$, this also makes sense due to the exchanging of dipoles and relaxation to the initial dipole length. Exceptions to this are found in the separations of vortices with the same circulation, i.e. $\ell_{1,3}$ and $\ell_{2,4}$. This again is intuitively obvious, as vortices with the same circulation cannot form a dipole and so the dipole separation is never reached. As we see the minimum lengths become less than the initial dipole separation length in the direct scattering region, and the minimum separations converge to the initial dipole separation in the exchange scattering case, there is a strong analogy to the minimum lengths in the three-vortex case, when the same overall behavior was observed. We notice strange behavior in the case of $\ell_{3,4}$, whereupon in the region $L = 1, \phi < 2.094$ we see an extremely sudden drop in the minimum length values much below the expected d value, even more strangely this particular behavior is not seen in the minimum lengths of the other dipole separation $\ell_{1,2}$. Interestingly this sudden drop occurs at the same parameters that the sudden jump in scattering angle occurred at, and the minimum length appears to be close to the value $0.5d$, which was the exact value observed in the boundary between direct scattering and exchange scattering in the three vortex case. Again this may be hinting that the case of vortex collapse as mentioned by Aref occurs in this region, or at least some other form of atypical motion. Clearly understanding of the dipole-dipole case is hidden in the behavior of the collision at these critical points, it is then important in future to simulate these regions specifically in order to better understand the results observed here.

Chapter 5

Conclusions

5.1 Final Statements

Over the course of this review we have built an understanding of the dynamics of the two vortex dipole propagation and of the extensions thereof. In chapter 1 we note the fundamentals of fluid turbulence, the interesting case of quantum turbulence and the analogy of point vortex dynamics to this. In chapter 2 we detailed the basic principles of point vortex motion in the general case and explained the numerical method used in order to solve the point vortex system. We also use this system to briefly investigate the two vortex system as a way of conducting numerical diagnostics. We found our numerical method to be very reliable when compared to analytial calculations and thus the algorithm is suitable for use in the more complicated vortex systems to be considered later. We also use our algorithm to form animations that can be useful in visualizing the dynamics of vortices that otherwise would not be possible. In chapter 3 we look at the specific case of a dipole-vortex collision, whereupon our dipole case is extended by the addition of a stationary vortex which the dipole will collide with. The procedures here are inspired in part by the work of Aref as mentioned [5]. We note however the apparent mistakes in Aref's derivation of the scattering angles, and go on to extend this work by discovering the minimum lengths and scattering lengths of the system. Hence the results in this section can be considered an extension and a correction of Aref's original work. We note the complete agreement between numerical and theoretical results in this case and so conclude our results are the definite solutions of the dipole-vortex collision. In chapter 4 we again extend the dipole case to now have the dipole approach a target point where it will collide into another dipole. We recall the non-integrability of this case as mentioned by Aref and so restrict our analysis to purely a numerical one. We solve and plot the scattering angles of the system in the form of a heat mapping of the scattering angle θ. We also note the symmetries that exist in the system about $\phi = \pi$ and $L = 1.00$. Also we acknowledge analogies to three vortex scattering, regions of atypical behavior, and the disappointing lack of chaotic motion in this case, again as predicted by Aref. This then concludes our analysis of the point vortex collisions.

5.2 Future Prospects

Here we consider the possibilities of extending the current work. Firstly, each section of the current body functions as an extension of the previous, i.e. the dipole-vortex collision acts as extension of the previously considered dipole where we place a stationary vortex in the path of the dipole and investigate the scattering, whereas in the four vortex case instead of a stationary vortex we form another dipole aimed at a target point along with the initial dipole. Thus we could continue this method of extension this time with the five vortex case and examine the behavior of the two dipoles colliding with a stationary vortex. In theory we could continue

extending the system indefinitely after these results are found, it would be interesting to observe any similarities in the results found for different N vortices, such as the similarities found in the dipole-vortex and dipole-dipole collision for example. This procedure however has some caveats, namely the increasingly complexity of the system after each additional vortex. Each vortex added results in an additional 2 iterations of the Dormand-Prince algorithm at each time point as the algorithm has to solve for an additional x and y coordinate. This will result in a substantial increase in runtime after every vortex addition, so this method of extension quickly becomes unfeasible. Nevertheless it would be interesting to see our method to higher vortex systems and noting the results.

It is also important to realize that the examples we have here considered only hold for a specific case of point vortex scattering, namely in the case of an infinite domain, in other words x_i and y_i of each vortex are allowed to be any real number. This of course does not have to be the case, as for example point vortices on a sphere have before been considered. Of particular interest is the case of periodic boundaries. This involves calculating the dynamics of vortices as before but this time vortices will be contained within a periodic box (torus). The equations of motions were discussed by Weiss and McWilliams [50], again as a Hamiltonian system given by the equations:

$$\dot{x}_i = -\frac{1}{4\pi}\sum_{j}^{N\prime}\kappa_j\Big[\sum_{m=-\infty}^{m=\infty}\frac{\sin(y_{i,j})}{\cosh(x_{i,j})-2\pi m)-\cos(y_{i,j})}\Big],$$
$$\dot{y}_i = -\frac{1}{4\pi}\sum_{j}^{N\prime}\kappa_j\Big[\sum_{m=-\infty}^{m=\infty}\frac{\sin(x_{i,j})}{\cosh(y_{i,j})-2\pi m)-\cos(x_{i,j})}\Big].$$

These can be derived from the same Hamilton canonical equations (2.3) as before with the Hamiltonian being given by:

$$H = -\frac{1}{4\pi}\sum_{i,j}^{N\prime}\kappa_i\kappa_j\Bigg[\sum_{m=-\infty}^{\infty}\ln\Big[\frac{\cosh(x_{i,j}-2\pi m)-\cos(y_{i,j})}{\cosh(2\pi m)}\Big]-\frac{x_{i,j}}{2\pi}\Bigg].$$

The goal of analysis here is to derive as before the key quantities and compare these to the infinite motion case to see how it differs (if at all).

Also we note the limited scope of the investigation into the dipole-dipole collision in the current work. We observe regions of atypical behavior in certain regions, as well as generally near the direct/exchange scattering boundary. This therefore should warrant further investigation in order to determine what is actually happening at these points, whether it is the phenomenon of self-similar vortexl collapse as described by Aref or something else entirely. There are also similar four-vortex collisions that exist that have not been investigated here. As already mentioned there exists the dipole-dipole integrable case, this can be considered similar to the dipole-vortex collision with one single impact parameter ρ. It is also possible to investigate the dynamics of the dipole colliding with two identical rotating point vortices. Alternatively it is possible to consider systems with more general κ values. Such a system is then not analogous to quantum turbulence, as in the case of quantum turbulence circulations are quantized, but doing this may instead provide better insight into the point vortex system.

Finally, as one of the main motivations in the study of point vortices is the analogy to quantum vortices, a sensible continuation of the research would be direct modelling of the quantum point vortices specifically. This would involve numerically solving the 2D Gross-Pitaevskii equation, similar to what has been done before by Griffin in the analysis of a dipole in a BEC being scattered by an impurity [51]. Note the similarity to the periodic boundary case (the Gross-Pitaevskii requires periodic boundaries to ensure periodicity of the wave-function).

Ultimately it will be interesting to analyze the closeness to point vortex dynamics in this case. It is also of interest to see if we can recover phenomena of sound and vortex annihilation in these simulations.

Bibliography

[1] Andrew W. Baggaley, Jason Laurie, and Carlo F. Barenghi. Vortex-density fluctuations, energy spectra, and vortical regions in superfluid turbulence. *Physical Review Letters.*, 109:205304, 2012.

[2] N. A. Worth and T. B. Nickels. Some characteristics of thin shear layers in homogeneous turbulent flow. *Philosophical Transactions of the Royal Society of London A: Mathematical, Physical and Engineering Sciences*, 369:709–722, 2011.

[3] J. Kim, P. Moin, and R. Moser. Turbulence statistics in fully developed channel flow at low Reynolds number. *Journal of Fluid Mechanics*, 177:133166, 1987.

[4] C. G. Speziale, S. Sarkar, and T. B. Gatski. Modelling the pressure-strain correlation of turbulence: an invariant dynamical systems approach. *Journal of Fluid Mechanics*, 227:245272, 1991.

[5] H. Aref. Motion of three vortices. *The Physics of Fluids*, 22(3):393–400, 1979.

[6] H. Aref. Point vortex dynamics: a classical mathematics playground. *Journal of Mathematical Physics*, 48(6), 2007.

[7] E.A. Novikov. Dynamics and statistics of a system of vortices. *Zh. Eksp. Teor. Fiz.*, 68:937–943, 1975.

[8] V.L. Streeter. *Handbook of Fluid Dynamics*. McGraw-Hill, 1st edition, 1961.

[9] D.J. Acheson. *Elementary Fluid Mechanics*. Oxford University Press, 1990.

[10] Wm. T. Ashurst, A. R. Kerstein, R. M. Kerr, and C. H. Gibson. Alignment of vorticity and scalar gradient with strain rate in simulated Navier-Stokes turbulence. *The Physics of Fluids*, 30(8):2343–2353, 1987.

[11] H. J. H. Clercx and G. J. F. van Heijst. Two-dimensional Navier-Stokes turbulence in bounded domains. *Applied Mechanics Reviews*, 62(2):020802, 2009.

[12] Z.S. She, S. Chen, G. Doolen, R. H. Kraichnan, and S. A. Orszag. Reynolds number dependence of isotropic Navier-Stokes turbulence. *Physical Review Letters*, 70:3251–3254, 1993.

[13] L. Onsager. Statistical hydrodynamics. *Il Nuovo Cimento*, 6:279–287, 1949.

[14] P.K. Newton. *The N-Vortex Problem*. Springer, 1st edition, 2001.

[15] V.L. Streeter and E.B. Wylie. *Fluid Mechanics*. Civil and Mechanical Engineering Series. McGraw-Hill, 9th edition, 1998.

[16] R. Fitzpatrick. Vortex lines, vortex tubes, and vortex filaments. http://farside.ph.utexas.edu/teaching/336L/Fluidhtml/node61.html/, 2016. [Online; accessed 15-August-2018].

[17] H. Helmholtz. Über Integrale der hydrodynamischen Gleichungen, welche den Wirbelbewegungen entsprechen. *Journal für die reine und angewandte Mathematik*, 55:25–55, 1858.

[18] A.M. Kuethe and C. Chow. *Foundations of Aerodynamics*. Wiley, 5th edition, 1998.

[19] M. Nitsche. Vortex dynamics. http://www.math.unm.edu/~nitsche/pubs/2006EMP.pdf/, 2006. [Online; accessed 20-July-2018].

[20] H. Adachi, S. Fujiyama, and M. Tsubota. Steady state of counterflow quantum turbulence: Vortex filament simulation with the full Biot-Savart law. *Physical Review B*, 81(10), 2018.

[21] Wm.T. Ashurst and D.I. Merion. Numerical study of vortex reconnection. *Physical Review Letters*, 58(16):1632–1635, 1986.

[22] J. Jiménez and W.A. Alan. On the characteristics of vortex filaments in isotrophic turbulence. *Journal of Fluid Mechanics*, 373:255–285, 1998.

[23] G. Boffetta and R.H. Ecke. Two-dimensional turbulence. *Annual Review of Fluid Mechanics*, 44:427–451, 2011.

[24] R.H. Kraichnan and D. Montgomery. Two-dimensional turbulence. *Reports on Progress in Physics*, 43(5):547, 1980.

[25] J. Laurie, G. Boffetta, G. Falkovich, I. Kolokolov, and V. Lebedev. Universal profile of the vortex condensate in two-dimensional turbulence. *Physical Review Letters*, 113:254503, 2014.

[26] C.F. Barenghi, L. Skrbek, and K.R. Sreenivasan. Introduction to quantum turbulence. *Proceedings of the National Academy of Sciences*, 111(201400033), 2014.

[27] R.P. Feynman. Chapter II Application of quantum mechanics to liquid helium. volume 1 of *Progress in Low Temperature Physics*, pages 17 – 53. Elsevier, 1955.

[28] K. W. Schwarz. Critical velocity for a self-sustaining vortex tangle in superfluid helium. *Phys. Rev. Lett.*, 50:364–367, 1983.

[29] J. Rogel-Salazar. The Gross-Pitaevksii equation and Bose-Einstein condensates. *European Journal of Physics*, 34(2), 2013.

[30] M. D. Bustamante and S. Nazarenko. Derivation of the Biot-Savart equation from the nonlinear Schrödinger equation. *Physical Review E*, 92:053019, 2015.

[31] Additional background material on the Nobel prize in physics 1996. https://www.nobelprize.org/prizes/physics/1996/advanced-information/. [Online; accessed 12-July-2018].

[32] C.J. Pethick and H. Smith. *Bose-Einstein Condensation in Dilute Gases*. Cambridge University Press, 2 edition, 2008.

[33] Makoto Tsubota. Turbulence in quantum fluids. *Journal of Statistical Mechanics: Theory and Experiment*, 2014(2), 2014.

[34] E. Madelung. Eine anschauliche Deutung der Gleichung von Schrödinger. *Naturwissenschaften*, 14:1004, 1926.

[35] S. Nazarenko and M. Onorato. Wave turbulence and vortices in bose-einstein condensation. *Physica D: Nonlinear Phenomena*, 219:1–12, 2006.

[36] M. Drela. MIT: Course number 16.03-16.04: Lecture number f6: 3d vortex filaments, lifting line theory. `https://ocw.mit.edu/courses/aeronautics-and-astronautics/16-01-unified-engineering-i-ii-iii-iv-fall-2005-spring-2006/fluid-mechanics/f06_sp.pdf`, 2005. [Online; accessed 12-July-2018].

[37] E.W. Weisstein. Wolfram mathworld: Cylindrical coordiantes. `http://mathworld.wolfram.com/CylindricalCoordinates.html`. [Online; accessed 20-September-2018].

[38] G. Kirchhoff. *Vorlesungen über Mathematische Physik*, volume 1. Leipzig, B. G. Teubner, 3rd edition, 1883.

[39] H. Goldstein, C.P. Poole, and J. Safko. *Classical Mechanics*. Addison-Wesley, 3rd edition, 2001.

[40] R.L. Burden and J.D. Faires. *Numerical Analysis*. Brooks Cole, 9th edition, 2010.

[41] J.R. Dormand and P.J. Prince. A family of embedded Runge-Kutta formulae. *Journal of Computational and Applied Mathematics*, 6(1):19–26, 1980.

[42] G. Söderling and L. Wang. Adaptive time-stepping and computational stability. *Journal of Computational and Applied Mathematics*, 185(2):225–243, 2006.

[43] Animations showing each scattering regime. `https://drive.google.com/drive/folders/1jbJcwEuGoGxTD4t98IAqsagWnYf8HjTn?usp=sharing`. [Online; accessed 23-September-2018].

[44] Mathematica product page. `https://www.wolfram.com/mathematica/`. [Online; accessed 16-July-2018].

[45] M. Abramowitz and Stegun I.A. *Handbook of Mathematical Functions with Formulas, Graphs, and Mathematical Tables*. Dover, 9 edition, 1964.

[46] G. Labahn and M. Mutrie. Reduction of elliptic integrals to Legendre normal form. `https://pdfs.semanticscholar.org/3a41/3ed6779db174ff01c0debea7f41e12a215d0.pdf/`, 1997. [Online; accessed 12-July-2018].

[47] H. Aref and M.A. Stremler. Four-vortex motion with zero total circulation and impulse. *Physics of Fluids*, 11(12):3704–3715, 1999.

[48] B. Eckhardt. Integrable four vortex motion. *Physics of Fluids*, 31(10):2796–2801, 1988.

[49] L. Tophøj and H. Aref. Chaotic scattering of two identical point vortex pairs revisited. *Physics of Fluids*, 20(9), 2008.

[50] J. B. Weiss and J. C. McWilliams. Nonergodicity of point vortices. *Physics of Fluids A: Fluid Dynamics*, 3(5):835–844, 1991.

[51] A. Griffin, G.W. Stagg, N.P. Proukakis, and C.F. Barenghi. Vortex scattering by impurities in a Bose-Einstein condensate. *Journal of Physics B: Atomic, Molecular and Optical Physics*, 50(11), 2017.

Appendix A

Derivations

A.1 Vortex Equations of Motion $\dot{x}_i$ and $\dot{y}_i$

We complete the differentiation of the Hamiltonian as such:

$$\begin{aligned}\dot{x}_i &= \frac{1}{\kappa_i}\frac{\partial H}{\partial y_i} = -\frac{1}{4\pi\kappa_i}\sum_{i,j}^{N\prime}\frac{\partial}{\partial y_i}[\kappa_i\kappa_j ln(\ell_{i,j})],\\ &= -\frac{1}{4\pi}\sum_{j}^{N\prime}\frac{2\kappa_j}{\ell_{i,j}}\frac{\partial \ell_{i,j}}{\partial y_i} = -\frac{1}{2\pi}\sum_{j}^{N}\frac{\kappa_j}{2\ell_{i,j}^2}\frac{\partial}{\partial y_i}[x_{i,j}^2 + y_{i,j}^2],\\ &= -\frac{1}{2\pi}\sum_{j}^{N\prime}\frac{\kappa_j y_{i,j}}{\ell_{i,j}^2}.\end{aligned}$$

We can complete the derivation of $\dot{y}_i$ in the same fashion to complete the equations of motion.

A.2 Momentum invariance with respect to time

Here we show that linear momentum is constant during system evolution, we also show that rotational momentum is constant, and use these facts to show that the relative motion conserved quantity R is constant with respect to motion. We first consider the linear momentums P and Q, the conservation of these can be proven using the same procedure; we begin by stating the equations for the linear momenta:

$$P = \sum_{i=1}^{N}\kappa_i x_i, \quad Q = \sum_{i=1}^{N}\kappa_i y_i. \tag{A.1}$$

We now consider the derivative of P with respect to time, the key is to note $y_{i,j} = -y_{j,i}$ which gives:

$$P=\sum_{i=1}^{N}\kappa_i x_i \implies \dot{P}=\sum_{i=1}^{N}\kappa_i\dot{x}_i=\sum_{i=1}^{N}\kappa_i\left(-\frac{1}{2\pi}\sum_{j=1}^{N}{}'\frac{\kappa_j y_{i,j}}{\ell_{i,j}^2}\right)=-\frac{1}{2\pi}\sum_{i,j}^{N}{}'\frac{\kappa_i\kappa_j y_{i,j}}{\ell_{i,j}^2},$$
$$\begin{aligned}
&=-\frac{1}{2\pi}\Bigg(\kappa_1\kappa_2\frac{y_{1,2}}{\ell_{1,2}^2}+\kappa_1\kappa_3\frac{y_{1,3}}{\ell_{1,3}^2}+\cdots+\kappa_2\kappa_1\frac{y_{2,1}}{\ell_{1,2}^2}+\cdots+\kappa_3\kappa_1\frac{y_{3,1}}{\ell_{1,3}^2}\\
&\quad+\kappa_N\kappa_{N-1}\frac{y_{N,N-1}}{\ell_{N,N-1}^2}+\cdots+\kappa_{N-1}\kappa_N\frac{y_{N-1,N}}{\ell_{N-1,N}^2}\Bigg),\\
&=-\frac{1}{2\pi}\Bigg(\kappa_1\kappa_2\frac{y_{1,2}}{\ell_{1,2}^2}+\kappa_1\kappa_3\frac{y_{1,3}}{\ell_{1,3}^2}+\cdots-\kappa_2\kappa_1\frac{y_{1,2}}{\ell_{1,2}^2}+\cdots-\kappa_3\kappa_1\frac{y_{1,3}}{\ell_{1,3}^2}\\
&\quad+\kappa_N\kappa_{N-1}\frac{y_{N,N-1}}{\ell_{N,N-1}^2}+\cdots-\kappa_{N-1}\kappa_N\frac{y_{N-1,N}}{\ell_{N,N-1}^2}\Bigg),\\
&=-\frac{1}{2\pi}\Bigg[\left(\kappa_1\kappa_2\frac{y_{1,2}}{\ell_{1,2}^2}-\kappa_2\kappa_1\frac{y_{1,2}}{\ell_{1,2}^2}\right)+\left(\kappa_1\kappa_3\frac{y_{1,3}}{\ell_{1,3}^2}-\kappa_3\kappa_1\frac{y_{1,3}}{\ell_{1,3}^2}\right)+\left(\kappa_1\kappa_2\frac{y_{1,2}}{\ell_{1,2}^2}-\kappa_2\kappa_1\frac{y_{1,2}}{\ell_{1,2}^2}\right)\\
&\quad+\cdots+\left(\kappa_N\kappa_{N-1}\frac{y_{N-1,N}}{\ell_{N,N-1}^2}-\kappa_N\kappa_{N-1}\frac{y_{N,N-1}}{\ell_{N,N-1}^2}\right)\Bigg]=0.
\end{aligned}$$

Hence the x momentum time derivative gives a sum of differences between $y_{i,j}$ lengths that are equivalent. Thus the x momentum derivative gives zero as shown. The same procedure applies for the y momentum Q.

Now for the angular momentum for M we have that:

$$\begin{aligned}
M=\sum_{i=1}^{N}\kappa_i(x_i^2+y_i^2) \implies \dot{M}&=2\sum_{i=1}^{N}\kappa_i(x_i\dot{x}_i+y_i\dot{y}_i)=2\left(\sum_{i=1}^{N}\kappa_i x_i\dot{x}_i+\sum_{i=1}^{N}\kappa_i y_i\dot{y}_i\right),\\
&=\frac{1}{\pi}\left(-\sum_{i=1}^{N}\kappa_i x_i\sum_{j}^{N}{}'\frac{\kappa_j y_{i,j}}{\ell_{i,j}^2}+\sum_{i=1}^{N}\kappa_i y_i\sum_{j}^{N}{}'\frac{\kappa_j x_{i,j}}{\ell_{i,j}^2}\right),\\
&=\frac{1}{\pi}\left(-\sum_{i,j}^{N}{}' x_i\frac{\kappa_i\kappa_j y_{i,j}}{\ell_{i,j}^2}+\sum_{i,j}^{N}{}' y_i\frac{\kappa_i\kappa_j x_{i,j}}{\ell_{i,j}^2}\right),\\
&=\frac{1}{\pi}\sum_{i,j}^{N}{}'\frac{\kappa_i\kappa_j}{\ell_{i,j}^2}[y_i(x_i-x_j)-x_i(y_i-y_j)],\\
&=\frac{1}{\pi}\sum_{i,j}^{N}{}'\frac{\kappa_i\kappa_j}{\ell_{i,j}^2}(x_iy_j-x_jy_i)=0.
\end{aligned}$$

So therefore all absolute momentums P, Q, M are conserved. We now turn our attention to the relative conserved quantity R. We show the invariance of this by first proving the relation:

$$R=\frac{1}{2}\sum_{i,j}^{N}{}'\kappa_i\kappa_j\ell_{i,j}^2=\left(\sum_{i=1}^{N}\kappa_i\right)M-P^2-Q^2.$$

We have that:

$$
\begin{aligned}
R &= \frac{1}{2}\sum_{i,j}^{N}{}' \kappa_i\kappa_j\ell_{i,j}^2 = \frac{1}{2}\sum_{i,j}^{N}{}' \kappa_i\kappa_j[x_i^2+y_i^2+x_j^2+y_j^2-2(x_ix_j+y_iy_j)],\\
&= \sum_{i,j}^{N}{}' \kappa_i\kappa_j(x_j^2+y_j^2) - \sum_{i,j}^{N}{}' \kappa_i\kappa_j(x_ix_j+y_iy_j),\\
&= \sum_{i,j}^{N}{}' \kappa_i\kappa_j(x_j^2+y_j^2) + \sum_{i=1}^{N}\kappa_i^2x_i^2 - \sum_{i=1}^{N}\kappa_i^2x_i^2 + \sum_{i=1}^{N}\kappa_i^2y_i^2 - \sum_{i=1}^{N}\kappa_i^2y_i^2 - \sum_{i,j}^{N}{}' \kappa_i\kappa_j(x_ix_j+y_iy_j),\\
&= \sum_{i,j}^{N}\kappa_i\kappa_j(x_j^2+y_j^2) - \left(\sum_{i=1}^{N}\kappa_i^2x_i^2 + \sum_{i,j}^{N}{}' \kappa_i\kappa_jx_ix_j\right) - \left(\sum_{i=1}^{N}\kappa_i^2y_i^2 + \sum_{i,j}^{N}{}' \kappa_i\kappa_jy_iy_j\right),\\
&= \sum_{i=1}^{N}\kappa_i\sum_{j=1}^{N}\kappa_j(x_i^2+y_i^2) - \left(\sum_{i=1}^{N}\kappa_ix_i\right)^2 - \left(\sum_{i=1}^{N}\kappa_iy_i\right)^2,\\
&= \left(\sum_{i=1}^{N}\kappa_i\right)M - P^2 - Q^2.
\end{aligned}
$$

It is then easy to show the invariance of R from this identity as:

$$
R = \left(\sum_{i=1}^{N}\kappa_i\right)M - P^2 - Q^2 \implies \dot{R} = \left(\sum_{i=1}^{N}\kappa_i\right)\dot{M} - 2P\dot{P} - 2Q\dot{Q}.
$$

We have already found that $\dot{P} = \dot{Q} = \dot{M} = 0$ so therefore each term on the right side of the equality above vanishes so finally:

$$
\dot{R} = 0.
$$

As corollary to this we also have that the center of vorticity $\boldsymbol{x}_\Omega$ is constant with respect to time as:

$$
\boldsymbol{x}_\Omega = \frac{1}{\sum_{i=1}^{N}\kappa_i}(P,Q) \implies \frac{d}{dt}\boldsymbol{x}_\Omega = \frac{1}{\sum_{i=1}^{N}\kappa_i}(\dot{P},\dot{Q}) = (0,0).
$$

Hence the center of vorticity does not depend upon time and so is a fixed point in the fluid flow.

A.3 Equation of Motion of $\ell_{i,j}^2$

$$
\begin{aligned}
&\ell_{i,j}^2 = x_{i,j}^2 + y_{i,j}^2,\\
\implies &\frac{d\ell_{i,j}^2}{dt} = \frac{d}{dt}x_{i,j}^2 + \frac{d}{dt}y_{i,j}^2 = 2x_{i,j}\frac{d}{dt}x_{i,j} + 2y_{i,j}\frac{d}{dt}y_{i,j}.
\end{aligned}
$$

Use (2.3) with above so therefore:

$$\ell_{i,j}^2 = 2x_{i,j}\left(-\frac{1}{2\pi}\right)\left(\sum_k^N{}' \kappa_k \frac{y_{i,k}}{\ell_{i,k}^2} - \sum_k^N{}' \kappa_k \frac{y_{j,k}}{\ell_{j,k}^2}\right) + 2y_{i,j}\left(-\frac{1}{2\pi}\right)\left(\sum_k^N{}' \kappa_k \frac{x_{j,k}}{\ell_{j,k}^2} - \sum_k^N{}' \kappa_k \frac{x_{i,k}}{\ell_{i,k}^2}\right),$$
$$= \frac{1}{\pi}\sum_k^N{}'' \kappa_k \left(\frac{x_{i,j}y_{j,k} - x_{j,k}y_{i,j}}{\ell_{j,k}^2} - \frac{x_{i,j}y_{i,k} - x_{i,k}y_{i,j}}{\ell_{i,k}^2}\right).$$

Focusing on the term inside the sum. Factoring out $(\frac{1}{\ell_{j,k}^2} - \frac{1}{\ell_{i,k}^2})$ we have:

$$= \left(\frac{1}{\ell_{j,k}^2} - \frac{1}{\ell_{i,k}^2}\right)\frac{1}{\ell_{i,k}^2 - \ell_{j,k}^2}\left(\ell_{i,k}^2(x_{j,k}y_{i,j} - x_{i,j}y_{j,k}) - \ell_{j,k}^2(x_{i,j}y_{i,k} - x_{i,k}y_{i,j})\right).$$

Now using Cramer's rule for the area of a triangle (Here A is the area of the triangle):

$$2A = \pm\begin{vmatrix} x_i & y_i & 1 \\ x_j & y_j & 1 \\ x_k & y_k & 1 \end{vmatrix}.$$

Note that by definition the determinant is multilinear i.e. the following holds:

$$2A = \pm\begin{vmatrix} x_i & y_i & 1 \\ x_j & y_j & 1 \\ x_k & y_k & 1 \end{vmatrix} = \pm\begin{vmatrix} x_{i,j} & y_{i,j} & 1 \\ 0 & 0 & 1 \\ x_{k,j} & y_{k,j} & 1 \end{vmatrix} = \pm\begin{vmatrix} 0 & 0 & 1 \\ x_{j,i} & y_{j,i} & 1 \\ x_{k,i} & y_{k,i} & 1 \end{vmatrix}.$$

Where again the $\pm$ is selected such that 2A is positive. Using the above we have

$$\left(\frac{1}{\ell_{j,k}^2} - \frac{1}{\ell_{i,k}^2}\right)\frac{1}{\ell_{i,k}^2 - \ell_{j,k}^2}(\ell_{i,k}^2(x_{j,k}y_{i,j} - x_{i,j}y_{j,k}) - \ell_{j,k}^2(x_{i,j}y_{i,k} - x_{i,k}y_{i,j})),$$
$$= \left(\frac{1}{\ell_{j,k}^2} - \frac{1}{\ell_{i,k}^2}\right)\frac{1}{\ell_{i,k}^2 - \ell_{j,k}^2}(2A\sigma\ell_{i,k}^2 - 2A\sigma\ell_{j,k}^2) = 2A\sigma\left(\frac{1}{\ell_{j,k}^2} - \frac{1}{\ell_{i,k}^2}\right).$$

Where σ is chosen between -1 and 1 such that $2A\sigma$ is always positive. To determine this consider an arbitrary triangle with vertices i,j,k and applying the determinant.

$$\begin{vmatrix} x_i & y_i & 1 \\ x_j & y_j & 1 \\ x_k & y_k & 1 \end{vmatrix}.$$

We find that for an arbitrary triangle of i,j,k as vertices then

$$\sigma_{i,j,k} = \begin{cases} -1 & \text{if } (i,j,k) \text{ appear clockwise,} \\ 1 & \text{if } (i,,k) \text{ appear anticlockwise.} \end{cases}$$

So finally combining the above we achieve the required result as:

$$\ell_{i,j}^2 = \frac{2}{\pi}\sum_{k}^{N}{}'' \kappa_k \sigma_{i,j,k} A_{i,j,k}\left(\frac{1}{\ell_{j,k}^2} - \frac{1}{\ell_{i,k}^2}\right).$$

A.4 $\frac{\rho}{d} < 0$ Critical Lengths

In the case that $\frac{\rho}{d} < 0$ we have that $\ell_{1,3}^* = \ell_{1,2}^* + \ell_{2,3}^*$. We also have the conserved quantities:

$$\begin{aligned}\tilde{H} &= \frac{\ell_{1,2}}{\ell_{1,3}\ell_{2,3}},\\ R &= \ell_{1,2}^2 - \ell_{1,3}^2 - \ell_{2,3}^2.\end{aligned}$$

Applying our collinearity constraint:

$$\begin{aligned}\tilde{H} = \frac{\ell_{1,2}^*}{(\ell_{1,2}^* + \ell_{2,3}^*)\ell_{2,3}^*} \implies (\ell^{*2}_{2,3} + \ell_{1,2}^*\ell_{2,3}^*)\tilde{H} = \ell_{1,2}^*,\\ R = \ell^{*2}_{1,2} - (\ell_{1,2}^* + \ell_{2,3}^*)^2 - \ell^{*2}_{2,3} = -2(\ell^{*2}_{2,3} + \ell_{1,2}^*\ell_{2,3}^*).\end{aligned}$$

Solving these equations we have:

$$\ell_{1,2}^* = -\frac{R\tilde{H}}{2}.$$

Now note that using the above we have that:

$$\begin{aligned}\tilde{H}\ell^{*2}_{2,3} - \frac{R\tilde{H}^2}{2}\ell_{2,3}^* + \frac{R\tilde{H}}{2} = 0,\\ \implies \ell_{2,3}* = \frac{\frac{R\tilde{H}^2}{2} \pm \sqrt{\frac{R^2\tilde{H}^4}{4} - 4\tilde{H}\frac{R\tilde{H}}{2}}}{2\tilde{H}},\\ = \frac{R\tilde{H}}{4} + \frac{1}{2}\sqrt{R\left(\frac{R\tilde{H}^2}{4} - 2\right)}.\end{aligned}$$

And finally using the constraint $\ell_{1,3}^* = \ell_{1,2}^* + \ell_{2,3}^*$ we have:

$$\begin{aligned}\ell_{1,3}^* = -\frac{R\tilde{H}}{2} + \frac{R\tilde{H}}{4} \pm \frac{1}{2}\sqrt{R\left(\frac{R\tilde{H}^2}{4} - 2\right)},\\ = -\frac{R\tilde{H}}{4} + \frac{1}{2}\sqrt{R\left(\frac{R\tilde{H}^2}{4} - 2\right)}.\end{aligned}$$

Where positive roots are chosen such that lengths cannot be negative. Now note that:

$$\begin{aligned}\tilde{H} = \frac{\sqrt{(\rho + \frac{3d}{2})^2 + L^2}}{d\sqrt{(\rho + \frac{d}{2})^2 + L^2}},\\ R = 2\rho d + d^2.\end{aligned}$$

So by substitution we have that:

$$\ell^*_{1,2} = -\frac{(2\rho d + d^2)\sqrt{(\rho + \frac{3d}{2})^2 + L^2}}{2d\sqrt{(\rho + \frac{d}{2})^2 + L^2}} = -\left(\rho + \frac{d}{2}\right)\frac{\sqrt{\frac{\rho^2}{L^2} + 3\frac{\rho d}{L^2} + \frac{9}{4}\frac{d^2}{L^2} + 1}}{\sqrt{\frac{\rho^2}{L^2} + \frac{\rho d}{L^2} + \frac{1}{4}\frac{d^2}{L^2} + 1}},$$

$$\ell^*_{2,3} = \left(\frac{\rho + \frac{d}{2}}{2}\right)\frac{\sqrt{\frac{\rho^2}{L^2} + 3\frac{\rho d}{L^2} + \frac{9}{4}\frac{d^2}{L^2} + 1}}{\sqrt{\frac{\rho^2}{L^2} + \frac{\rho d}{L^2} + \frac{1}{4}\frac{d^2}{L^2} + 1}} + \frac{1}{2}\sqrt{(2\rho d + d^2)(\frac{[2\rho d + d^2][(\rho + \frac{3d}{2})^2 + L^2]}{4d^2[(\rho + \frac{d}{2})^2 + L^2]} - 2)}.$$

Now note that by definition of our system $\rho \ll L$ and $d \ll L$ so therefore:

$$\lim_{L\to\infty}\frac{\rho}{L} = 0, \quad \lim_{L\to\infty}\frac{d}{L} = 0.$$

So we have that

$$\lim_{L\to\infty}\frac{\sqrt{\frac{\rho^2}{L^2} + 3\frac{\rho d}{L^2} + \frac{9}{4}\frac{d^2}{L^2} + 1}}{\sqrt{\frac{\rho^2}{L^2} + \frac{\rho d}{L^2} + \frac{1}{4}\frac{d^2}{L^2} + 1}} = 1.$$

Using this in the limit as $L \to \infty$ our lengths become:

$$\begin{aligned}
\ell^*_{1,2} &= -\frac{2\rho + d}{2} + \mathcal{O}\left(\left(\frac{\rho}{d}\right)^2\right) + \mathcal{O}\left(\left(\frac{d}{L}\right)^2\right), \\
\ell^*_{2,3} &= \frac{2\rho + d}{4} + \frac{1}{2}\sqrt{\frac{(2\rho d + d^2)^2}{4d^2} - 4\rho d - 2d^2} + \mathcal{O}\left(\left(\frac{\rho}{L}\right)^2\right) + \mathcal{O}\left(\left(\frac{d}{L}\right)^2\right), \\
&= \frac{2\rho + d}{4} + \frac{1}{4}\sqrt{4\rho^2 - 7d^2 - 12\rho d} + \mathcal{O}\left(\left(\frac{\rho}{L}\right)^2\right) + \mathcal{O}\left(\left(\frac{d}{L}\right)^2\right), \\
\ell^*_{1,3} &= \ell^*_{1,2} + \ell^*_{2,3} = -\frac{2\rho + d}{4} + \frac{1}{4}\sqrt{4\rho^2 - 7d^2 - 12\rho d} + \mathcal{O}\left(\left(\frac{\rho}{L}\right)^2\right) + \mathcal{O}\left(\left(\frac{d}{L}\right)^2\right).
\end{aligned}$$

From here we will continue to use the fact that:

$$\lim_{L\to\infty}\tilde{H} = \frac{1}{d}.$$

A.5 $0 < \frac{\rho}{d} < \frac{9}{2}$ Critical Lengths

Here we have the case of exchange scattering giving the constraint:

$$\ell^*_{1,3} = \ell^*_{2,3} = \ell^*.$$

Using this with our constraints we have that:

$$\begin{aligned}
\tilde{H} &= \frac{\ell_{1,2}}{{\ell^*}^2}, \\
R &= {\ell^*_{1,2}}^2 - 2{\ell^*}^2.
\end{aligned}$$

Solving this we have:

$$\tilde{H}{\ell^*}_{1,2}^2 - 2\ell^*_{1,2} - R\tilde{H} = 0 \implies \ell^*_{1,2} = \frac{2 + \sqrt{4 + 4R\tilde{H}^2}}{2\tilde{H}} = \frac{1}{\tilde{H}} + \sqrt{\frac{1}{\tilde{H}^2} + R}.$$

Where there is a positive root as to avoid the length becoming negative. This gives the other ℓ^* lengths as:

$$\ell^* = \sqrt{\frac{1}{\tilde{H}^2} + \frac{1}{\tilde{H}}\sqrt{\frac{1}{\tilde{H}^2} + R}}.$$

Where again as we are talking about a length the positive root must be taken. As before we take the limit as $L \to \infty$ to find:

$$\ell^*_{1,2} = d + \sqrt{2d(\rho + d)} + \mathcal{O}\left(\left(\frac{\rho}{d}\right)^2\right) + \mathcal{O}\left(\left(\frac{d}{L}\right)^2\right),$$
$$\ell^* = \sqrt{d^2 + d\sqrt{2\rho d + 2d^2}} + \mathcal{O}\left(\left(\frac{\rho}{d}\right)^2\right) + \mathcal{O}\left(\left(\frac{d}{L}\right)^2\right).$$

A.6 $\frac{\rho}{d} > \frac{9}{2}$ Critical Lengths

This gives the condition that $\ell^*_{1,2} = \ell^*_{1,3} + \ell^*_{2,3}$. With our constraints this gives:

$$\tilde{H} = \frac{\ell^*_{1,2}}{\ell^*_{1,3}(\ell^*_{1,2} - \ell^*_{1,3})},$$
$$R = 2\ell^*_{1,2}\ell^*_{1,3} - 2{\ell^*}_{1,3}^2.$$

Solving this gives:

$$\ell^*_{1,2} = \frac{R\tilde{H}}{2}.$$

Now using the above we have:

$$2{\ell^*}_{1,3}^2 - R\tilde{H}\ell^*_{1,3} + R = 0,$$
$$\implies \ell^*_{1,3} = \frac{R\tilde{H} \pm \sqrt{R^2\tilde{H}^2 - 8R}}{4}.$$

Also:

$$\ell^*_{2,3} = \ell^*_{1,2} - \ell^*_{1,3} = -\frac{R\tilde{H}}{4} \mp \frac{1}{4}\sqrt{R^2\tilde{H}^2 - 8R}.$$

We must take the megative root of $\ell^*_{1,3}$ so that $\ell^*_{2,3}$ is not negative. We again take the expansion as $L \to \infty$ to get:

$$\ell_{1,2}^* = \frac{2\rho+d}{2} + \mathcal{O}\left(\left(\frac{\rho}{d}\right)^2\right) + \mathcal{O}\left(\left(\frac{d}{L}\right)^2\right),$$
$$\ell_{1,3}^* = \frac{2\rho+d}{4} - \frac{1}{4}\sqrt{4\rho^2 - 12\rho d - 15d^2} + \mathcal{O}\left(\left(\frac{\rho}{d}\right)^2\right) + \mathcal{O}\left(\left(\frac{d}{L}\right)^2\right),$$
$$\ell_{2,3}^* = -\frac{2\rho+d}{4} + \frac{1}{4}\sqrt{4\rho^2 - 12\rho d - 15d^2} + \mathcal{O}\left(\left(\frac{\rho}{d}\right)^2\right) + \mathcal{O}\left(\left(\frac{d}{L}\right)^2\right).$$

A.7 C Time Invariance

We show that C is invariant with respect to time:

$$C = -\frac{1}{3}(\ell_{1,2}^2 - \ell_{2,3}^2 - \ell_{1,3}^2) \implies \frac{d}{dt}C = -\frac{1}{3}(\frac{d}{dt}\ell_{1,2}^2 - \frac{d}{dt}\ell_{2,3}^2 - \frac{d}{dt}\ell_{1,3}^2).$$

By subsitution (3.2) we see:

$$\begin{aligned}
\frac{d}{dt}C &= -\frac{1}{3}\big[-\frac{2}{\pi}\sigma_{1,2,3}A\left(\frac{1}{\ell_{2,3}^2} - \frac{1}{\ell_{1,3}^2}\right) - \frac{2}{\pi}\sigma_{2,3,1}A\left(\frac{1}{\ell_{1,3}^2} - \frac{1}{\ell_{1,2}^2}\right) - \frac{2}{\pi}\sigma_{1,3,2}A\left(\frac{1}{\ell_{2,3}^2} - \frac{1}{\ell_{1,2}^2}\right)\big], \\
&= \frac{2A}{3\pi}\big[\sigma_{1,2,3}\left(\frac{1}{\ell_{2,3}^2} - \frac{1}{\ell_{1,3}^2}\right) + \sigma_{2,3,1}\left(\frac{1}{\ell_{1,3}^2} - \frac{1}{\ell_{1,2}^2}\right) + \sigma_{1,3,2}\left(\frac{1}{\ell_{2,3}^2} - \frac{1}{\ell_{1,2}^2}\right)\big], \\
&= \frac{2A}{3\pi}\big[-\frac{1}{\ell_{1,2}^2}(\sigma_{1,3,2} + \sigma_{2,3,1}) + \frac{1}{\ell_{1,3}^2}(\sigma_{2,3,1} - \sigma_{1,2,3}) + \frac{1}{\ell_{2,3}^2}(\sigma_{1,2,3} + \sigma_{1,3,2})\big].
\end{aligned}$$

Note that by definition $\sigma_{1,2,3} = \sigma_{2,3,1} = -\sigma_{1,3,2}$ so each term on the right side of the equality above gives 0. So therefore:

$$\frac{d}{dt}C = 0.$$

A.8 θ and b_m Relation

First note that

$$e^{-4\pi H} = e^{2[\ln(\ell_{1,2}) - \ln(\ell_{1,3}) - \ln(\ell_{2,3})]} = \frac{\ell_{1,2}^2}{\ell_{1,3}^2\ell_{2,3}^2}.$$

So now using our dimensionless variables:

$$\begin{aligned}
|C|e^{-4\pi H} &= -|C|\frac{b_3}{Cb_1b_2}, \\
&= \begin{cases} \frac{-b_3}{b_1b_2} & \text{if } C > 0, \\ \frac{b_3}{b_1b_2} & \text{if } C < 0. \end{cases}
\end{aligned}$$

Now note that $C > 0 \implies b_3 < 0$ and $C < 0 \implies b_3 > 0$ so therefore:

$$\theta = |C|e^{-4\pi H} = \frac{|b_3|}{b_1b_2}.$$

Finally this gives:

$$\frac{1}{\theta} = \frac{b_1 b_2}{|b_3|}.$$

A.9 Derivation of dimensionless equation of relative motion $\dot{b}_3$

We use (3.2) i.e. consider $\frac{db_3}{dt} = -\frac{1}{C}\frac{d\ell_{1,2}^2}{dt}$. Therefore using (3.16):

$$\begin{aligned}
\frac{db_3}{dt} &= \left(-\frac{1}{C}\right)\frac{2}{\pi}\kappa_3\sigma A\left(\frac{1}{\ell_{2,3}^2} - \frac{1}{\ell_{1,3}^2}\right), \\
&= \pm\frac{2}{C\pi}A\left(\frac{\ell_{1,3}^2 - \ell_{2,3}^2}{\ell_{1,3}^2\ell_{2,3}^2}\right), \\
&= \pm\frac{2}{C^2\pi}A\left(\frac{b_2 - b_1}{b_1 b_2}\right).
\end{aligned}$$

We now express the area A in terms of b_3. Using Heron's formula for the area for a triangle i.e. $A = \sqrt{r(r-\ell_{1,2})(r-\ell_{2,3})(r-\ell_{1,3})}$ where $r = \frac{1}{2}(\ell_{1,2}+\ell_{1,3}+\ell_{2,3})$. Therefore:

$$\begin{aligned}
A &= \sqrt{\left(\frac{\ell_{1,2}+\ell_{1,3}+\ell_{2,3}}{2}\right)\left(\frac{\ell_{1,3}+\ell_{2,3}-\ell_{1,2}}{2}\right)\left(\frac{\ell_{1,2}+\ell_{1,3}-\ell_{2,3}}{2}\right)\left(\frac{\ell_{2,3}+\ell_{1,2}-\ell_{1,3}}{2}\right)}, \\
&= \frac{1}{4}\sqrt{(\ell_{1,3}^2 - \ell_{1,2}^2 + \ell_{2,3}^2 + 2\ell_{2,3}\ell_{1,3})(\ell_{1,2}^2 - \ell_{2,3}^2 - \ell_{1,3}^2 + 2\ell_{2,3}\ell_{1,3})}, \\
&= \frac{1}{4}\sqrt{4\ell_{2,3}^2\ell_{1,3}^2 - (\ell_{1,3}^2 - \ell_{1,2}^2 + \ell_{2,3}^2)^2}.
\end{aligned}$$

Using (3.16) and our constraints (3.17) and (3.19) we find:

$$\begin{aligned}
A &= \frac{1}{4}\sqrt{4C^2 b_1 b_2 - (Cb_2 + Cb_3 + Cb_1)^2}, \\
&= \frac{C}{4}\sqrt{4\frac{|b_3|}{\theta} - 9}, \\
&= \frac{C}{2\sqrt{\theta}}\sqrt{|b_3| - \frac{9}{4}\theta}.
\end{aligned}$$

Focusing on the $\frac{b_2-b_1}{b_1 b_2}$ term now we have:

$$\begin{aligned}
\frac{b_2 - b_1}{b_1 b_2} &= \frac{\theta}{|b_3|}\sqrt{(b_2-b_1)^2} = \frac{\theta}{|b_3|}\sqrt{b_1^2 + b_2^2 - 2b_1 b_2}, \\
&= \frac{\theta}{|b_3|}\sqrt{(b_1+b_2+b_3)^2 - b_3^2 - 4b_1 b_2 - 2b_1 b_3 - 2b_2 b_3}, \\
&= \frac{9+\theta}{|b_3|}\sqrt{b_3^2 - 6b_3 - 4\frac{|b_3|}{\theta}}, \\
&= \frac{\theta}{|b_3|}\sqrt{(3-b_3)^2 - 4\frac{|b_3|}{\theta}}.
\end{aligned}$$

Now finally this gives:

$$\begin{aligned}\frac{db_3}{dt} &= \pm\frac{2}{C^2\pi}A\left(\frac{b_2-b_1}{b_1b_2}\right),\\ &= \pm\frac{\sqrt{\theta}}{C\pi b_3}\sqrt{(|b_3|-\frac{9}{4}\theta)\big[(3-b_3)^2-4\frac{|b_3|}{\theta}\big]}.\end{aligned}$$

With the $\pm$ cancelling the modulus of the b_3 term.

A.10 Roots of $\dot{b}_3$

We observe the equation for $\dot{b}_3$ in the $C>0$ case as:

$$\dot{b}_3 = \pm\frac{\sqrt{\theta}}{C\pi b_3}\sqrt{-\left(b_3+\frac{9}{4}\theta\right)\big[(3-b_3)^2+4\frac{b_3}{\theta}\big]}.$$

Note that it is not possible for $\theta=0$, so therefore $\dot{b}_3=0$ if and only if:

$$-\left(b_3+\frac{9}{4}\theta\right)\left[(3-b_3)^2+4\frac{b_3}{\theta}\right]=0.$$

Which implies

$$b_3+\frac{9}{4}\theta=0 \text{ or } (3-b_3)^2+4\frac{b_3}{\theta}=0$$

Already this gives the root $b_3=-(9/4)\theta=\alpha$, and by solving the quadratic we have that:

$$\begin{aligned}b_3^2+\left(\frac{4}{\theta}-6\right)b_3+9=0,&\\ \implies b_3 &= \frac{6-\frac{4}{\theta}\pm\sqrt{\left(\frac{4}{\theta}-6\right)^2-36}}{2},\\ &= 3-\frac{2}{\theta}\pm\frac{2}{\theta}\sqrt{1-3\theta}.\end{aligned}$$

Which we can factor as

$$b_3=-\frac{1}{\theta}[1\pm\sqrt{1-3\theta}]^2$$

Giving us the roots:

$$\beta=-\frac{1}{\theta}[1-\sqrt{1-3\theta}]^2,\quad \gamma=-\frac{1}{\theta}[1+\sqrt{1-3\theta}]^2.$$

We can verify the interpretation of the vortex dynamics at the roots above as such; first examine the case of colinear vortices i.e. $\ell_{1,2}=\ell_{1,3}+\ell_{2,3} \implies \ell_{1,2}^2=\ell_{1,3}^2+\ell_{2,3}^2+2\sqrt{\ell_{1,3}^2\ell_{2,3}^2}$, we apply our dimensionless b variables so that:

$$-Cb_3=Cb_1+Cb_2+2\sqrt{C^2b_1b_2} \implies -b_3=b_1+b_2+2\sqrt{b_1b_2}.$$

By applying constraints (3.17) and (3.19) to the above this gives:

$$-3=2\sqrt{\frac{-b_3}{\theta}} \implies b_3=-\frac{9}{4}\theta=\alpha.$$

Hence collinear vortex alignment corresponds to where $b_3 = \alpha$. Now examine where $\ell_{1,3} = \ell_{2,3} \implies b_1 = b_2$, if we let $b = b_1 = b_2$ the above constraints become:

$$2b + b_3 = 3, \quad b^2 = -\frac{b_3}{\theta}.$$

This gives the quadratic equation $(3 - b_3)^2 + \frac{4}{\theta} b_3 = 0$ already solved above to give:

$$b_3 = -\frac{1}{\theta}[1 \pm \sqrt{1 - 3\theta}]^2 \implies b_3 = \beta \text{ or } b_3 = \gamma.$$

Hence $b_3 = \beta$ or $b_3 = \gamma$ corresponds to where $\ell_{1,3} = \ell_{2,3}$. Following similar logic as the above gives the same result in the case of $C < 0$ and the roots $\bar{\alpha}, \bar{\beta}, \bar{\gamma}$.

A.11 Hamilton's Canonical Equations in Polar Coordinates

In cartesian coordinates we have that:

$$\kappa_i \dot{x}_i = \frac{\partial H}{\partial y_i}, \quad \kappa_i \dot{y}_i = -\frac{\partial H}{\partial x_i}.$$

Now using the polar coordinates we can say:

$$\begin{aligned} \frac{\partial H}{\partial \phi_i} = \frac{\partial H}{\partial x_i}\frac{dx_i}{d\phi_i} + \frac{\partial H}{\partial y_i}\frac{dy_i}{d\phi_i} &= -\kappa_i \dot{y}_i(-r_i \sin\phi_i) + \kappa_i \dot{x}_i(r_i \cos\phi_i), \\ &= \kappa_i(\dot{y}_i y_i + \dot{x}_i x_i). \end{aligned}$$

Now as $r_i^2 = x_i^2 + y_i^2$ we have:

$$\begin{aligned} 2r_i\dot{r}_i = 2x_i\dot{x}_i + 2y_i\dot{y}_i &\implies r_i\dot{r}_i = x_i\dot{x}_i + y_i\dot{y}_i, \\ &\implies \frac{\partial H}{\partial \phi_i} = \kappa_i r_i \dot{r}_i. \end{aligned}$$

We also have:

$$\begin{aligned} \frac{\partial H}{\partial r_i} = \frac{\partial H}{\partial x_i}\frac{dx_i}{dr_i} + \frac{\partial H}{\partial y_i}\frac{dy_i}{dr_i} &= -\kappa_i \dot{y}_i \cos\phi_i + \kappa_i \dot{x}_i \sin\phi_i, \\ &= \frac{\kappa_i}{r_i}[\dot{x}_i y_i - \dot{y}_i x_i]. \end{aligned}$$

Now examining equation for ϕ_i:

$$\begin{aligned} \phi_i = \arctan\left(\frac{y_i}{x_i}\right) \implies \dot{\phi}_i &= \frac{1}{1 + [\frac{y_i}{x_i}]^2}\frac{d}{dt}\left(\frac{y_i}{x_i}\right), \\ &= \frac{x_i^2}{x_i^2 + y_i^2}\left(\frac{\dot{y}_i}{x_i} - \frac{\dot{x}_i y_i}{x_i^2}\right) = \frac{\dot{y}_i x_i - \dot{x}_i y_i}{x_i^2 + y_i^2}. \end{aligned}$$

Therefore:

$$\frac{\partial H}{\partial r_i} = -\kappa_i r_i \dot{\phi}_i.$$

A.12 Polar Equation of Motion $\dot{\phi}_3$

Using these equations of motion we express for the third vortex angle i.e.:

$$\dot{\phi}_3 = \frac{1}{r_3}\frac{\partial H}{\partial r_3}.$$

Now using the definitions above and the cosine rule on the triangles formed by the vortices and the centre of vorticity we see that:

$$\begin{aligned}
\ell_{1,2}^2 &= r_1^2 + r_2^2 - 2r_1 r_2 \cos(\phi_1 - \phi_2),\\
\ell_{1,3}^2 &= r_1^2 + r_3^2 - 2r_1 r_3 \cos(\phi_1 - \phi_3),\\
\ell_{2,3}^2 &= r_2^2 + r_3^2 - 2r_2 r_3 \cos(\phi_2 - \phi_3).
\end{aligned}$$

We write these equations in dimensionless form, to do this we define the variables $\bar{r}_m = \frac{r_m}{\sqrt{C}}$. Using these we then have the identities as:

$$\begin{aligned}
b_1 = \frac{\ell_{2,3}^2}{C} &= \bar{r}_2^2 + \bar{r}_3^2 - 2\bar{r}_2\bar{r}_3\cos(\phi_2 - \phi_3),\\
b_2 = \frac{\ell_{1,3}^2}{C} &= \bar{r}_1^2 + \bar{r}_3^2 - 2\bar{r}_1\bar{r}_3\cos(\phi_1 - \phi_3),\\
b_3 = -\frac{\ell_{1,2}^2}{C} &= 2\bar{r}_1\bar{r}_2\cos(\phi_1 - \phi_2) - \bar{r}_1^2 - \bar{r}_2^2.
\end{aligned}$$

Now let us assume the centre of vorticity is at the origin, from the definition of centre of vorticity this gives the condition that:

$$(x_1 + x_2 - x_3, y_1 + y_2 - y_3) = (0, 0).$$

by substitution of the polar coordinates this gives:

$$\begin{aligned}
x_1 + x_2 &= x_3,\\
y_1 + y_2 &= y_3,\\
\implies r_1\cos\phi_1 + r_2\cos\phi_2 &= r_3\cos\phi_3,\\
r_1\sin\phi_1 + r_2\sin\phi_2 &= r_3\sin\phi_3,\\
\implies r_1^2\cos^2\phi_1 + r_2^2\cos^2\phi_2 + 2r_1r_2\cos\phi_1\cos\phi_2 &= r_3^2\cos^2\phi_3,\\
r_1^2\sin^2\phi_1 + r_2^2\sin^2\phi_2 + 2r_1r_2\sin\phi_1\sin\phi_2 &= r_3^2\sin^2\phi_3.
\end{aligned}$$

Adding equations gives:

$$r_3^2 = r_1^2 + r_2^2 + 2r_1r_2\cos\phi_1\cos\phi_2 + 2r_1r_2\sin\phi_1 sin\phi_2 = r_1^2 + r_2^2 + 2r_1r_2\cos(\phi_1 - \phi_2).$$

Alternatively the condition for the centre of vorticity being at origin can be expressed as:

$$\begin{aligned}
x_1 - x_3 &= -x_2,\\
y_1 - y_3 &= -y_2,\\
\implies r_1\cos\phi_1 - r_3\cos\phi_3 &= -r_2\cos\phi_2,\\
r_1\sin\phi_1 - r_3\sin\phi_3 &= -r_2\sin\phi_2,\\
\implies r_1^2\cos^2\phi_1 + r_3^2\cos^2\phi_3 - 2r_1r_3\cos\phi_1\cos\phi_3 &= r_2^2\cos^2\phi_2,\\
r_1^2\sin^2\phi_1 + r_3^2\sin^2\phi_3 - 2r_1r_3\sin\phi_1\sin\phi_3 &= r_2^2\sin^2\phi_2.
\end{aligned}$$

Again adding equations we have that:

$$r_2^2 = r_1^2 + r_3^2 - 2r_1r_3\cos\phi_1\cos\phi_3 - 2r_1r_3\sin\phi_1\sin\phi_3 = r_1^2 + r_3^2 - 2r_1r_3\cos(\phi_1 - \phi_3).$$

And by similar logic:

$$r_1^2 = r_2^2 + r_3^2 - 2r_2r_3\cos(\phi_2 - \phi_3).$$

Now by dividing through by C we get these dimensionless relations:

$$\begin{aligned}\bar{r}_1^2 &= \bar{r}_2^2 + \bar{r}_3^2 - 2\bar{r}_2\bar{r}_3\cos(\phi_2 - \phi_3),\\ \bar{r}_2^2 &= \bar{r}_1^2 + \bar{r}_3^2 - 2\bar{r}_1\bar{r}_3\cos(\phi_2 - \phi_3),\\ \bar{r}_3^2 &= \bar{r}_1^2 + \bar{r}_2^2 + 2\bar{r}_1\bar{r}_2\cos(\phi_1 - \phi_2).\end{aligned}$$

We will now express each b_m in terms of $\bar{r}_m$. We note that comparing relations above we have that:

$$b_1 = \bar{r}_1^2, \quad b_2 = \bar{r}_2^2.$$

Now as

$$b_3 = 2\bar{r}_1\bar{r}_2\cos(\phi_1 - \phi_2) - \bar{r}_1^2 - \bar{r}_2^2.$$

By substitution of the cosine term we have that

$$b_3 = \bar{r}_3^2 - 2\bar{r}_1^2 - 2\bar{r}_2^2 = \bar{r}_3^2 - 2(\bar{r}_1^2 + \bar{r}_2^2) = \bar{r}_3^2 - 2(3 - b_3).$$

By rearrangement:

$$b_3 = 6 - \bar{r}_3^2.$$

So finally:

$$\begin{aligned}b_1 &= \bar{r}_1^2,\\ b_2 &= \bar{r}_2^2,\\ b_3 &= 6 - \bar{r}_3^2.\end{aligned}$$

We now look back to our original equation for $\dot{\phi}_3$ i.e.

$$\dot{\phi}_3 = \frac{1}{r_3}\frac{\partial H}{\partial r_3}.$$

We now will introduce our dimensionless varieables into this equation using the identities:

$$\begin{aligned}\sqrt{C}\bar{r}_3 &= r_3,\\ \frac{\partial H}{\partial r_3} &= \frac{\partial \bar{r}_3}{\partial r}\frac{\partial H}{\partial \bar{r}_3} = \frac{1}{\sqrt{C}}\frac{\partial H}{\partial \bar{r}_3}.\end{aligned}$$

Therefore we have that:

$$\dot{\phi}_3 = \frac{1}{r_3}\frac{\partial H}{\partial r_3} = \frac{1}{C\bar{r}_3}\frac{\partial H}{\partial \bar{r}_3},$$
$$\implies \dot{\phi}_3 = -\frac{1}{4\pi C}\frac{1}{\bar{r}_3}\frac{\partial}{\partial \bar{r}_3}\left[2\ln(\ell_{1,2}) - 2\ln(\ell_{1,3}) - 2\ln(\ell_{2,3})\right] = \frac{1}{2\pi C}\frac{1}{\bar{r}_3}\frac{\partial}{\partial \bar{r}_3}\ln\left(\frac{\ell_{1,3}\ell_{2,3}}{\ell_{1,2}}\right),$$
$$= \frac{1}{2\pi C}\frac{1}{2\bar{r}_3}\frac{\partial}{\partial \bar{r}_3}\ln(\frac{\ell_{1,3}^2\ell_{2,3}^2}{\ell_{1,2}^2}) = \frac{1}{2\pi C}\frac{1}{2\bar{r}_3}\frac{\partial}{\partial \bar{r}_3}\ln\left(C\frac{b_1b_2}{|b_3|}\right) = \frac{1}{2\pi C}\frac{1}{2\bar{r}_3}\frac{\partial}{\partial \bar{r}_3}\ln\left(\frac{b_1b_2}{|b_3|}\right).$$

Now by differentiating and using our identity for θ we have that

$$\dot{\phi}_3 = \frac{1}{2\pi C}\frac{1}{2\bar{r}_3}\frac{\partial}{\partial \bar{r}_3}\ln\left(\frac{b_1b_2}{|b_3|}\right), = \frac{1}{2\pi C}\frac{1}{2\bar{r}_3}\frac{|b_3|}{b_1b_2}\frac{\partial}{\partial \bar{r}_3}\frac{b_1b_2}{|b_3|}$$
$$= \frac{\theta}{4\pi C}\frac{1}{\bar{r}_3}\frac{\partial}{\partial \bar{r}_3}\frac{b_1b_2}{|b_3|}.$$

Now we focus on the derivative, Using the product rule and $\bar{r}_m$ identities:

$$\frac{\partial}{\partial \bar{r}_3}\frac{b_1b_2}{|b_3|} = \frac{1}{|b_3|}[b_1\frac{\partial}{\partial \bar{r}_3}b_2 + b_2\frac{\partial}{\partial \bar{r}_3}b_1],$$
$$= \frac{1}{|b_3|}[b_1\frac{\partial}{\partial \bar{r}_3}(\bar{r}_1^2 + \bar{r}_3^2 + 2\bar{r}_1\bar{r}_3\cos(\phi_1 - \phi_3)) + b_2\frac{\partial}{\partial \bar{r}_3}(\bar{r}_2^2 + \bar{r}_3^2 + 2\bar{r}_2\bar{r}_3\cos(\phi_2 - \phi_3))],$$
$$= \frac{1}{|b_3|}[b_1(2\bar{r}_3 + 2\bar{r}_1\cos(\phi_1 - \phi_3)) + b_2(2\bar{r}_3 + 2\bar{r}_2\cos(\phi_2 - \phi_3))],$$
$$= \frac{1}{\bar{r}_3|b_3|}[b_1(2\bar{r}_3^2 + 2\bar{r}_1\bar{r}_3\cos(\phi_1 - \phi_3)) + b_2(2\bar{r}_3^2 + 2\bar{r}_2\bar{r}_3\cos(\phi_2 - \phi_3))],$$
$$= \frac{1}{\bar{r}_3|b_3|}[b_1(\bar{r}_3^2 + \bar{r}_2^2 - \bar{r}_1^2) + b_2(\bar{r}_3^2 + \bar{r}_1^2 - \bar{r}_2^2)] = \frac{1}{\bar{r}_3|b_3|}[\bar{r}_3^2(b_1 + b_2) + b_1(\bar{r}_2^2 - \bar{r}_1^2) + b_2(\bar{r}_1^2 - \bar{r}_2^2)],$$
$$= \frac{1}{\bar{r}_3|b_3|}[(6 - b_3)(b_1 + b_2) + b_1(b_2 - b_1) + b_2(b_1 - b_2)] = \frac{1}{\bar{r}_3|b_3|}[(6 - b_3)(3 - b_3) + 2b_1b_2 - (b_1^2 + b_2^2)],$$
$$= \frac{1}{\bar{r}_3|b_3|}[(6 - b_3)(3 - b_3) + 2b_1b_2 - (b_1 + b_2 + b_3)^2 + b_3^2 + 2b_1b_2 + 2b_1b_3 + 2b_2b_3],$$
$$= \frac{1}{\bar{r}_3|b_3|}[18 + b_3^2 - 9b_3 + b_3^2 + 4b_1b_2 - (b_1 + b_2 + b_3)^2 + b_3^2 + 2b_3(3 - b_3)],$$
$$= \frac{1}{\bar{r}_3|b_3|}[9 - 3b_3 + \frac{4}{\theta}|b_3|].$$

Finally we will substitute back:

$$\dot{\phi}_3 = \frac{\theta}{4\pi C}\frac{1}{\bar{r}_3^2|b_3|}[9 - 3b_3 + \frac{4}{\theta}|b_3|].$$

So now the derivation is complete:

$$\dot{\phi}_3 = \frac{\theta}{4\pi C}\frac{9 - 3b_3 + \frac{4}{\theta}|b_3|}{(6 - b_3)|b_3|}.$$

A.13 Forming $\Delta\phi_3$ integrals

Here we will derive the integral formula for $\Delta\phi_3$, the change of polar angle after scattering. We will use the formula given by Aref:

$$\Delta\phi_3 = \lim_{t\to+\infty}\phi_3(t) - \lim_{t\to-\infty}\phi_3(t) = \int_{-\infty}^{+\infty} dt\dot{\phi}_3(t).$$

Now note that, as derived in previous sections:

$$\dot{\phi}_3 = \frac{\theta}{4\pi C}\frac{9-3b_3+\frac{4}{\theta}|b_3|}{|b_3|(6-b_3)}, \quad \dot{b}_3 = \pm\frac{\sqrt{\theta}}{C\pi b_3}\sqrt{(\alpha+|b_3|)\left[(3-b_3)^2-4\frac{|b_3|}{\theta}\right]}.$$

Therefore:

$$dt = \pm\frac{C\pi b_3}{\sqrt{\theta(\alpha+|b_3|)[(3-b_3)^2-4\frac{|b_3|}{\theta}]}}db_3.$$

We use these to transform the $\Delta\phi_3$ integral as such:

$$\int_{-\infty}^{+\infty} dt\dot{\phi}_3(t) = \pm\frac{\sqrt{\theta}}{4}\int_{L_1}^{L_2}\frac{b_3(9-3b_3+\frac{4}{\theta}|b_3|)db_3}{|b_3|\sqrt{(\alpha+|b_3|)[(3-b_3)^2-4\frac{|b_3|}{\theta}]}}.$$

Where $L_1 = \lim_{t\to-\infty} b_3$, $\quad L_2 = \lim_{t\to+\infty} b_3$ Which will depend upon both C and θ. Note how the integral changes with respect to C. As when $C > 0 \implies |b_3| = -b_3$ and $C < 0 \implies |b_3| = b_3$. Our integral becomes(with b_3 left as b for convenience):

$$\Delta\phi_3 = \begin{cases} \mp\frac{\sqrt{\theta}}{4}\int_{L_1}^{L_2}\frac{9-(3+\frac{4}{\theta})bdb}{\sqrt{(\alpha-b)[(3-b)^2+4\frac{b}{\theta}]}} & \text{if} \quad C>0, \\ \pm\frac{\sqrt{\theta}}{4}\int_{L_1}^{L_2}\frac{9-(3-\frac{4}{\theta})bdb}{\sqrt{(\alpha+b)[(3-b)^2-4\frac{b}{\theta}]}} & \text{if} \quad C<0. \end{cases}$$

Note also that for the case that $C > 0$ the quadratic in the square root term has roots β and γ. Also notice the quadratic in the square root term of the C¡0. We can find the roots as:

$$\begin{aligned}(3-b)^2-4\frac{b}{\theta}=0 \implies b &= \frac{(6+\frac{4}{\theta})\pm\sqrt{\frac{48}{\theta}+\frac{16}{\theta^2}}}{2}, \\ &= \frac{1}{\theta}(3\theta+2\pm2\sqrt{3\theta+1}), \\ &= \frac{1}{\theta}(1\pm\sqrt{3\theta+1})^2.\end{aligned}$$

also note $\beta(-\theta) = \frac{1}{\theta}(1-\sqrt{3\theta+1})^2$, $\gamma(-\theta) = \frac{1}{\theta}(1+\sqrt{3\theta+1})^2$. So it is clear that in the case where $C < 0$ the equation in the square root term has roots $\alpha(-\theta), \beta(-\theta), \gamma(-\theta)$. We will refer to these quantities as $\bar{\alpha}, \bar{\beta}, \bar{\gamma}$ from here. This means that the $\Delta\phi_3$ integral now becomes:

$$\Delta\phi_3 = \begin{cases} \mp\frac{\sqrt{\theta}}{4}\int_{L_1}^{L_2}\frac{9-(3+\frac{4}{\theta})bdb}{\sqrt{(\alpha-b)(\beta-b)(\gamma-b)}} & \text{if} \quad C>0, \\ \pm\frac{\sqrt{\theta}}{4}\int_{L_1}^{L_2}\frac{9-(3-\frac{4}{\theta})bdb}{\sqrt{(b-\bar{\alpha})(b-\bar{\beta})(b-\bar{\gamma})}} & \text{if} \quad C<0. \end{cases}$$

Now we contend with the boundaries for θ and so solve for the limits L_1 and L_2. Here θ dictates whether the particular scattering considered will be exchange scattering or direct scattering. We will consider each particular case.

A.13.1 Integrals in the Region $\theta < \frac{1}{3}$, $C > 0$

This will be a case of exchange scattering and as such at a point we will reach the configuration $b_1 = b_2$ i.e. $b_3 = \gamma$. This means that over the entire scattering of b_3 will begin at $-\infty$ reach a singularity where $b_3 = \gamma \implies (\alpha - b)(\beta - b)(\gamma - b) = 0$ and rebound back to $-\infty$ (see phase point diagrams for clarification of this). We must update our integral to reflect this:

$$\begin{aligned}\Delta\phi_3 &= \frac{\sqrt{\theta}}{4}[\int_{-\infty}^{\gamma} \frac{9 - (3 + \frac{4}{\theta})bdb}{\sqrt{(\alpha - b)(\beta - b)(\gamma - b)}} - \int_{\gamma}^{-\infty} \frac{9 - (3 + \frac{4}{\theta})bdb}{\sqrt{(\alpha - b)(\beta - b)(\gamma - b)}}], \\ &= \frac{\sqrt{\theta}}{2} \int_{-\infty}^{\gamma} \frac{9 - (3 + \frac{4}{\theta})bdb}{\sqrt{(\alpha - b)(\beta - b)(\gamma - b)}}.\end{aligned}$$

Note that coefficients for the first expression are determined by the direction in which b_3 is moving, e.g. in the first integral b_3 is moving along the trajectory $-\infty \to \gamma$, as $-\infty < \gamma$ this means that $\dot{b_3} > 0$ hence the $+1$ coefficient.

A.13.2 Integrals in the Region $\theta > \frac{1}{3}, C > 0$

We continue as before, except this time the stationary point γ is not reached as both β and γ are complex in this case, this means that b_3 will increase from $-\infty$ until it reaches the physical boundary α, whereupon it again rebounds back to $-\infty$. As before:

$$\begin{aligned}\Delta\phi_3 &= \frac{\sqrt{\theta}}{4}[\int_{-\infty}^{\alpha} \frac{9 - (3 + \frac{4}{\theta})bdb}{\sqrt{(\alpha - b)(\beta - b)(\gamma - b)}} - \int_{\alpha}^{-\infty} \frac{9 - (3 + \frac{4}{\theta})bdb}{\sqrt{(\alpha - b)(\beta - b)(\gamma - b)}}], \\ &= \frac{\sqrt{\theta}}{2} \int_{-\infty}^{\alpha} \frac{9 - (3 + \frac{4}{\theta})bdb}{\sqrt{(\alpha - b)(\beta - b)(\gamma - b)}}.\end{aligned}$$

A.13.3 Integrals in the Region $\theta < \frac{8}{3}, C < 0$

This is again similar to the previous, except here the integral to contend with is different i.e:

$$\Delta\phi_3 = \pm\frac{\sqrt{\theta}}{4} \int_{L_1}^{L_2} \frac{9 - (3 - \frac{4}{\theta})bdb}{\sqrt{(b - \bar{\alpha})(b - \bar{\beta})(b - \bar{\gamma})}}.$$

We note that here $b_3 > 0$, therefore when $t \to \infty \implies b_3 \to \infty$, so therefore in the case of exchange scattering the phase point will begin at the limit $b_3 = \infty$ will decrease to the point where $b_3 = \bar{\gamma}$ i.e. $\dot{b_3} < 0$. Then b_3 will increase back to the starting limit:

$$\begin{aligned}\Delta\phi_3 &= \frac{\sqrt{\theta}}{4}[-\int_{\infty}^{\bar{\gamma}} \frac{9 - (3 - \frac{4}{\theta})bdb}{\sqrt{(b - \bar{\alpha})(b - \bar{\beta})(b - \bar{\gamma})}} + \int_{\bar{\gamma}}^{\infty} \frac{9 - (3 - \frac{4}{\theta})bdb}{\sqrt{(b - \bar{\alpha})(b - \bar{\beta})(b - \bar{\gamma})}}], \\ &= \frac{\sqrt{\theta}}{2} \int_{\bar{\gamma}}^{\infty} \frac{9 - (3 - \frac{4}{\theta})bdb}{\sqrt{(b - \bar{\alpha})(b - \bar{\beta})(b - \bar{\gamma})}}.\end{aligned}$$

A.13.4 Integrals in the Region $\theta > \frac{8}{3}, C < 0$

This is the same as previous section except in this case we have direct scattering, therefore as already discussed b_3 will reach the physical boundary $\bar{\alpha}$ before the points $\bar{\beta}$ and $\bar{\gamma}$. So here the

phase point will begin at the limit $b_3 = \infty$, decrease until $b_3 = \bar{\alpha}$, and then increase back to the limit $b_3 = \infty$. So our integral becomes:

$$\begin{aligned}\Delta\phi_3 &= \frac{\sqrt{\theta}}{4}[-\int_{\infty}^{\bar{\alpha}} \frac{9-(3-\frac{4}{\theta})bdb}{\sqrt{(b-\bar{\alpha})(b-\bar{\beta})(b-\bar{\gamma})}} + \int_{\bar{\alpha}}^{\infty} \frac{9-(3-\frac{4}{\theta})bdb}{\sqrt{(b-\bar{\alpha})(b-\bar{\beta})(b-\bar{\gamma})}}], \\ &= \frac{\sqrt{\theta}}{2}\int_{\bar{\alpha}}^{\infty} \frac{9-(3-\frac{4}{\theta})bdb}{\sqrt{(b-\bar{\alpha})(b-\bar{\beta})(b-\bar{\gamma})}}.\end{aligned}$$

A.13.5 Complete $\Delta\phi_3$ Integrals

From the above we can give the $\Delta\phi_3$ formula as:

$$\Delta\phi_3 = \begin{cases} \frac{\sqrt{\theta}}{2}\int_{-\infty}^{\gamma} \frac{9-(3+\frac{4}{\theta})bdb}{\sqrt{(\alpha-b)(\beta-b)(\gamma-b)}} \text{ if } & C>0, \theta<\frac{1}{3} \\ \frac{\sqrt{\theta}}{2}\int_{-\infty}^{\alpha} \frac{9-(3+\frac{4}{\theta})bdb}{\sqrt{(\alpha-b)(\beta-b)(\gamma-b)}} \text{ if } & C>0, \theta>\frac{1}{3}, \\ \frac{\sqrt{\theta}}{2}\int_{\bar{\gamma}}^{\infty} \frac{9-(3-\frac{4}{\theta})bdb}{\sqrt{(b-\bar{\alpha})(b-\bar{\beta})(b-\bar{\gamma})}} \text{ if } & C<0, \theta<\frac{8}{3}, \\ \frac{\sqrt{\theta}}{2}\int_{\bar{\alpha}}^{\infty} \frac{9-(3-\frac{4}{\theta})bdb}{\sqrt{(b-\bar{\alpha})(b-\bar{\beta})(b-\bar{\gamma})}} \text{ if } & C<0, \theta>\frac{8}{3}. \end{cases}$$

A.14 Reduction of Integrals to Normal Form

We can reduce the integrals found to their Legendre Normal forms by simple substitutions found in Labahn and Mutrie. We note that we want to reduce into the two Legendre forms for the first and third complete elliptic integrals given by(note we are using the *characteristic* n):

$$K(k) = \int_0^1 \frac{d\phi}{\sqrt{1-k^2 sin^2\phi}}, \quad \Pi(n,k) = \int_0^1 \frac{d\phi}{(nsin^2\phi+1)\sqrt{1-k^2sin^2\phi}}.$$

A.14.1 Normal Forms in the Region $\theta < \frac{1}{3}, C > 0$

We first examine the case of $C > 0$ and $\theta < \frac{1}{3}$. The scattering angle in this case is given by the integral:

$$\Delta\theta = \frac{\sqrt{\theta}}{2}\int_{-\infty}^{\gamma} \frac{9-(3+\frac{4}{\theta})bdb}{(6-b)\sqrt{(\alpha-b)(\beta-b)(\gamma-b)}}.$$

Note if $y = \sqrt{(\alpha-b)(\beta-b)(\gamma-b)}$:

$$\begin{aligned}\frac{\sqrt{\theta}}{2}\int_{-\infty}^{\gamma} \frac{9-(3+\frac{4}{\theta})bdb}{(6-b)y} &= \frac{\sqrt{\theta}}{2}\int_{-\infty}^{\gamma} \frac{9-6(3+\frac{4}{\theta})+(6-b)(3+\frac{4}{\theta})db}{(6-b)y}, \\ &= \frac{\sqrt{\theta}}{2}\big[(3+\frac{4}{\theta})\int_{-\infty}^{\gamma}\frac{db}{y} + [9-6(3+\frac{4}{\theta})]\int_{-\infty}^{\gamma}\frac{db}{(6-b)y}\big], \\ &= \frac{\sqrt{\theta}}{2}\big[(3+\frac{4}{\theta})\int_{-\infty}^{\gamma}\frac{db}{y} + (9+\frac{24}{\theta})\int_{-\infty}^{\gamma}\frac{db}{(b-6)y}\big].\end{aligned}$$

Thus the problem has been reduced to transferring the integrals $\int_{-\infty}^{\gamma}\frac{db}{y}$ and $\int_{-\infty}^{\gamma}\frac{db}{(b-6)y}$ into the Legendre normal forms in order to implement them in the numerical calculations. We start

with the first integral. We first must analyse the root structure of the polynomial y^2, we find that:

$$\gamma < \beta < \alpha.$$

whenever $\theta < \frac{1}{3}$. So using this we find our substiution to be:

$$\begin{aligned} sin^2\phi &= \frac{\alpha-\gamma}{\alpha-b}, \\ \implies 2sin\phi cos\phi d\phi &= \frac{\alpha-\gamma}{(\alpha-b)^2}db, \\ \implies 2\frac{cos\phi}{sin^3\phi}(\alpha-\gamma)d\phi &= db. \end{aligned}$$

With $k^2 = \frac{\alpha-\beta}{\alpha-\gamma}$. Thus the polynomial y becomes:

$$\begin{aligned} y = \sqrt{(\alpha-b)(\beta-b)(\gamma-b)} &= \sqrt{(\frac{\alpha-\gamma}{sin^2\phi})(\beta-\alpha+\frac{\alpha-\gamma}{sin^2\phi})(\gamma-\alpha+\frac{\alpha-\gamma}{sin^2\phi})}, \\ &= \frac{\alpha-\gamma}{sin^3\phi}\sqrt{\alpha-\gamma}\sqrt{(\frac{\beta-\alpha}{\alpha-\gamma}sin^2\phi+1)(1-sin^2\phi)}, \\ &= \frac{cos\phi}{sin^3\phi}(\alpha-\gamma)\sqrt{\alpha-\gamma}\sqrt{1-k^2sin^2\phi}. \end{aligned}$$

So therefore:

$$\begin{aligned} \int_{-\infty}^{\gamma}\frac{db}{y} &= \int_0^{\frac{\pi}{2}}\frac{2\frac{cos\phi}{sin^3\phi}(\alpha-\gamma)d\phi}{\frac{cos\phi}{sin^3\phi}(\alpha-\gamma)\sqrt{\alpha-\gamma}\sqrt{1-k^2sin^2\phi}}, \\ &= \frac{2}{\sqrt{\alpha-\gamma}}\int_0^{\frac{\pi}{2}}\frac{d\phi}{\sqrt{1-k^2sin^2\phi}} = \frac{2}{\sqrt{\alpha-\gamma}}K(k). \end{aligned}$$

We now move to our other integral, by the same logic we have that:

$$\begin{aligned} \int_{-\infty}^{\gamma}\frac{db}{(b-6)y} &= \frac{2}{\sqrt{\alpha-\gamma}}\int_0^1\frac{d\phi}{(\frac{\alpha sin^2\phi-(\alpha-\gamma)}{sin^2\phi}-6)\sqrt{1-k^2sin^2\phi}}, \\ &= \frac{2}{(\alpha-6)\sqrt{\alpha-\gamma}}\int_0^1\frac{(\alpha-6)sin^2\phi+(\alpha-\gamma)-(\alpha-\gamma)d\phi}{[(\alpha-6)sin^2\phi-(\alpha-\gamma)]\sqrt{1-k^2sin^2\phi}}, \\ &= \frac{2}{(\alpha-6)\sqrt{\alpha-\gamma}}\big[\int_0^1\frac{d\phi}{\sqrt{1-k^2sin^2\phi}} \\ &+ (\alpha-\gamma)\int_0^1\frac{d\phi}{[(\alpha-6)sin^2\phi-(\alpha-\gamma)]\sqrt{1-k^2sin^2\phi}}\big], \\ &\frac{2}{(\alpha-6)\sqrt{\alpha-\gamma}}\big[K(k)-\int_0^1\frac{d\phi}{[\frac{\alpha-6}{\gamma-\alpha}sin^2\phi+1]\sqrt{1-k^2sin^2\phi}}\big], \\ &= \frac{2}{(\alpha-6)\sqrt{\alpha-\gamma}}\big[K(k)-\Pi(n,k)\big]. \end{aligned}$$

Where $n = \frac{\alpha-6}{\gamma-\alpha}$. Finally substituting back:

$$\begin{aligned}
\Delta\theta &= \frac{\sqrt{\theta}}{2}\big[(3+\frac{4}{\theta})\int_{-\infty}^{\gamma}\frac{db}{y} + (9+\frac{24}{\theta})\int_{-\infty}^{\gamma}\frac{db}{(b-6)y}\big], \\
&= \frac{\sqrt{\theta}}{2}\big[(3+\frac{4}{\theta})\frac{2}{\sqrt{\alpha-\gamma}}K(k) + (9+\frac{24}{\theta})\frac{2}{(\alpha-6)\sqrt{\alpha-\gamma}}[K(k)-\Pi(n,k)]\big], \\
&= \sqrt{\frac{\theta}{\alpha-\gamma}}\big[(3+\frac{4}{\theta})K(k) + (\frac{9+\frac{24}{\theta}}{\alpha-6})[K(k)-\Pi(n,k)]\big], \\
&= \sqrt{\frac{\theta}{\alpha-\gamma}}\big[\frac{3\alpha+\frac{4}{\theta}\alpha-9}{\alpha-6}K(k) - \frac{9+\frac{24}{\theta}}{\alpha-6}\Pi(n,k)\big].
\end{aligned}$$

And as $\alpha = -\frac{9}{4}\theta \implies \frac{4}{\theta} = -\frac{9}{\alpha}$

$$\begin{aligned}
\implies \Delta\theta &= \sqrt{\frac{\theta}{\alpha-\gamma}}\big[\frac{3\alpha-18}{\alpha-6}K(k) - \frac{9-6\frac{9}{\alpha}}{\alpha-6}\Pi(n,k)\big], \\
&= \sqrt{\frac{\theta}{\alpha-\gamma}}\big[3K(k) - \frac{9}{\alpha}\Pi(n,k)\big], \\
&= \sqrt{\frac{\theta}{\alpha-\gamma}}\big[3K(k) + \frac{4}{\theta}\Pi(n,k)\big].
\end{aligned}$$

A.14.2 Normal Forms in the Region $\theta > \frac{1}{3}, C > 0$

Now we move on to the case where $C > 0$ and this time $\theta > \frac{1}{3}$. We perform the root analysis as before and we find that in this region $1 - 3\theta < 0$ so β and γ are complex conjugates as:

$$\begin{aligned}
\beta &= -\frac{1}{\theta}[2 - 3\theta - 2\sqrt{1-3\theta}], \\
\gamma &= -\frac{1}{\theta}[2 - 3\theta + 2\sqrt{1-3\theta}].
\end{aligned}$$

We calculate the integrals using the same process as before with the additional quantity $A = \sqrt{(\beta-\alpha)(\gamma-\alpha)}$. Now our first integral will integrate from $-\infty$ to $\alpha - A$ and our second integral will integrate from $\alpha - A$ to α using several substitutions. For our first we shall consider the integral

$$\int_{-\infty}^{\alpha-A}\frac{db}{y}.$$

We use the substitution:

$$\begin{aligned}
b &= \frac{(\alpha+A)sin^2\phi - 2A - 2Acos\phi}{sin^2\phi}, \\
\implies db &= \frac{2Asin^2\phi + 4Acos\phi + 4Acos^2\phi}{sin^2\phi}d\phi = \frac{2A(cos\phi+1)^2}{sin^3\phi}.
\end{aligned}$$

Where in this case we have:

$$k^2 = \frac{A - (\frac{\beta+\gamma}{2}) + \alpha}{2A},$$
$$2A - 4Ak^2 = (\beta + \gamma) - 2\alpha.$$

Now we have that:

$$\sqrt{\alpha - b} = \sqrt{\frac{-Asin^2\phi + 2A + 2Acos\phi}{sin^2\phi}} = \sqrt{A}(\frac{cos\phi + 1}{sin\phi}),$$
$$\sqrt{(\beta - b)(\gamma - b)} = \sqrt{(\beta - \alpha + \frac{A(cos\phi+1)^2}{sin^2\phi})(\gamma - \alpha + \frac{A(cos\phi+1)^2}{sin^2\phi})},$$
$$= \frac{A}{Z}\sqrt{[(\beta - \alpha)\frac{Z}{A} + 1][(\gamma - \alpha)\frac{Z}{A} + 1]}.$$

Where here $Z = \frac{sin^2\phi}{(cos\phi+1)^2}$. Continuing:

$$\sqrt{(\beta - b)(\gamma - b)} = \frac{A}{Z}\sqrt{(\beta - \alpha)(\gamma - \alpha)\frac{Z^2}{A^2} + (\beta + \gamma - 2\alpha)\frac{Z}{A} + 1},$$
$$= \frac{A}{Z}\sqrt{Z^2 + 2Z - 4k^2Z + 1} = \frac{A}{Z}\sqrt{(Z+1)^2 - 4k^2Z}.$$

Now

$$Z + 1 = \frac{sin^2\phi}{(cos\phi + 1)^2} + 1 = \frac{sin^2\phi + cos^2\phi + 2cos\phi + 1}{(cos\phi + 1)^2} = \frac{2}{cos\phi + 1}.$$

So:

$$\sqrt{(\beta - b)(\gamma - b)} = \frac{A}{Z}\sqrt{\frac{4}{(cos\phi+1)^2} - 4k^2Z},$$
$$= \frac{A(cos\phi+1)^2}{sin^2\phi}\sqrt{\frac{4}{(cos\phi+1)^2} - 4k^2\frac{sin^2\phi}{(cos\phi+1)^2}},$$
$$= \frac{2A(cos\phi+1)}{sin^2\phi}\sqrt{1 - k^2sin^2\phi}.$$

Hence for the final integral we have that:

$$\int_{-\infty}^{\alpha-A}\frac{db}{y} = \int_0^1 \frac{\frac{2A(cos\phi+1)^2}{sin^3\phi}d\phi}{\sqrt{A}(\frac{cos\phi+1}{sin\phi})\frac{2A(cos\phi+1)}{sin^2\phi}\sqrt{1 - k^2sin^2\phi}} = \frac{1}{\sqrt{A}}\int_0^1 \frac{d\phi}{\sqrt{1 - k^2sin^2\phi}},$$
$$= \frac{1}{\sqrt{A}}K(k).$$

Now for our other integral $\int_{\alpha-A}^{\alpha}\frac{db}{y}$ we proceed using the same logic. Again $A = \sqrt{(\beta - \alpha)(\gamma - \alpha)}$ and $k^2 = \frac{A-(\frac{\beta+\gamma}{2})+\alpha}{2A} \implies 2A - 4Ak^2 = (\beta + \gamma) - 2\alpha$. We now use the substitution;

$$b = \frac{(\alpha + A)sin^2\phi - 2A + 2Acos\phi}{sin^2\phi},$$
$$\implies db = \frac{-2Asin^2\phi + 4Acos\phi - 4Acos^2\phi}{sin^3\phi}d\phi = -2A\frac{(cos\phi - 1)^2}{sin^3\phi}d\phi.$$

And

$$\sqrt{\alpha - b} = \sqrt{\frac{-Asin^2\phi + 2A - 2Acos\phi}{sin^2\phi}} = \sqrt{A}(\frac{cos\phi - 1}{sin\phi}),$$
$$\sqrt{(\beta - b)(\gamma - b)} = \sqrt{(\beta - \alpha + \frac{A(cos\phi - 1)^2}{sin^2\phi})(\gamma - \alpha + \frac{A(cos\phi - 1)^2}{sin^2\phi})},$$
$$= \frac{A}{Z}\sqrt{[(\beta - \alpha)\frac{Z}{A} + 1][(\gamma - \alpha)\frac{Z}{A} + 1]}.$$

Where $Z = \frac{sin^2\phi}{(cos\phi - 1)^2}$ We follow as before:

$$\sqrt{(\beta - b)(\gamma - b)} = \frac{A}{Z}\sqrt{(\beta - \alpha)(\gamma - \alpha)\frac{Z^2}{A^2} + (\beta + \gamma - 2\alpha)\frac{Z}{A} + 1},$$
$$= \frac{A}{Z}\sqrt{(Z + 1)^2 - 4k^2Z}.$$

Again as before:

$$Z + 1 = \frac{sin^2\phi}{(cos\phi - 1)^2} + 1 = \frac{sin^2\phi + cos^2\phi - 2cos\phi + 1}{(cos\phi - 1)^2} = \frac{2}{cos\phi - 1}.$$

So therefore:

$$\sqrt{(\beta - b)(\gamma - b)} = \frac{A}{Z}\sqrt{\frac{4}{(cos\phi - 1)^2} - 4k^2Z},$$
$$= \frac{2A(cos\phi - 1)}{sin^2\phi}\sqrt{1 - k^2sin^2\phi}.$$

So finally we calculate the integral as:

$$\int_{\alpha - A}^{\alpha}\frac{db}{y} = \int_1^0 \frac{-2A\frac{(cos\phi - 1)^2}{sin^3\phi}d\phi}{\sqrt{A}(\frac{cos\phi - 1}{sin\phi})\frac{2A(cos\phi - 1)}{sin^2\phi}\sqrt{1 - k^2sin^2\phi}} = \frac{1}{\sqrt{A}}\int_0^1 \frac{1}{\sqrt{1 - k^2sin^2\phi}},$$
$$= \frac{1}{\sqrt{A}}K(k).$$

At last we find the integral in the required form as:

$$\int_{-\infty}^{\alpha}\frac{db}{y} = \int_{-\infty}^{\alpha - A}\frac{db}{y} + \int_{\alpha - A}^{\alpha}\frac{db}{y} = \frac{2}{\sqrt{A}}K(k).$$

Now to calculate the second integral:

$$\int_{-\infty}^{\alpha} \frac{db}{(b-6)y} = \int_{-\infty}^{\alpha-A} \frac{db}{(b-6)y} + \int_{\alpha-A}^{\alpha} \frac{db}{(b-6)y}.$$

Using substitutions and the same logic as before:

$$\begin{aligned}
\int_{-\infty}^{\alpha-A} \frac{db}{(b-6)y} + \int_{\alpha-A}^{\alpha} \frac{db}{(b-6)y} &= \frac{1}{\sqrt{A}}\Big[\int_0^1 \frac{sin^2\phi d\phi}{[(\alpha+A-6)sin^2\phi + 2A + 2Acos\phi]\sqrt{1-k^2sin^2\phi}} \\
&\quad + \int_0^1 \frac{sin^2\phi d\phi}{[(\alpha+A-6)sin^2\phi + 2A - 2Acos\phi]\sqrt{1-k^2sin^2\phi}}\Big], \\
&= \frac{1}{\sqrt{A}}\int_0^1 \frac{sin^2\phi d\phi}{\sqrt{1-k^2sin^2\phi}}\Big[\frac{2(\alpha+A-6)sin^2\phi - 4A}{[sin^2\phi(\alpha+A-6) - 2A]^2 - 4A^2cos^2\phi}\Big], \\
&= \frac{2}{\sqrt{A}(\alpha+A-6)}\int_0^1 \frac{(\alpha+A-6)^2sin^2\phi - 2A(\alpha+A-6)d\phi}{[sin^2\phi(\alpha+A-6)^2 - 4A(\alpha-6)]\sqrt{1-k^2sin^2\phi}}, \\
&= \frac{2}{\sqrt{A}(\alpha+A-6)}\big[K(k) + \frac{1}{2}(\frac{A}{\alpha-6} - 1)\Pi(n,k)\big].
\end{aligned}$$

With $n = \frac{(\alpha+A-6)^2}{-4A(\alpha-6)}$So we finally substitute to find

$$\begin{aligned}
\Delta\phi_3 &= \frac{\sqrt{\theta}}{2}\big[(3+\frac{4}{\theta})\int_{-\infty}^{\gamma}\frac{db}{y} + (9+\frac{24}{\theta})\int_{-\infty}^{\gamma}\frac{db}{(b-6)y}\big], \\
&= \frac{\sqrt{\theta}}{2}\big[(3+\frac{4}{\theta})\frac{2}{\sqrt{A}}K(k) + (9+\frac{24}{\theta})\frac{2}{\sqrt{A}(\alpha+A-6)}\big[K(k) + \frac{1}{2}(\frac{A}{\alpha-6} - 1)\Pi(n,k)\big]\big], \\
&= \sqrt{\frac{\theta}{A}}\big[(3+\frac{4}{\theta} + \frac{9+\frac{24}{\theta}}{\alpha+A-6})K(k) + \frac{(\frac{A}{\alpha-6}-1)(9+\frac{24}{\theta})}{2(\alpha+A-6)}\Pi(n,k)\big].
\end{aligned}$$

A.14.3 Normal Forms in the Region $\theta < \frac{8}{3}, C < 0$

We now move to the case where $C < 0$. Note that in this case y becomes:

$$y = \sqrt{[\alpha+b_3][(3-b_3)^2 - \frac{4}{\theta}b_3]}.$$

We notice that the quadratic polynomial has roots $\beta(-\theta)$ and $\gamma(-\theta)$ i.e.

$$\beta(\theta) = \frac{1}{\theta}[1-\sqrt{1+3\theta}]^2, \quad \gamma(\theta) = \frac{1}{\theta}[1+\sqrt{1+3\theta}]^2.$$

Are roots of the quadratic term, therefore we can factor as:

$$y = \sqrt{(b_3 - (-\alpha))(b_3 - \beta(-\theta))(b_3 - \gamma(-\theta))}.$$

And as $\alpha(-\theta) = -\alpha$

$$y = \sqrt{[b_3 - \alpha(-\theta)][b_3 - \beta(-\theta)][b_3 - \gamma(-\theta)]} = \sqrt{(b_3 - \bar{\alpha})(b_3 - \bar{\beta})(b_3 - \bar{\gamma})}.$$

Where the bar notation represents the previous negative θ terms. We continue as before with the root analysis. We note that in the region $\theta < \frac{8}{3}$:

$$\bar{\beta} < \bar{\alpha} < \bar{\gamma}.$$

Now to reduce the integral into elementary forms:

$$\Delta\phi_3 = \frac{\sqrt{\theta}}{2}\int_{\bar{\gamma}}^{\infty}\frac{9-(3-\frac{4}{\theta})bdb}{(6-b)y} = \frac{\sqrt{\theta}}{2}\big[(3-\frac{4}{\theta})\int_{\bar{\gamma}}^{\infty}\frac{db}{y} + [9-6(3-\frac{4}{\theta})]\int_{\bar{\gamma}}^{\infty}\frac{db}{(6-b)y}\big],$$
$$= \frac{\sqrt{\theta}}{2}\big[(3-\frac{4}{\theta})\int_{\bar{\gamma}}^{\infty}\frac{db}{y} + (9-\frac{24}{\theta})\int_{\bar{\gamma}}^{\infty}\frac{db}{(b-6)y}\big].$$

Here $k^2 = \frac{\bar{\alpha}-\bar{\beta}}{\bar{\gamma}-\bar{\beta}}$. We use the substitution

$$b = \frac{\bar{\alpha}sin^2\phi - \bar{\gamma}}{sin^2\phi - 1},$$
$$\implies db = \big[\frac{2\bar{\alpha}sin\phi cos\phi}{sin^2\phi-1} - 2sin\phi cos\phi\frac{\bar{\alpha}sin^2\phi-\bar{\gamma}}{(sin^2\phi-1)^2}\big]d\phi,$$
$$= 2(\bar{\gamma}-\bar{\alpha})\frac{sin\phi}{cos^3\phi}d\phi.$$

and so:

$$y = \sqrt{(b-\bar{\alpha})(b-\bar{\beta})(b-\bar{\gamma})} = \sqrt{(\frac{\bar{\alpha}-\bar{\gamma}}{sin^2\phi-1})(\bar{\alpha}-\bar{\beta}+\frac{\bar{\alpha}-\bar{\gamma}}{sin^2\phi-1})(\bar{\alpha}-\bar{\gamma}+\frac{\bar{\alpha}-\bar{\gamma}}{sin^2\phi-1})},$$
$$= (\bar{\alpha}-\bar{\gamma})\frac{sin\phi}{sin^2\phi-1}\sqrt{(\bar{\alpha}-\bar{\beta}+\frac{\bar{\alpha}-\bar{\gamma}}{sin^2\phi-1})},$$
$$= (\bar{\alpha}-\bar{\gamma})\frac{sin\phi}{sin^2\phi-1}\sqrt{\frac{1}{sin^2\phi-1}}\sqrt{(\bar{\alpha}-\bar{\beta})sin^2\phi+\bar{\beta}-\bar{\gamma}},$$
$$= (\bar{\gamma}-\bar{\alpha})\frac{sin\phi}{cos^3\phi}\sqrt{\bar{\gamma}-\bar{\beta}}\sqrt{1-k^2sin^2\phi}.$$

So as before:

$$\int_{\bar{\gamma}}^{\infty}\frac{db}{y} = \int_0^1\frac{2(\bar{\gamma}-\bar{\alpha})\frac{sin\phi}{cos^3\phi}d\phi}{(\bar{\gamma}-\bar{\alpha})\frac{sin\phi}{cos^3\phi}\sqrt{\bar{\gamma}-\bar{\beta}}\sqrt{1-k^2sin^2\phi}},$$
$$= \frac{2}{\sqrt{\bar{\gamma}-\bar{\beta}}}\int_0^1\frac{d\phi}{\sqrt{1-k^2sin^2\phi}} = \frac{2}{\sqrt{\bar{\gamma}-\bar{\beta}}}K(k).$$

And again by the same logic, if $n = \frac{\bar{\alpha}-6}{6-\bar{\gamma}}$:

$$\int_{\bar{\gamma}}^{\infty}\frac{db}{(b-6)y} = \frac{2}{\sqrt{\bar{\gamma}-\bar{\beta}}}\int_0^1\frac{d\phi}{(\frac{\bar{\alpha}sin^2\phi-\bar{\gamma}}{sin^2\phi-1}-6)\sqrt{1-k^2sin^2\phi}},$$
$$= \frac{2}{\sqrt{\bar{\gamma}-\bar{\beta}}}\int_0^1\frac{sin^2\phi-1}{[(\bar{\alpha}-6)sin^2\phi+6-\bar{\gamma}]\sqrt{1-k^2sin^2\phi}}d\phi,$$
$$= \frac{2}{(6-\bar{\gamma})\sqrt{\bar{\gamma}-\bar{\beta}}}\int_0^1\frac{sin^2\phi-1}{[nsin^2\phi+1]\sqrt{1-k^2sin^2\phi}}d\phi,$$
$$= \frac{2}{(\bar{\alpha}-6)\sqrt{\bar{\gamma}-\bar{\beta}}}\big[K(k) - \frac{\bar{\alpha}-\bar{\gamma}}{6-\bar{\gamma}}\Pi(n,k)\big].$$

Now we finally substitute back:

$$\begin{aligned}\Delta\phi_3 &= \frac{\sqrt{\theta}}{2}\big[(3-\frac{4}{\theta})\int_{\bar\gamma}^{\infty}\frac{db}{y}+(9-\frac{24}{\theta})\int_{\bar\gamma}^{\infty}\frac{db}{(b-6)y}\big],\\ &= \frac{\sqrt{\theta}}{2}\big[(3-\frac{4}{\theta})\frac{2}{\sqrt{\bar\gamma-\bar\beta}}K(k)+(9-\frac{24}{\theta})\frac{2}{(\bar\alpha-6)\sqrt{\bar\gamma-\bar\beta}}\big[K(k)-\frac{\bar\alpha-\bar\gamma}{6-\bar\gamma}\Pi(n,k)\big]\big],\\ &= \sqrt{\frac{\theta}{\bar\gamma-\bar\beta}}\big[\frac{3\bar\alpha-\frac{4}{\theta}\bar\alpha-9}{\bar\alpha-6}K(k)-\frac{(9-\frac{24}{\theta})(\bar\alpha-\bar\gamma)}{(\bar\alpha-6)(6-\bar\gamma)}\Pi(n,k)\big].\end{aligned}$$

And again as $\bar\alpha=\frac{9}{4}\theta \implies \frac{4}{\theta}=\frac{9}{\bar\alpha}$

$$\Delta\phi_3=\sqrt{\frac{\theta}{\bar\gamma-\bar\beta}}\big[3K(k)-\frac{(9-\frac{24}{\theta})(\bar\alpha-\bar\gamma)}{(\bar\alpha-6)(6-\bar\gamma)}\Pi(n,k)\big].$$

A.14.4 Normal Forms in the Region $\theta > \frac{8}{3}, C < 0$

We now move to the final case of direct scattering with $C<0$. We need to derive the integrals:

$$\int_{\bar\alpha}^{\infty}\frac{db}{y},\quad \int_{\bar\alpha}^{\infty}\frac{db}{(b-6)y}.$$

We continue as before with a root analysis. We find that in the region where $\theta>\frac{8}{3}$:

$$\bar\alpha>\bar\gamma>\bar\beta.$$

We will use the substitution:

$$\begin{aligned}b &= \frac{\bar\gamma sin^2\phi-\bar\alpha}{sin^2\phi-1},\\ \implies db &= [\frac{2\bar\gamma sin\phi cos\phi}{sin^2\phi-1}-2sin\phi cos\phi\frac{\bar\gamma sin^2\phi-\bar\alpha}{(sin^2\phi-1)^2}]d\phi,\\ &= 2(\bar\alpha-\bar\gamma)\frac{sin\phi}{cos^3\phi}d\phi.\end{aligned}$$

With $k^2=\frac{\bar\gamma-\bar\beta}{\bar\alpha-\bar\beta}$. We note that:

$$\begin{aligned}y=\sqrt{(b-\bar\alpha)(b-\bar\beta)(b-\bar\gamma)} &= \sqrt{\frac{(\bar\alpha-\bar\gamma)sin^2\phi}{cos^2\phi}(\bar\alpha-\bar\beta+\frac{(\bar\alpha-\bar\gamma)sin^2\phi}{cos^2\phi})(\bar\alpha-\bar\gamma+\frac{(\bar\alpha-\bar\gamma)sin^2\phi}{cos^2\phi})},\\ &= (\bar\alpha-\bar\gamma)\frac{sin\phi}{cos^3\phi}\sqrt{\bar\alpha-\bar\beta+(\bar\beta-\bar\gamma)sin^2\phi},\\ &= (\bar\alpha-\bar\gamma)\frac{sin\phi}{cos^3\phi}\sqrt{\bar\alpha-\bar\beta}\sqrt{1-k^2sin^2\phi}.\end{aligned}$$

So we can say:

$$\begin{aligned}\int_{\bar\alpha}^{\infty}\frac{db}{y} &= \int_0^1\frac{2(\bar\alpha-\bar\gamma)\frac{sin\phi}{cos^3\phi}d\phi}{(\bar\alpha-\bar\gamma)\frac{sin\phi}{cos^3\phi}\sqrt{\bar\alpha-\bar\beta}\sqrt{1-k^2sin^2\phi}},\\ &= \frac{2}{\sqrt{\bar\alpha-\bar\beta}}\int_0^1\frac{d\phi}{\sqrt{1-k^2sin^2\phi}}=\frac{2}{\sqrt{\bar\alpha-\bar\beta}}K(k).\end{aligned}$$

We complete the final integral as before, with $n = \frac{\bar{\gamma}-6}{6-\bar{\alpha}}$:

$$\begin{aligned}
\int_{\bar{\alpha}}^{\infty} \frac{db}{(b-6)y} &= \frac{2}{\sqrt{\bar{\alpha}-\bar{\beta}}} \int_0^1 \frac{sin^2\phi - 1 d\phi}{[(\bar{\gamma}-6)sin^2\phi + 6 - \bar{\alpha}]\sqrt{1-k^2sin^2\phi}}, \\
&= \frac{2}{(6-\bar{\alpha})\sqrt{\bar{\alpha}-\bar{\beta}}} \int_0^1 \frac{sin^2\phi - 1 d\phi}{(nsin^2\phi + 1)\sqrt{1-k^2sin^2\phi}}, \\
&= \frac{2}{(\bar{\gamma}-6)\sqrt{\bar{\alpha}-\bar{\beta}}} \big[\int_0^1 \frac{d\phi}{\sqrt{1-k^2sin^2\phi}} - (n+1) \int_0^1 \frac{d\phi}{(nsin^2\phi+1)\sqrt{1-k^2sin^2\phi}} \big], \\
&= \frac{2}{(\bar{\gamma}-6)\sqrt{\bar{\alpha}-\bar{\beta}}} \big[K(k) - \frac{\bar{\gamma}-\bar{\alpha}}{6-\bar{\alpha}} \Pi(n,k) \big].
\end{aligned}$$

So we calculate the final elliptic integral as:

$$\begin{aligned}
\Delta\phi_3 &= \frac{\sqrt{\theta}}{2} \big[(3 - \frac{4}{\theta}) \int_{\bar{\gamma}}^{\infty} \frac{db}{y} + (9 - \frac{24}{\theta}) \int_{\bar{\gamma}}^{\infty} \frac{db}{(b-6)y} \big], \\
&= \frac{\sqrt{\theta}}{\sqrt{\bar{\alpha}-\bar{\beta}}} \big[(3 - \frac{4}{\theta}) K(k) + \frac{(9 - \frac{24}{\theta})}{\bar{\gamma}-6} [K(k) - \frac{\bar{\gamma}-\bar{\alpha}}{6-\bar{\alpha}} \Pi(n,k)] \big], \\
&= \frac{\sqrt{\theta}}{\sqrt{\bar{\alpha}-\bar{\beta}}} \big[\frac{3\bar{\gamma} - \frac{4}{\theta}\bar{\gamma} - 9}{\bar{\gamma}-6} K(k) - \frac{(9 - \frac{24}{\theta})(\bar{\gamma}-\bar{\alpha})}{(\bar{\gamma}-6)(6-\bar{\alpha})} \Pi(n,k) \big].
\end{aligned}$$

So finally for the case where $\theta > \frac{8}{3}, C < 0$ with $k^2 = \frac{\bar{\gamma}-\bar{\beta}}{\bar{\alpha}-\bar{\beta}}$ and $n = \frac{\bar{\gamma}-6}{6-\bar{\alpha}}$, we reduce the final scattering angle as:

$$\Delta\phi_3 = \frac{\sqrt{\theta}}{\sqrt{\bar{\alpha}-\bar{\beta}}} \big[\frac{3\bar{\gamma} - \frac{4}{\theta}\bar{\gamma} - 9}{\bar{\gamma}-6} K(k) - \frac{(9 - \frac{24}{\theta})(\bar{\gamma}-\bar{\alpha})}{(\bar{\gamma}-6)(6-\bar{\alpha})} \Pi(n,k) \big].$$

A.15 θ in the limit $\rho \ll L$, $d \ll L$ and $\frac{C}{d}^2 \to \frac{\rho}{d}$ relation

We have from our original definition of θ:

$$\theta = |C| e^{-4\pi H}.$$

Note that this is equivalent to:

$$\theta = |C| \tilde{H}^2.$$

And as before we derived that:

$$\lim_{L\to\infty} \tilde{H} = \frac{1}{d}.$$

So therefore

$$\lim_{L\to\infty} \theta = \lim_{L\to\infty} |C| \tilde{H}^2 = \frac{|C|}{d^2}.$$

We also prove the relation between ρ/d and C/d^2, we have:

$$
\begin{aligned}
\frac{C}{d^2} &= -\frac{1}{3}\frac{\ell_{1,2}^2 - \ell_{1,3}^2 - \ell_{2,3}^2}{d^2}, \\
&= -\frac{1}{3}\frac{[(\rho + \frac{3d}{2})^2 + L^2] - [(\rho + \frac{d}{2})^2 + L^2] - d^2}{d^2}, \\
&= -\frac{1}{3}\frac{2\rho d - d^2}{d^2}, \\
&= -\frac{1}{3}(2\frac{\rho}{d} - 1).
\end{aligned}
$$